# Maternal High Fat Nutrition is Associated with Placental Dysfunction: Insight in Pathophysiology and Potential Mechanisms

INAUGURAL DISSERTATION

zur

Erlangung des Doktorgrades
Dr. nat. med.

der Medizinischen Fakultät

und

der Mathematisch-Naturwissenschaftlichen Fakultät

der Universität zu Köln

vorgelegt von

Tobias Kretschmer, M.Sc.

aus Lennestadt

sedruck, Köln

2020

Betreuer: Prof. Dr. Jörg Dötsch

Referenten: Prof. Dr. Mario Fabri

Prof. Dr. Matthias Hammerschmidt

Datum der mündlichen Prüfung: 21.07.2020

„Wir neigen dazu, die messbare Welt für die Welt zu halten.“

**Richard David Precht**

# I. Short Contents

# II. Table of Contents

## Abstract

The prevalence of overweight (BMI >25 kg/m²) and obesity (BMI >30 kg/m²) are increasing on a global scale, and as a consequence, obesity among women of reproductive age has also increased within the last decades. Obesity before and during pregnancy is associated with a higher risk for the mother and the unborn child to develop pregnancy related complications, including gestational diabetes and disturbed fetal growth. Abnormal fetal growth has been linked to placental dysfunction and can translate into childhood and adolescence health issues, resulting in high socio-economic costs.

Obesity and pregnancy are both linked to a state of increased inflammation and oxidative stress, which in case of pregnancy may be relevant to initiate the birth process at the end of pregnancy, but concomitant with obesity, can also attribute to placental dysfunction. The placenta provides essential tasks during pregnancy in both oxygen and nutrient supply, as well as waste removal and contributes to the success of pregnancy also by the production of hormones. In order to properly fulfill its function, placental cell homeostasis, structure and vascularization are of tremendous importance. However, it is still not fully understood how maternal obesity (MO) affects placental cells and processes like vascularization and placental transfer capacity. Therefore, we aimed to decipher the effects of MO on the placental feto-maternal transfer zone which constitutes the interface for transport of oxygen, nutrients and removal of waste products between maternal and fetal circulation.

In order to address these questions, we induced obesity in C57BL/6N mice via feeding a high fat diet (HFD) after weaning until the end of the experiment and collected serum, placentas and epigonadal white adipose tissue (egWAT) for analyses at various gestation days (E11.5, E15.5 and E18.5). Lean mice, receiving a standard diet (SD), served as control.

We discovered that in obese dams, gestation was prolonged for about 1 day compared to lean dams, and speculate that this might be due to a reduced leukocyte-infiltration of placentas and pro-inflammatory factor expression in egWAT of obese dams compared to lean dams shortly before parturition (E18.5). Furthermore, in our mouse model of maternal obesity, embryos of obese dams developed an intrauterine growth restriction (IUGR) at the beginning of the third trimester of gestation (E15.5). At the same time, protein and mRNA level of endothelial cell (EC) marker were reduced in placentas, and stereological analysis revealed impaired vascularization in placentas of obese dams. This was accompanied by increased EC senescence in the transfer zone of placentas under MO. We also found elevated interleukin-6 (IL-6) level in maternal serum and observed a trend towards an increase in IL-6 mRNA and protein level in egWAT of obese dams compared to controls, suggesting this tissue as the source of elevated circulating IL-6 level. In cell culture assays using human placental EC, we then confirmed that stimulation with IL-6 can induce senescence, suggesting a link between elevated serum IL-6 level, placental EC senescence and impaired placental vasculature.

Based on the findings regarding IL-6 induced EC senescence in vitro and altered placental vascularization in vivo, we subjected obese dams to an anti-IL-6 signaling antibody therapy. We found that under this therapy, placental IL-6 protein level were elevated and down-stream signaling marker level seemed reduced, which indicates successful IL-6 signaling blockade. However, antibody therapy

did not prevent lower fetal weight at E15.5, and placental vascular marker level were reduced compared to obese controls without antibody therapy. In summary, anti-IL-6 signaling therapy may not alleviate HFD-induced defects in placental vascularization and IUGR, and warrants further investigation with additional dosing.

Proteomic profiling of the feto-maternal transfer zone moreover revealed a reduced level of the adherens junctions (AJ) marker E-cadherin in obese compared to lean dams at E15.5. This was confirmed in whole placenta lysates of obese compared to lean dams concomitant with a strong tendency towards reduced β-catenin level, an intracellular adaptor protein of AJ. These changes persisted until the end of pregnancy (E18.5) in placentas of obese dams, while at mid-gestation (E11.5) we could not observe altered AJ marker level. In addition, it was found that at E15.5 the ultrastructure and cell homeostasis in the transfer zone were affected by MO, as demonstrated by defective syncytial fusion and a disrupted basement membrane. In functional assays we then showed that passive transfer across the placenta was significantly increased under MO, while active glucose transport was unaltered at E15.5. Moreover, our in vitro studies suggest that fatty acids, present in excess in our HFD, can alter trophoblast cell layer permeability and cause reduced β-catenin level. Collectively, these findings strongly suggest that MO causes disruptions in the feto-maternal transfer zone via disturbed EC and trophoblast homeostasis, leading to a “leaky” placental barrier while embryos develop an IUGR.

A healthy lifestyle with limited intake of fatty acids and prevention of obesity in women of childbearing age could therefore, in case of pregnancy, support proper placental function and reduce the risk of fetal growth restriction.

## Zusammenfassung

Die Prävalenz von Übergewicht (BMI >25 kg/m²) und Adipositas (BMI >30 kg/m²) haben in der Bevölkerung weltweit deutlich zugenommen, und infolgedessen sind über die letzten Jahrzehnte auch immer mehr Frauen im gebärfähigen Alter von Übergewicht betroffen. Übergewicht und Adipositas vor und während der Schwangerschaft sind mit einem höheren Risiko für die Mutter und das ungeborene Kind verbunden Schwangerschafts-Komplikationen wie beispielsweise Gestationsdiabetes und ein gestörtes fötales Wachstum zu entwickeln. Anormales fötales Wachstum wird dabei oft mit einer Funktionsstörung der Plazenta in Verbindung gebracht und kann zu langfristigen gesundheitlichen Problemen bis ins Erwachsenenalter führen, was hohe sozioökonomische Kosten zur Folge hat.

Übergewicht und Schwangerschaft sind jeweils mit einem Zustand erhöhter systemischer Inflammation und oxidativem Stress verbunden, die, im Fall einer Schwangerschaft allein, für das Einsetzen des Geburtsvorgangs von Bedeutung sein können, doch in Verbindung mit Übergewicht auch zu einer plazentaren Dysfunktion führen können. Die Plazenta erfüllt wesentliche Aufgaben, insbesondere die Versorgung des Fötus mit Sauerstoff und Nährstoffen sowie den Abtransport von Abfallstoffen und trägt durch die Produktion von Hormonen und anderen Faktoren zu einer gesunden Schwangerschaft bei. Für eine optimale Funktion der Plazenta sind Faktoren wie die Homöostase der plazentaren Zellen sowie die Vaskularisierung und der korrekte Aufbau der plazentaren Struktur von enormer Bedeutung. Es ist jedoch noch nicht hinreichend bekannt, wie mütterliches Übergewicht (MÜ) die Zellen und Gefäßentwicklung der Plazenta nebst der plazentaren Transferkapazität beeinflusst.

Aus diesem Grund ist es Ziel der vorliegenden Arbeit, die Effekte des MÜ auf die plazentare feto-maternale Transferzone, welche die entscheidende Schnittstelle für den Transfer von Sauerstoff, Nährstoffen und Abfallstoffen zwischen mütterlichem und fötalem Kreislauf darstellt, zu entschlüsseln.

Zur Erforschung dieser Fragestellung wurde mütterliches Übergewicht mittels Hochfett-Diät (HFD) in C57BL/6N-Mäusen induziert, um Blutserum, Plazenten und epigonadales weißes Fettgewebe (egWAT) von verschiedenen Trächtigkeitstagen (E11.5, E15.5, E18.5) für Analysen zu gewinnen. Normalgewichtige Mäuse, die eine Standard-Diät (SD) erhielten, dienten als Kontrollgruppe.

Wir konnten feststellen, dass sich, verglichen mit schlanken Kontrolltieren, in übergewichtigen Muttertieren die Trächtigkeit um einen Tag verlängerte. Unsere Daten lassen den Schluss zu, dass eine verminderte Leukozyten-Infiltration der Plazenten sowie eine verminderte Expression pro-inflammatorischer Faktoren im egWAT übergewichtiger Muttertiere kurz vor Ende der Trächtigkeit (E18.5) als Ursache für diese Beobachtung in Frage kommen.

Embryos der übergewichtigen Muttertiere zeigten zu Beginn des letzten Trimenon der Trächtigkeit (E15.5) eine intrauterine Wachstumsretardierung (IUGR). Zeitgleich waren Protein- und mRNA-Level von Endothelzellmarker herunterreguliert und stereologische Analysen zeigten eine gestörte Gefäßentwicklung in Plazenten übergewichtiger Muttertiere. Dies wurde begleitet von erhöhter Endothelzell (EC)-Seneszenz in der plazentaren feto-maternalen Transferzone. Wir fanden ebenso erhöhte Interleukin-6 (IL-6) Level im mütterlichem Serum und konnten einen deutlichen Trend hin zu erhöhten IL-6 mRNA- und Protein-Leveln im egWAT der übergewichtigen Muttertiere, verglichen mit

schlanken Kontrolltieren, erkennen. Dies deutet auf das egWAT als Quelle der erhöhten IL-6 Level in übergewichtigen Muttertieren hin. Wir konnten ferner bestätigen, dass eine Stimulation von humanen plazentaren EC mit IL-6 eine Seneszenz induziert, was eine Verbindung zwischen erhöhten IL-6 Serumlevel, plazentarer EC-Seneszenz und gestörter Gefäßentwicklung suggeriert.

Ausgehend von diesen Ergebnissen, dass IL-6 in EC eine Seneszenz *in vitro* herbeiführen kann und die plazentare Gefäßbildung *in vivo* gestört erscheint, wurde mittels Antikörper-Therapie eine Blockade des IL-6-Signalwegs in übergewichtigen Muttertieren induziert. Wir konnten zeigen, dass unter dieser Therapie die plazentare IL-6-Proteinmenge signifikant anstieg und nachgeschaltete Signalwege beeinträchtigt waren, was auf eine erfolgreiche Blockade des IL-6-Signalwegs hindeutet. Jedoch kam es auch unter der Antikörper-Therapie zu einem verringerten Körpergewicht der Föten an E15.5, und plazentare Gefäßmarker-Level waren im Vergleich zu den nicht-therapierten, übergewichtigen HFD-Kontrolltieren reduziert. Insgesamt deutet dies darauf hin, dass die Antikörper-Therapie die HFD-induzierten Schädigungen in der plazentaren Gefäßentwicklung nicht abschwächen kann und es weiterhin zu einer IUGR kommt, so dass weitere Untersuchungen mit alternativen Dosierungen angebracht sind.

Eine Proteom-Analyse der feto-maternalen Transferzone zeigte darüber hinaus, dass eine Reduktion des Adherens Junction (AJ)-Markers E-cadherin in Plazenten übergewichtiger Tiere, verglichen mit schlanken Kontrolltieren, an E15.5 vorliegt, was wiederum auf eine Destabilisierung der AJ hinweist. Die Reduktion von AJ-Markern wurde in Analysen von Gesamtplazenta-Lysaten übergewichtiger Muttertiere gegenüber Kontrolltieren bestätigt. Außerdem zeigte sich eine starke Tendenz hin zu einem reduzieren β-catenin Level, einem intrazellulären Adapterprotein der AJ. Diese Veränderungen wurden ebenso in Plazenten von übergewichtigen Muttertieren kurz vor Ende der Trächtigkeit gemessen (E18.5), während zur Mitte der Trächtigkeit hin (E11.5) keine Veränderungen der AJ-Marker Level festgestellt wurden. Ferner zeigte sich, dass an E15.5 die Ultrastruktur und Zell-Homöostase der Transferzone unter MÜ verändert sind, wie anhand der defekten „Synzytialfusion“ und der geschädigten Basalmembran zu erkennen ist. Wir konnten anhand funktionaler Untersuchungen zeigten, dass an E15.5 unter MÜ der passive Transfer über die Plazenta signifikant zunahm, während ein aktiver Glukose-Transport unverändert blieb. Ebenso lassen *in vitro*-Studien vermuten, dass Fettsäuren, die auch in der HFD im Übermaß vorhanden sind, die Durchlässigkeit der Trophoblasten-Zellschicht verändern sowie zu erniedrigten β-catenin Level führen können. Dies deutet darauf hin, dass MÜ über die vermehrte Aufnahme von Fettsäuren zu einer gestörten Integrität der feto-maternalen Transferzone beitragen könnte. Insgesamt lassen unsere Ergebnisse vermuten, dass MÜ die Transferzone durch Störung der EC-Homöostase und Trophoblasten-Differenzierung schädigt und es zu einer durchlässigeren Plazentabarriere kommt, während Föten eine IUGR entwickeln.

Ein gesunder Lebensstil mit einer begrenzten Aufnahme von Fettsäuren sowie die Prävention von Übergewicht und Adipositas könnten dementsprechend zu einer uneingeschränkten Plazentafunktion und einem geringeren Risiko einer IUGR beitragen.

# 1. Introduction

## 1.1 Development and function of the placenta

At the beginning of mammalian, rodent and all human life occurs conception, the fusion of gametes from male and female which is the initiation of development of one or multiple new organisms [1]. Subsequent to this fertilization event, the development of a zygote starts which can divide by mitosis into a multi-cellular blastomere. During this process in humans, the blastomere travels towards the uterus which is the implantation site, and implantation takes place at about day 5 after conception in the form of a blastocyst. The attachment and subsequent implantation of the blastocyst into the endometrial tissue are crucial events for gestation and the development of a placenta to occur. During this process, cells of the trophectoderm, the outer cell layer of the blastocyst, anchor to the endometrium and give rise to the developing placenta, while the inner cell mass of the blastocyst gives rise to the embryo [2, 3]. Though the mammalian placenta is an impermanent organ only required during development of the conceptus *in utero*, its formation and function are tightly regulated and pivotal for a healthy development of the embryo [2].

In humans, just about 2 days after the blastocyst reaches the endometrium, trophoblast cells which are cells of the outer cell layer of the blastocyst, invade maternal tissue with finger-like formations. These trophoblast cells ultimately reach maternal blood vessels by migrating through extracellular matrix (ECM), a prerequisite to establish blood supply to the forming placenta and therefore the embryo [4, 5]. Trophoblast invasion during implantation and placenta development is crucial and if impaired, it may cause stress during early pregnancy which can lead to placental dysfunction later and result in maternal and fetal complications [6]. Alterations in the endometrial lining as a consequence of blastocyst adhesion and trophoblast invasion lead to the formation of a decidual structure which is only present during pregnancy. Decidualization, as the formation of this structure from the endometrium between maternal and fetal tissues is called, limits trophoblast invasion, protects the endometrium and myometrium from invasion by trophoblasts, and permits preliminary supply for the developing embryo. Later, the maternal portion of the placenta consists of the decidua basalis (Db) which harbors a vascular network of spiral arteries that are invaded by the trophoblast cells to enable blood supply of the placenta [2]. These tightly controlled steps are very similar in human and murine placental development, and many studies in murine animal models have contributed substantially to the understanding of molecular and genetic aspects of placental development [7, 8]. Since both fetal and maternal cells are involved in the development of the placenta, it is considered a feto-maternal organ. A schematic overview of the human and murine placenta is shown in Figure 1.1.1.

Mouse strains used in the laboratory have proven valuable, even if gestation takes only about 20 days in these animals, to study gene function, embryogenesis and placental development; and it is especially the genetic manipulation that also revealed placental defects often as cause of lethality of the embryo. While about one in three knock-outs of individual genes cause fetal death, it is not known how many of those are due to placental defects, and the contribution of the placenta to lethality could thus frequently be underestimated or even misinterpreted [9-11]. The placenta in mice starts to form at about day 4 of

embryonic development (day 0.5 being the next morning when mating takes place overnight) as seen by the formation of extraembryonic cell lineages and the yolk sac. At embryonic day 8.5 (E8.5) chorioallantoic fusion which forms the placenta has occurred, branching morphogenesis starts taking place and highlights in full materno-fetal material exchange at around E12.5 [12, 13]. Roughly 2 days later, at E14.5, placental development and peak velocity of the vitelline artery have reached their maximum. At the same time, the exponential embryo weight-gain reaches the steepest phase as the organogenesis is completed. Technically, the embryo would from then on be called “fetus”, however it is convention to refer to the fetus as embryo also after E14.5 or use both terms interchangeably from E14.5 onwards [12].

The growing embryo requires nutrients and oxygen during its development, and the placenta is responsible for the transfer of such nutrients and oxygen additional to the removal of carbon dioxide ($CO_2$) and other waste products from fetal metabolism. This is achieved by supplying the embryo with oxygenized blood through the umbilical vein and removing waste-containing deoxygenized blood through two umbilical arteries. Both arteries spiral around the larger vein, and these three vessels together form the umbilical cord. In the umbilical cord, the vessels are embedded in what is called Wharton’s jelly. The vessels reach the placenta and enter into the chorionic plate where the arteries branch and ultimately form an arteriovenous system [2]. This system and thus the interior compartmentalization of the placenta differs among mammalian species and shows distinct architectures in human and mice [3, 14]. In murine placentas, trophoblasts of chorionic origin begin differentiation and fuse to give rise to the multinucleated syncytiotrophoblast (SynT), organized in two layers, which engulfs fetal endothelium of capillaries. A forth cell layer is situated on the other side of the SynT, i.e. the mononuclear trophoblast which is in contact with maternal blood sinuses carrying the oxygenated blood. In total, these 4 cell layers form the placental transfer barrier with markedly branched villi, giving the murine placenta its labyrinthine appearance (Figure 1.1.1 G). This interface for material exchange and transfer zone of the murine placenta is therefore called the labyrinth zone (Lz) [7, 8]. In humans, the transfer zone corresponds to the villous part of the placenta and comprises a multinucleated SynT, followed by a layer of villous mononuclear cytotrophoblast. Each of the so-formed floating villi can contain multiple fetal capillaries (Figure 1.1.1 D). In both human and mice, maternal blood on one side of the placental barrier and fetal blood in the fetal capillaries flow counter-currently to increase nutrient transport in the transfer zone, making both murine and human placentas hemochorial. Another similarity of murine and human placentas is the discoid shape (Figure 1.1.1 A & E) which adds to the value of mouse models to study the placenta and extrapolate to human placentas. In contrast, horse and pig have a diffuse epitheliochorial placenta, and cats, dogs and other carnivores have a zonary endotheliochorial placenta [14]. The flow characteristics within the transfer zone of the placenta underpin that adequate vascularization is necessary for appropriate nutrient and oxygen transfer [15, 16]. As a consequence, disturbances in trophoblast differentiation and defects in Lz or human villous development can severely impact on embryonic development and even lead to pregnancy termination [4, 17].

In both humans and mice, regulation of material exchange in the placenta is achieved by a variety of mechanisms and can be divided in passive and active transfer. In murine placentas, the SynT expresses specific nutrient transporters for glucose, amino acids, free fatty acids and other molecules, therefore actively mediating supply across the placental barrier to the fetus. Regarding glucose, the transporters GLUT1, GLUT3 and GLUT4 are found in the murine transfer zone and facilitate active glucose transport towards the fetal circulation [8, 18]. Additionally, fetal growth depends on the ability of the placenta to provide glucose, and for periods of glucose shortage the placenta can utilize glycogen which is stored in clusters within the murine placenta [19]. Passive transfer of substances without active carriers or transporters mediates oxygen supply and also transfer of predominantly hydrophobic molecules with a size of 600 Da or less. As pregnancy progresses, increased placental blood flow, increased transfer zone surface area and reduction in the SynT cell layer thickness lead to enhanced passive transfer [20]. Transporter expression on the surface of SynT and fetal endothelial cells (EC) determine active carrier-mediated transport. These placental cells also form junctions between each other, which have been implicated in vascular permeability and intestinal barrier function and thus in the transfer of substances [21, 22]. However, to best of our knowledge, the influence of these junctions on placental passive transfer capacity has not been described.

A third tissue layer in murine placenta, the so called junctional zone (Jz), is present between the maternal Db and the Lz consisting of spongiotrophoblasts and trophoblast glycogen cells, as well as arterial and venous channels of trophoblastic origin, but the Jz contains no fetal blood (vessels). The spongiotrophoblast layer is analogous to the placental column cytotrophoblasts in humans [8]. Spongiotrophoblasts and (trophoblast) glycogen cells are collectively forming the Jz of the murine placenta. The glycogen cells probably derive from spongiotrophoblasts and form clusters that can be seen from the second trimester of murine gestation in the Jz. Though the precise function of this zone and its inhabitant cells are not fully understood today, it is known that the Jz produces hormones and is absolutely required for placental function and successful pregnancy [3]. Primary trophoblast giant cells, originating from mural trophectoderm, do not contribute to the mature placenta, however a secondary trophoblast giant cell layer which derives from polar trophectoderm is located at the boundary between the Jz and the Db. Furthermore, the relative extent of the three layers, Lz, Jz and Db change during the course of gestation to meet fetal demands. This includes an increase in the size of the Lz for example, concomitant with enhanced complexity to allow exponential fetal growth towards the end of pregnancy. Exponential fetal growth similarly requires a drastic increase in nutrient transfer capacity by upregulation of transporters and morphological changes to enhance passive transfer [3, 23]. Conversely, the Jz starts decreasing in size from the third trimester onwards and has its maximum size before this time-point [24, 25].

### 1.2 The placental transfer zone

As mentioned above, the murine placental transfer zone consists of various cell types: the mononuclear trophoblasts which are in contact with maternal blood; the two layered SynT which lies beneath mononuclear trophoblasts and is in contact with the basement membrane (BM). Opposite of the BM is

the fetal endothelium with EC that are in contact with fetal blood, and the development of all these cell layers is precisely regulated (Figure 1.1.1) [7, 24]. The SynT can be described as a form of epithelium in human placentas which separates maternal and fetal blood while being heavily involved in transport of substances, oxygen and waste products in addition to producing certain hormones [8, 26, 27].

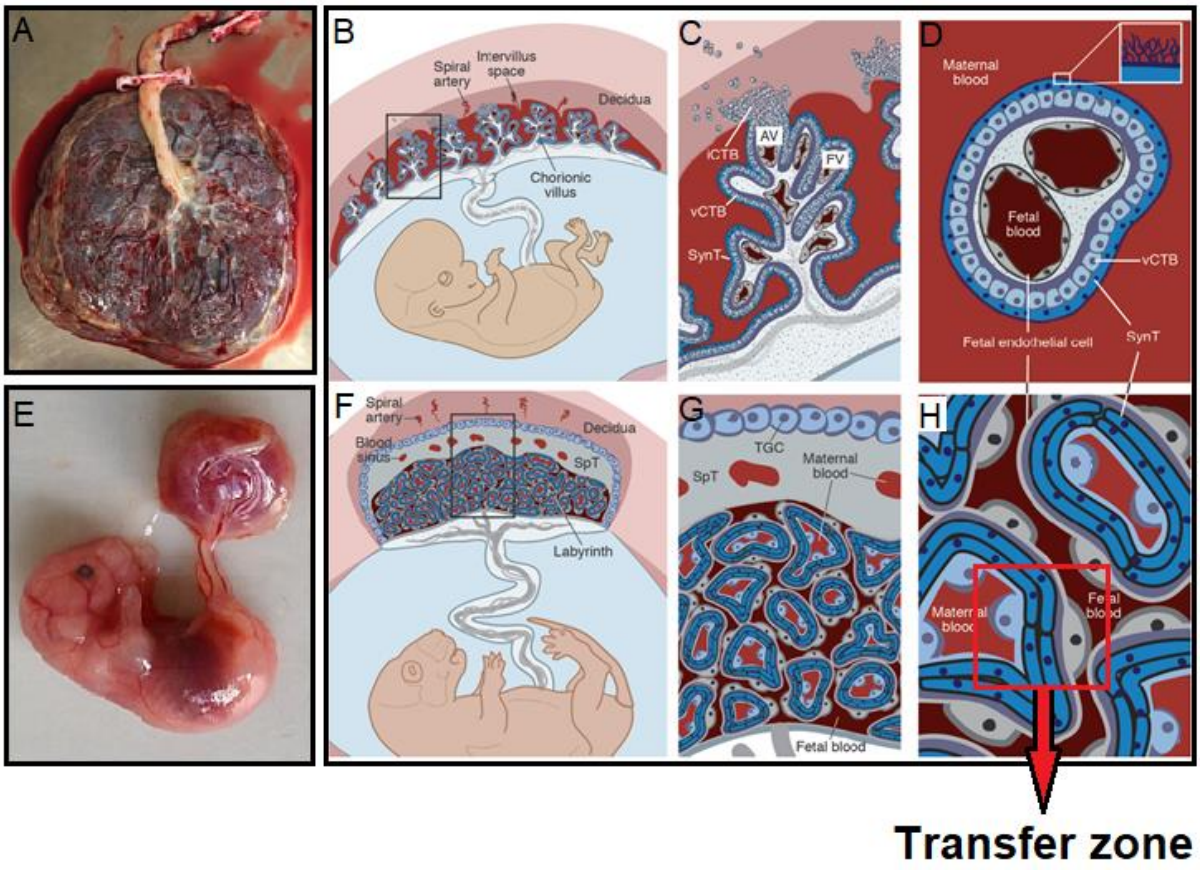


**Figure 1.1.1: Comparative appearance of the human and murine placenta.** (A) Photograph of a human placenta at term from a cesarean section. (B) Schematic drawing of the human placenta showing a villous tree in the black frame (close up in C) perfused by maternal spiral arterial blood. The FV are surrounded by a continuous layer of SynT that is in contact with maternal blood, and the extravillous trophoblasts invade from AV in order to anchor the villi within the decidua. (D) The human hemodichorial transfer zone with SynT towards maternal blood, vCTB underneath, and fetal EC of capillaries containing fetal blood. (E) The murine placenta has a disc-like shape similar to human placentas, however the placental layers are distinct as there is a labyrinth of villi (F). The black frame in (F) is shown in (G) and highlights the Lz, over which the Jz can be seen with its boundary of trophoblast giant cells. Additionally, the murine hemotrichorial transfer zone of maternal trophoblasts, two layers of SynT and fetal EC becomes evident in (H). AV: anchoring villi; FV: floating villi; iCTB: invasive cytotrophoblast; vCTB: villous cytotrophoblast; SpT: spongiotrophoblasts; TGC: trophoblast giant cell. Adapted and modified from Maltepe et al. [7].

The SynT and EC in the transfer zone are interconnected by adhesion molecules to the BM, but also to other SynT or EC, respectively, by the formation of adherens junctions (AJ). AJ contain molecules of the cadherin family of proteins to form cell-cell adhesions. In contrast, cell-BM or cell-ECM contact is mediated by other forms of adhesion, e.g. integrin binding and focal adhesion. The epithelial cadherin, E-cadherin, is mostly found on epithelial cells but also on villous trophoblasts in human placentas.

Already before the definitive placenta is formed, cells of the trophectoderm rely on the formation and distribution of AJ [7]. In the placenta and other organs, vascular cells, like fetal EC, rather express vascular endothelial cadherin, VE-cadherin [28, 29]. The cadherin molecules in EC and epithelial cells establish polarity of cells by forming AJ and creating cell-cell contacts which are required for vascular lumen formation and permeability regulation by EC [30, 31]. VE-cadherin clusters in human placentas on EC have been reported to co-localize and then bind to β-catenin, which is an intracellular adaptor molecule. Catenins are important anchoring proteins for cadherins to peri-junctional actin and thus, the cytoskeleton [32]. It has been shown that β-catenin knock-out specifically in EC can lead to altered vascularization in the placenta and embryos, and that *in vitro* β-catenin knock-out led to disorganized junctions in EC [33]. Furthermore, catenins can be released from these junctions and are then involved in regulation of transcription in the nucleus [32]. In this regard, β-catenin is part of canonical Wnt signaling which plays a relevant role in trophoblast development and other reproductive functions. Impaired Wnt signaling has been associated with infertility and placental defects, however there is still much to be discovered in pathological circumstances regarding involvement of β-catenin [34].

As mentioned above, EC and SynT together form an important barrier in the transfer zone to regulate material exchange between mother and fetus. Both cell layers express transport molecules that influence resource allocation. The placenta's ability to alter efficiency of resource allocation due to environmental conditions has been suggested to maintain fetal growth with consequences for the health of the offspring after birth [23]. This concept of inadequate fetal supply during intrauterine development, mediated by the placenta for a great part, has been termed fetal programming and affects not only metabolic health [35, 36], but also e.g. cardiovascular pathology [37] in later life.

### 1.3 Maternal obesity and placental pathologies

Since healthy fetal development requires a proper functioning placenta and the placenta is partially made up of maternal tissue and transports maternal blood, maternal health translates to placental physiology and ultimately fetal health. Numerous studies of the past decades have looked into factors of maternal origin and their influence on development and function of the placenta on the one hand, as well as perinatal outcome and offspring health on the other hand [4, 38-40]. Among those factors associated with adverse consequences on the placenta and fetal health is maternal obesity (MO), i.e. obesity before and during pregnancy. In Germany and worldwide, numbers of women at child-bearing age with overweight, defined by the World Health Organization by a body mass index (BMI) ≥25 kg/m², or obesity, defined by a BMI ≥30 kg/m², have increased since the 1990s [41, 42]. Depending on the severity of obesity, the associated complications for mothers differ and fall into a spectrum of pathologies, including decreased probability of conception, increased relative risk for preeclampsia and gestational diabetes mellitus (GDM), but also the risk for intrauterine death of the fetus [38, 43, 44]. Moreover, research in recent years showed that maternal nutrition and its effect on offspring health extent beyond pregnancy by fetal programming. Fetal programming occurs for example as a consequence of epigenetic changes in the offspring and may contribute to an increased obesity prevalence. Various tissues in the offspring can be affected by epigenetic changes, leading to an

involvement of multiple organs and the development of diabetes and the metabolic syndrome [45]. In the US as well as Europe, the increase in such diseases linked to obesity from an early age has been estimated to cost the health care systems between $100 billion to $200 billion per year [46]. Additionally, diagnosed obesity among pregnant women is associated with longer hospitalization and impacts the hospitalization costs [47]. These findings show the relevance for understanding and limiting adverse factors for maternal health before and during pregnancy to improve offspring health and reduce the potential burden on healthcare systems. The concept of developmental origins for/of health and disease (DOHaD) has reached many disciplines of biomedical science and has generated novel insight from many research fields to further public leadership for healthier life-style [48]. As a result, it is often collectively advised for obese women to adapt a healthy lifestyle before and during pregnancy to mitigate potential negative effects of obesity. However, it is still a matter of debate how this can be achieved most effectively, and many studies are difficult to compare due to variations in e.g. diets and study endpoints [49, 50]. Furthermore, such cohort studies provide limited insight into the direct effect on placental function and mechanisms of placental defects. As a result, studies with established and novel animal models are required to decipher mechanisms of placental function under MO.

Intrauterine growth restriction (IUGR) is occurring in approximately 3% to 8% of human pregnancies worldwide and the defined growth potential at a certain gestational age is not reached by fetuses suffering from IUGR. IUGR is, amongst others, associated with preeclampsia, a serious hypertensive disorder occurring during pregnancy [51] and can be caused by various factors like embryo genetics combined with maternal factors. In the majority of cases, it is assumed that placental dysfunction is the leading cause of IUGR, where the nutrient supply to the fetus is inadequate despite sufficient maternal nutrition [52-56]. Not only IUGR has been associated with insufficient placental function and vascularization, MO itself was associated with negatively affected placental vascular development in humans [57, 58], as well as mice [44] and rats [59, 60]. Furthermore, induction of obesity and diabetes in mice through feeding of a specific diet led to a reduction in placental trophoblast and EC density resulting in vascular changes [44] which could also affect the Lz development.

The effects of MO on the placenta are manifold and comprise exaggerated saturated fatty acid profiles that can e.g. cause inflammatory responses in the placenta and altered mitochondrial function which in turn may lead to oxidative stress in the placenta. Moreover, the metabolic environment in the placenta of obese mothers probably affects the epigenome of placental cells, thereby influencing placental function [36]. Additionally, human and primate studies have shown excessive macrophage accumulation and reduced blood flow in placentas of obese individuals [61, 62]. In obese mice, elevated placental cytokine level and macrophage infiltration were described in placentas [63]. Regarding inflammatory responses, obesity and pregnancy are both associated with systemic inflammation of low grade, which may constitute the underlying mechanism of adverse placenta function [63, 64]. Longitudinal studies have reported that level of pro-inflammatory cytokines, like Interleukin-6 (IL-6), are elevated during pregnancy concomitant with higher BMI especially after the first half of pregnancy [65-67]. IL-6 is a cytokine that can have both pro-inflammatory and anti-inflammatory effects which are dependent on either classic IL-6 receptor (IL-6R)-mediated signaling or trans-signaling, respectively. The trans-

signaling is dependent on coupling of a soluble IL-6R (sIL-6R) with the membrane-bound gp130 receptor for its pro-inflammatory activities on cells of various types, e.g. EC [68, 69]. Furthermore, trans-signaling of IL-6 could also affect placental EC via gp130 receptor. It has been shown that IL-6 stimulation of EC is associated with lower VE-cadherin level and reduced AJ expression [70], and IL-6 may regulate AJ in breast cancer cells [71]. Other inflammatory markers, like IL-1β and TGF-β have been suggested to affect placental tight junctions and weaken the placental barrier by regulating the tight junction marker occludin [72, 73]. Under obesity, such systemic pro-inflammatory factors like IL-6 are elevated, may arise from adipose tissue and be secreted into the circulation to reach and affect different organs including the placenta [64, 74]. The placenta is highly vascularized and molecules of many kinds that are found in the circulation of the mother will pass the vasculature and thus, may reach and affect cells within the placenta. Adipokines and hormones, like leptin and insulin, are associated with MO and could play important regulatory roles in the placenta, since they can be produced both here and in adipose tissue from which they reach the placenta via the circulation. These substances affect signaling in placental cells such as Stat3 and Akt/mTOR pathway activation which translates to regulation of placental nutrient transport and ultimately fetal supply and growth [75]. However, in pregnant mice it was shown that leptin was not involved in inflammatory responses in the placenta [76]. Nevertheless, it could be important to further investigate mechanisms of placental function mediated by inflammatory molecules.

The chain of evidence more and more pinpoints towards placental dysfunction under MO as a cause for maternal and fetal health consequences, which makes it worthwhile to study placenta function and develop strategies to mitigate adverse effects of MO on the placenta. Studies on the mechanisms of placental dysfunction in many contexts, including MO, have however, not yielded sufficient results to elucidate the precise origin of IUGR and other complications under MO. As a consequence, further studies are required on placental dysfunction.

### 1.4 Study aims and hypothesis

The association of MO with placental dysfunction, together with possible implications for fetal health and development, permit investigations into the mechanisms behind these clinically relevant effects. Previous studies of our group showed that it is possible to induce MO by feeding a high fat diet (HFD) after weaning [76, 77]. Herein, we aimed to advance our insight into placental dysfunction and the placenta-associated programming effects on offspring health under MO.

The inflammatory responses in adipose tissue and the placenta during pregnancy in obese women are still not understood in great detail and we aimed to elucidate the inflammatory response in adipose tissue and the placenta of both obese and lean mice before the onset of parturition.

Since the placenta is a highly vascularized organ and its main function is the exchange of nutrients and waste via blood circulation to ensure proper fetal growth, we aimed to elucidate the effects of MO on placental vascularization together with EC homeostasis. Based on previous reports and preliminary data from our group, we hypothesize that MO affects maternal serum level of the pro-inflammatory marker

IL-6 and in this study we aimed to clarify the effects of IL-6 on placental EC. To this end, obese dams were also assigned to an antibody therapy in order to block IL-6 signaling and study potentially positive effects on the placenta under MO. An obese mouse model in which IL-6 was genetically knocked-out was used to gain further insight into IL-6 signaling related processes in placental and fetal development under MO.

Previous studies suggest that HFD consumption could cause reduced expression level of cell junction markers [21, 22] which might also translate to placental cells and therefore affect integrity and function of the transfer zone. We hence aimed to analyze the proteome of the transfer zone to find new hints regarding altered marker level of cell junctions and AJ. Moreover, localization of such markers was investigated, and the morphology and ultrastructure of the transfer zone was studied in detail. We furthermore hypothesized that morphological and molecular changes in the transfer zone could have an impact on materno-fetal transfer of substances and aimed to determine the transfer capacity across the placental barrier in obese dams.

Collectively, it is assumed that MO can disrupt the placental transfer zone and cause structural and molecular changes in the cells of the transfer zone, resulting in adverse placental function and impaired fetal development.

# 2. Materials

## 2.1 Chemicals, materials and reagents

Table 2.1: Chemicals, materials and reagents used in this work.

| Chemical / material / reagent | Company |
|---|---|
| 1-tetradecanoic acid-$d_{27}$ | Sigma-Aldrich, Steinheim, Germany |
| 2-Chloroacetamide | Sigma-Aldrich, Steinheim, Germany |
| 2-mercaptoethanol | Carl Roth, Karlsruhe, Germany |
| 2N $H_2SO_4$ | Carl Roth, Karlsruhe, Germany |
| 4′,6-diamidino-2-phenylindole, DAPI | Sigma-Aldrich, Steinheim, Germany |
| 6-, 24- and 96-well plates | Sarstedt, Nümbrecht, Germany |
| Acetic acid | Carl Roth, Karlsruhe, Germany |
| Aceton | Carl Roth, Karlsruhe, Germany |
| Acetonitril, 80%, 20% water with 0.1% formic acid, Optima LC/MS (Puffer B) | Fisher Scientific, Waltham, Massachusetts, USA |
| Acrylamide (30%) and bisacrylamide (0.8%) mix ROTIPHORESE® Gel 30 (37.5:1) | Carl Roth, Karlsruhe, Germany |
| AdipoRed reagent | Lonza, Walkersville, Maryland, USA |
| Agarose | Sigma-Aldrich, Steinheim, Germany |
| Albumin bovine fraction V, BSA | SERVA Electrophoresis GmbH, Heidelberg, Germany |
| Ammonium persulfate, APS | Sigma-Aldrich, Steinheim, Germany |
| Antibody diluent | DAKO Agilent, Santa Clara, California, USA |
| Aprotinin from bovine lung | Sigma-Aldrich, Steinheim, Germany |
| Aqueous mounting medium, Fluoromount™ | Sigma-Aldrich, Steinheim, Germany |
| Bepanthen® | Bayer Vital GmbH, Leverkusen, Germany |
| Biosol | National Diagnostics, Atlanta, Georgia, USA |
| Buprenorphine | Bayer Vital GmbH, Leverkusen, Germany |
| CellStain®, from ECM642 | Merck, Darmstadt, Germany |
| Chloroacetamide, CAA | AppliChem, Darmstadt, Germany |

| | |
|---|---|
| Chloroform | Merck, Darmstadt, Germany and Sigma-Aldrich, Steinheim, Germany |
| Citrate buffer pH 6, target retrieval solution | DAKO, Glostrup, Denmark |
| cOmplete EDTA-free Protease Inhibitor Cocktail | Roche, Basel, Schweiz |
| Deoxycholic acid sodium salt | Carl Roth, Karlsruhe, Germany |
| Diethyl pyrocarbonate, DEPC ≥ 97% | Sigma-Aldrich, Steinheim, Germany |
| Dithiothreitol, DTT | AppliChem, Darmstadt, Germany |
| D-Mannitol, [1-$^{14}$C]-250 µCi, $^{14}$C-mannitol | Hartmann Analytic, Braunschweig, Germany |
| DNA ladder | Thermo Scientific, Vilnius, Lithuania |
| dNTP mix for genotyping and RT-qPCR (10 mM) | Thermo Scientific, Vilnius, Lithuania (Genotyping)<br>Thermo Scientific, Massachusetts, USA (RT-qPCR) |
| Dulbecco's phosphate-buffered saline (1X and 10X), D-PBS, $Ca^{2+}$/$Mg^{2+}$-free | Gibco, Life Technologies Ltd. Paisley, UK |
| ECL™ Prome Western Blot Detection Reagent | GE Healthcare, Solingen, Germany |
| Eosin G-solution 0.5% | Carl Roth, Karlsruhe, Germany |
| Ethanol ≥ 99.8% | Carl Roth, Karlsruhe, Germany |
| Ethanol absolute | Merck, Darmstadt, Germany |
| Ethylenediaminetetraacetic acid disodium salt dehydrate, EDTA | Sigma-Aldrich, Steinheim, Germany |
| Fetal calf serum, FBS | Biochrom GmbH, Berlin, Germany |
| Fibronectin from bovine plasma | Sigma-Aldrich, Steinheim, Germany |
| Flexi Green (5X) | Promega, Madison, Wisconsin, USA |
| Fludeoxyglucose ((18)F), $^{18}$F-FDG | Life Radiopharma GmbH, Bonn, Germany |
| Formaldehyde, phosohate-buffered Roti®-Histofix 4% | Carl Roth, Karlsruhe, Germany |
| Formic acid, puriss. p.a., ≥ 98% | Sigma-Aldrich, Steinheim, Germany |
| Gelatin, G1393 | Sigma-Aldrich, Steinheim, Germany |
| Glutaraldehyde, 50% | Electron Microscopy Sciences, Hatfield, Pennsylvania, USA |

| | |
|---|---|
| Glycerol | Carl Roth, Karlsruhe, Germany |
| Glycine | Carl Roth, Karlsruhe, Germany |
| goTaq polymerase (5 u/µL) | Promega, Madison, Wisconsin, USA |
| Heparin, 5000 IE/mL | B. Braun Melsungen AG, Melsungen, Germany |
| Hexane | Sigma-Aldrich, Steinheim, Germany |
| Hoechst 33342 stain | Fisher Scientific, Waltham, Massachusetts, USA |
| HPLC<br>Water for chromatography LiChrosolv® | Merck, Darmstadt, Germany |
| Hydrogen chloride | Sigma-Aldrich, Steinheim, Germany |
| Hydrophobic pen, Liquid Blocker | Daido Sangyo Co. Ltd., Japan |
| hyperIL-6, recombinant human IL-6/IL-6R Chimera, #8954-SR | R&D Systems, Minneapolis, Minnesota, USA |
| IGEPAL® CA-630 | Sigma-Aldrich, Steinheim, Germany |
| Inserts 0.4 µm for 24-well plates | Sarstedt, Nümbrecht, Germany |
| Isoflurane | Primal Healthcare, Northumberland, UK |
| Isopropyl alcohol (2-Propanol)<br>≥ 99.95% | Carl Roth, Karlsruhe, Germany |
| Leupeptin, ≥ 90% | Sigma-Aldrich, Steinheim, Germany |
| Linoleic acid sodium salt | Sigma-Aldrich, Steinheim, Germany |
| Liquid nitrogen | Linde AG, Köln, Germany |
| Lysyl Endopeptidase, Lys-C | WAKO, Neuss, Germany |
| Matrigel, growth factor reduced #356230 | BD Biosciences, Bedford, Massachusetts, USA |
| Mayer's hematoxylin | Carl Roth, Karlsruhe, Germany |
| Methanol, ≥99.8% | VWR, Radnor, Pennsylvania, USA |
| Methanol, 250 ppm BHT<br>(equals 0.025%) | Sigma-Aldrich, Steinheim, Germany |
| $MgCl_2$ ≥98,5% (water-free) | Carl Roth, Karlsruhe, Germany |
| $MgCl_2$, 25 mM | Promega, Madison, Wisconsin, USA |
| Micro(µ-)slide angiogenesis, #81506 | Ibidi GmbH, Graefelfing, Germany |

| | |
|---|---|
| Midori Green Advance DNA Stain | Nippon Genetics Europe GmbH, Düren, Germany |
| Milk powder, non-fat | Carl Roth, Karlsruhe, Germany |
| M-MLV Reverse Transcriptase (200 U/µL) | Promega, Mannheim, Germany |
| M-MLV RT 5X Buffer | Promega, Mannheim, Germany |
| Moloney Murine Leukemia Virus Reverse Transcriptase (M-MLV RT), DNA polymerase | Promega, Mannheim, Germany |
| N,N,N',N'-Tetramethylethylendiamin, TEMED | Sigma-Aldrich, Steinheim, Germany |
| Neo-Clear® | Sigma-Aldrich, Steinheim, Germany |
| Neo-Mount® | Sigma-Aldrich, Steinheim, Germany |
| Nitrocellulose Blotting Membrane | GE Healthcare, Solingen, Germany |
| Oil Red O | Sigma-Aldrich, Steinheim, Germany |
| Oligo-dT primer | Eurofins Genomics, Ebersberg, Germany |
| PEN-Membrane slides (No. 11600288) | Leica, Herborn, Germany |
| PenStrep | Sigma-Aldrich, Steinheim, Germany |
| Pepstatin A ≥ 75% | Sigma-Aldrich, Steinheim, Germany |
| Phalloidin, fluorescein isothiocyanate labeled, P5282 | Sigma-Aldrich, Steinheim, Germany |
| Phenylmethylsulfonyl fluoride, PMSF ≥ 98.5% | Sigma-Aldrich, Steinheim, Germany |
| Phosphate-buffered saline, PBS | Biochrom GmbH, Berlin, Germany |
| Platinum® qPCR SuperMix-UDG with ROX | Invitrogen, Carlsbad, California, USA |
| Ponceau S | Carl Roth, Karlsruhe, Germany |
| Procaine hydrochloride | Merck, Darmstadt, Germany |
| Protein ladder, PageRuler™ | Thermo Scientific, Vilnius, Lithuania |
| Proteinase K | Thermo Scientific, Vilnius, Lithuania |
| Random primer | Roche, Basel, Switzerland |
| RNasin® Ribonuclease Inhibitors (40 U/µL) | Promega, Mannheim, Germany |
| RQ1 DNase 10X Reaction Buffer | Promega, Mannheim, Germany |
| RQ1 DNase Stop Solution (20 mM EGTA) | Promega, Mannheim, Germany |

| | |
|---|---|
| RQ1 RNase-Free DNase (1 U/µL) | Promega, Mannheim, Germany |
| Sea Blocking buffer | Thermo Fisher, Rockford, Illinois, USA |
| Sodium chloride 0.9% solution | Fresenius Kabi Deutschland GmbH, Bad Homburg Germany |
| Sodium chloride, NaCl | Carl Roth, Karlsruhe, Germany |
| Sodium dodecyl sulfate, SDS | Carl Roth, Karlsruhe, Germany |
| Sodium fluoride, NaF ≥ 99% | Sigma-Aldrich, Steinheim, Germany |
| Sodium oleate | Sigma-Aldrich, Steinheim, Germany |
| Sodium orthovanadate, $Na_3VO_4$ ≥ 99% | Sigma-Aldrich, Steinheim, Germany |
| Sodium palmitate | Sigma-Aldrich, Steinheim, Germany |
| Streptavidin-HRP | R&D Systems, Minneapolis, Minnesota, USA |
| SYBR® Green Master Mix | Thermo Scientific, Vilnius, Lithuania |
| Tissue-Tek® OCT | Sakura Finetek, California, USA |
| TMB substrate solution | Sigma-Aldrich, Steinheim, Germany |
| Toluidine blue | Sigma-Aldrich, Steinheim, Germany |
| TRI Reagent® | Sigma-Aldrich, Steinheim, Germany |
| Triethylammonium bicarbonate, TEAB | Sigma-Aldrich, Steinheim, Germany |
| TRIS (hydrochloride) | Carl Roth, Karlsruhe, Germany |
| Trypan blue | Sigma-Aldrich, Steinheim, Germany |
| Trypsin (1 µg/µL) | Serva, Heidelberg, Germany |
| Trypsin-EDTA | Sigma-Aldrich, Steinheim, Germany |
| Tween 20 | Sigma-Aldrich, Steinheim, Germany |
| Urea ≥ 99.5% | Sigma-Aldrich, Steinheim, Germany |
| Urea-hydrogen peroxide (tablets) | Carl Roth, Karlsruhe, Germany |
| Water with 0.1% Formic Acid (v/v), Optima LC/MS Grade (Puffer A) | Fisher Scientific, Waltham, Massachusetts, USA |
| ZytoChem Plus HRP One-Step Polymer anti-Mouse/Rabbit/Rat | Zytomed Systems, Berlin, Germany |

## 2.2 Buffers, gels and solutions

Table 2.2: Buffers made in lab and used in this work.

| Buffer | Ingredients | Amount/Concentration |
|---|---|---|
| 10X Laemmli | TRIS-Hydrochloride | 0.184 M |
| pH 8.3 | Glycerine | 1.564 M |
| | SDS | 34.7 mM |
| | Water (de-ionized) | |
| 5X Western blot loading | Stacking gel buffer | 16.4% (v/v) |
| buffer | SDS | 2.06% (v/v) |
| | Bromphenol blue | 2.6% (v/v) |
| | Glycerol | 10% (v/v) |
| | 2- mercaptoethanol | 25% (v/v) |
| | Water (de-ionized) | |
| Main gel buffer | TRIS | 1.5 M |
| pH 8.8 | Water (de-ionized) | |
| Modified RIPA | TRIS-Hydrochloride | 50 mM |
| | NaCl | 150 mM |
| | IGEPAL® | 1% (v/v) |
| | Deoxycholic acid sodium salt | 0,25% (v/v) |
| | EDTA | 1 mM |
| | Aprotinin | 1 µg/mL |
| | Pepastatin A | 1 µg/mL |
| | Leupeptin | 1 µg/mL |
| | PMSF | 1 mM |
| | NaF | 1 mM |
| | $Na_3VO_4$ | 1 mM |
| SP3 lysis buffer | SDS | 5% (w/v) |
| | PBS | |
| Stacking gel buffer | TRIS | 0.5 M |
| pH 6.8 | Water (de-ionized) | |
| Stripping buffer | TRIS | 50 mM |
| | 2-mercaptoethanol | 100 mM |
| | SDS | 2% (v/v) |
| TAE buffer | TRIS | 2 M |
| pH 8 | EDTA | 50 mM |
| | Acetic acid | variable, pH-dependent |
| Tail lysis buffer | TRIS | 100 mM |
| pH 8 | EDTA | 5 mM |

| | | |
|---|---|---|
| | NaCl | 200 mM |
| | SDS | 0.2% (v/v) |
| Towbin buffer | TRIS | 250 mM |
| | Glycin | 1.92 M |
| | Water (de-ionized) | |
| Urea buffer (made by Proteomics core facility, CECAD) | Urea ≥ 99.5% | 8 M |
| | TEAB | 50 mM |

Table 2.3: Gels made in lab and used in this work.

| Gel | Ingredients | Amount |
|---|---|---|
| Agarose gel | Agarose | 1.5% (w/v) |
| | Midori Green | 10% (v/v) |
| | TAE buffer | |
| Main gel (SDS-PAGE) (8% to 12%) | Acrylamide mix (30%) | 27% to 40% (v/v) |
| | Main gel buffer | 25% (v/v) |
| | SDS | 0.1% (v/v) |
| | APS | 0.1% (v/v) |
| | TEMED | 0.04% to 0.06% (v/v) |
| | Water (de-ionized) | |
| Stacking gel | Acrylamide mix (30%) | 5.1% (v/v) |
| | Stacking gel buffer | 13% (v/v) |
| | SDS (10%) | 0.1% (v/v) |
| | APS (10%) | 0.1% (v/v) |
| | TEMED | 0.01% (v/v) |
| | Water (de-ionized) | |

Table 2.4: Solutions made in lab and used in this work.

| Solution | Ingredients | Amount/Concentration |
|---|---|---|
| AdipoRed staining solution | AdipoRed reagent | 0.5% (v/v) |
| | D-PBS | |
| Beta-gal staining solution | X-Gal | 1 mg/mL |
| | Potassium ferricyanide | 5 mM |
| | Potassium ferrocyanide | 5 mM |
| | $MgCl_2$ | 2 mM |
| | PBS (pH 6) | variable amounts |

| | | |
|---|---|---|
| EM fixation solution | Formaldehyde, phosphate-buffered<br>Glutaraldehyde<br>Cacodylate buffer, pH 7.35 | 2% (v/v)<br>2% (v/v)<br>0.1 M |
| Eosin G staining solution | Eosing G-solution 0.5%<br>acetic acid | 200 mL<br>one drop, approx. 50 µL |
| Oil Red O staining solution | Oil Red O<br>2-Propanol | 0.5% (w/v)<br>100 mL |
| PBS-T | PBS<br>Tween20 | 9.55 g/L<br>0.05% (v/v) |
| PCR Mastermix | 5X Flexi Green<br>25 mM $MgCl_2$<br>10 mM dNTP's<br>10 µM oIMR-0212 primer<br>10 µM oIMR-0213 primer<br>10 µM oIMR-0214 primer<br>5 u/µL goTaq DNA polymerase<br>Water (de-ionized) | 4 µL per sample<br>1.6 µL per sample<br>0.4 µL per sample<br>1 µL per sample<br>1 µL per sample<br>1 µL per sample<br>0.2 µL per sample<br>9.8 µL per sample |
| Ponceau S solution | Ponceau S<br>Trichloroacetic acid<br>Water (de-ionized) | 0.2% (w/v)<br>3% (v/v) |
| Pre-perfusion solution | Procaine hydrochloride<br>Heparin<br>Sodium chloride 0.9% solution | 5 g/L<br>2 mL/L |
| TBST<br>pH 7.45 | TRIS<br>NaCl<br><br>Tween20<br>Water (de-ionized) | 0.1 M<br>1 M<br><br>0.1% (v/v) |
| Toluidine blue staining solution | Toluidine blue<br>Water (de-ionized) | 1% (w/v) |

### 2.3 Kits

Table 2.5: Commercial kits used in this work.

| Kit | Company |
|---|---|
| Cell Proliferation ELISA, BrdU | Roche Diagnostics GmbH, Mannheim, Germany |
| IL-6 ELISA kit, EZMIL6 | Merck Millipore, Darmstadt Germany |
| ImmPACT™ DAB Substrate kit | Vector Laboratories, Burlingame, California, USA |
| In Situ Cell Death Detection Kit, Fluorescein, TUNEL kit | Roche Diagnostics GmbH, Mannheim, Germany |
| Lipid Peroxidation (MDA) assay kit | Sigma-Aldrich, Steinheim, Germany |
| Mouse SAA2 (Serum Amyloid A2) ELISA kit, E-EL-M1349 | Elabscience Biotechnology Inc., Houston, Texas, USA |
| Pierce™ BCA Protein Assay Kit | Thermo Scientific, Rockford, Illinois, USA |
| Tyramide SuperBoost™ kit with AlexaFluor™ | Invitrogen, Eugene, Oregon, USA |
| Caspase-GLO® 3/7 Assay Systems assay | Promega, Madison, Wisconsin, USA |

### 2.4 Antibodies

Table 2.6: Antibodies used in this work.

| Antibody | Isotype/species | Company |
|---|---|---|
| BrdU, #5292 | mouse | Cell Signaling Technology |
| Caspase 3, #9661 | rabbit | Cell Signaling Technology |
| CD31, ab28364 | rabbit | Abcam |
| CD45, ab10558 | rabbit | Abcam |
| Cleaved Caspase 3, #9662 | rabbit | Cell Signaling Technology |
| Cy3-conjugated, 111-165-003 (anti-rabbit), 115-165-003 (anti-mouse) | goat | Jackson Immuno Research |
| CyclinD1, ab134175 | rabbit | Abcam |
| DyLight488-conjugated, 115-485-003 (anti-mouse), 111-485-003 (anti-rabbit) | goat | Jackson Immuno Research |
| E-cadherin, #3195 | rabbit | Cell Signaling Technology |
| ERK1/2, #4696 | mouse | Cell Signaling Technology |
| HPRT, ab10479 | rabbit | Abcam |

| | | |
|---|---|---|
| HRP-conjugated anti-mouse IgG, #7076 | horse | Cell Signaling Technology |
| HRP-conjugated anti-rabbit IgG, #7074 | goat | Cell Signaling Technology |
| IL-6, MAB406 | rat | R&D Systems |
| mMR16-1, anti-IL6R | rat | Chugai Pharmaceutical Co. Ltd. |
| PARP, #9542 | rabbit | Cell Signaling Technology |
| P-cadherin, ab190076 | rabbit | Abcam |
| PCNA, M0879 | mouse | DAKO |
| phospho-ERK1/2, #4370 | rabbit | Cell Signaling Technology |
| phospho-S139-γH2A.X, ab11174 | rabbit | Abcam |
| phospho-Stat3, #9145 | rabbit | Cell Signaling Technology |
| phospho-Y654-β-catenin, E-AB-20830 | rabbit | Elabscience, Biozol, Eching, Germany |
| Rat IgG, isotype control, 10700 | rat | Thermo Fisher Scientific |
| SOCS3, ab16030 | rabbit | Abcam |
| Stat3, #9139 | mouse | Cell Signaling Technology |
| VE-cadherin, ab33168 | rabbit | Abcam |
| β-actin, #3700S | mouse | Cell Signaling Technology |
| β-catenin, #8480 | rabbit | Cell Signaling Technology |

## 2.5 Apparatus

Table 2.7: Apparatuses used in this work.

| Apparatus | Software | Company |
|---|---|---|
| BioDoc Analyze | BioDoc Analyze | Biometra, Analytik Jena, Germany |
| BX43F equipped with DP80 dual CCD camera | cellSens Dimension V1.8 | Olympus, Germany |
| ChemiDOC™ XRS+ | ImageLab v5.2.1 | Bio-Rad Laboratories, Munich, Germany |
| Cryostat CM3050 S | - | Leica, Germany |
| EASY nLC 1000 | - | Thermo Scientific™, USA |
| EVOS FL Auto2 | Evos software, Celleste | Thermo Scientific™ Invitrogen™, USA |

| | | |
|---|---|---|
| Fully-enclosed tissue processor ASP300 | Built-in | Leica, Germany |
| GloMax® Multi Detection System | Built-in | Promega, USA |
| Histoscan SCN400 | ImageScope 12.3.3 | Leica, Germany |
| Infinite M200 pro | Tecan i-control 2.0 | Tecan, Austria |
| LMD7000 Leica | AVC Standard | Leica, Germany |
| Meta 510 | Zeiss LSM software | Zeiss, Jena, Germany |
| Microtome RM2 | - | Leica, Germany |
| Mixer mill MM 400 | - | Retsch GmbH, Germany |
| Packard TriCarb 1900 TR Liquid Scintillation Analyzer | Built-in | Perkin Elmer, USA |
| Paraffin embedding module EG1150 H | - | Leica, Germany |
| PCR Biometra Tone | Built-in | Analytik Jena, Germany |
| PerfectBlue blot chamber | - | PeqLab, VWR, Germany |
| Q Exactive Plus Orbitrap | - | Thermo Scientific™, USA |
| Sonopuls HD | - | Bandelin electronic GmbH, Berlin, Germany |
| Steam heater FS 20 | - | Braun, Germany |
| Taqman 7500 | 7500 Software v2.0.6 | AppliedBiosystems, Life Technologies GmbH, Germany |
| TCS SP8 | LAS X | Leica, Germany |

### 2.6 Software

ImageJ-Fiji version 2011 (“Madison”), ImageLab 5.2, GraphPad Prism 6, Microsoft Paint, Omero web v5.4.10, Microsoft Office 2013, QuPath v0.2.0-m8 and EndNote were used for this work.

### 2.7 Animals

In this work, C57BL/6N mice from Janvier Labs, La Genest-Saint-Isle, France were purchased and animal handling and procedures for this work were performed in accordance with German regulations, legal requirements and animal welfare guidelines. Animals were housed at the Department of

Pharmacology, University of Cologne, Germany. The project was approved by local authorities, Landesamt für Natur, Umwelt und Verbraucherschutz, Nordrhein-Westfalen and the Bezirksregierung Köln, Germany under the licenses and identification codes 84-02.04.2014.A057 (project A057, organ harvest at E15.5 and E18.5) and 84-02.04.2016.A046 (project A046, organ harvest at E11.5, E15.5, E18.5, *in vivo* studies at E15.5, mMR16-1 or IgG therapy at E15.5 and interleukin-6 knock-out (IL-$6^{-/-}$) on HFD). IL-$6^{-/-}$ BL/6N mice were generated from B6.129S2-IL6tm1Kopf/J mice [78] purchased from The Jackson Laboratory, Bar Harbor, Maine, USA which were housed in the Center for Molecular Medicine Cologne (CMMC). Since wild type mice for HFD and SD groups were from a BL/6N strain, the B6.129S2-IL6tm1Kopf/J were backcrossed over 10 generations with wild type BL/6N mice. Preferably male IL-$6^{+/-}$ offspring were mated with wild type females and all offspring were genotyped to confirm knock-out of one allele. After 10 generations of backcrossing, IL-$6^{+/-}$ male offspring from one parent pair and IL-$6^{+/-}$ female offspring from another parent pair were mated to generate IL-$6^{-/-}$ animals that were used for experiments and received HFD.

# 3. Methods

The following sections have been partially published in (Appel, Schulze-Edinghausen, Kretschmer et al. 2017 [79], Nüsken et al. 2019 [80], Kretschmer et al. 2020 [81] or in revision for publication by Kretschmer et al. Biology of Reproduction, 2020).

### 3.1 Animal models, handling and *in vivo* studies

In this work, mice were maintained at 20 – 24°C, 45 – 65% humidity, 12 hours light/dark cycles, at a maximum of 4 control diet or 3 HFD mice per cage. Mice either received a control / standard diet (SD, R/M-H, Ssnif®, Soest, Germany) or HFD (C1057 modified, Altromin, Lage, Germany) *ad libitum* from week 3 of age and until the end of experiments, schematized in Figure 3.1.1.1. Mice were considered obese when they reached a body weight of more than 23.5 g. Male mice for mating were received at week 8 of age and kept solely on SD. For mating, one non-obese SD dam lighter than 23.5 g or one obese HFD dam was mated overnight (O/N) for approximately 20 hours, with a male mouse, while further receiving the respective diet *ad libitum*. The next morning was considered as E0.5. Dams were weighed once per week and before the section day to assess pregnancy, together with visual examination of the belly. Several SD and HFD dams (project A046) were allowed to give birth to determine pregnancy duration. Pregnant dams were transferred to the experimentation site at embryonic day E11.5, E15.5 or E18.5 for sacrifice and organ harvest, or at E15.5 for *in vivo* studies with $^{18}$F-FDG or $^{14}$C-mannitol. One and a half hour before sacrifice for organ harvest, dams from A046 projects were injected with 10 mg/mL BrdU dissolved in D-PBS. For *in vivo* studies and sacrifice for organ harvest, dams from A046 projects received subcutaneously 0.1 mg/kg bodyweight buprenorphine dissolved in sodium chloride 0.9% solution 30 minutes prior to sacrifice. For organ harvest, mice were euthanized under $CO_2$ and subsequently blood was drawn by cardiac puncture. The body was then opened along the linea alba to perform a caesarian section and retrieve the feto-placental units. Additionally, epigonadal white adipose tissue (egWAT) and other organs were collected by one dissector and egWAT weight as well as number of alive and resorbed fetuses were documented. At the same time, fetuses were removed, decapitated, weighed (only E15.5 and E18.5 fetuses) and collected by another dissector. Next, placentas were removed, weighed (if collected in total and removed of amniotic and uterus tissue for biochemical analysis) and collected. Some placentas were cut in halves and one of the resulting halves was either embedded in Tissue-Tek® OCT on dry ice or fixed in 4% (v/v) formaldehyde O/N. From the other placenta half, amnion sac and connective tissue were carefully removed and this half was snap frozen in liquid nitrogen. Placentas for stereological analysis were removed as a whole, thus undamaged with parts of the uterus and attached tissues, and immediately fixed in formaldehyde. After formaldehyde fixation, organs were stored for at least one additional night in 70% (v/v) 2-propanol in de-ionized water before paraffin-embedding in an ASP300.

### 3.1.1 *In vivo* studies involving radioactive tracers $^{18}$F-FDG and $^{14}$C-mannitol

For *in vivo* studies, pregnant dams were transferred to the experimentation site at E15.5 under adequate transportation conditions. Positron emission tomography (PET) was performed at the Department of Nuclear Medicine, University Hospital of Cologne with the help and under the supervision of PD Dr. Heike Endepols. Dams were put under general anesthesia using isoflurane inhalation (1,5 – 5% isoflurane, 30% $O_2$ and up to 70% medicinal air) which took place 30 minutes after dams received subcutaneously 0.1 mg/kg bodyweight buprenorphine dissolved in sodium chloride 0.9% solution. Mice were kept on warm plates (37°C), breathing was visually controlled and Bepanthen® was applied to the eyes. Starting with the injection of 125 µL with 10 MBq $^{18}$F-FDG dissolved in 125 µL sodium chloride 0.9% solution via a tail vein catheter and subsequent scanning for 60 minutes. After the emission scan, a transmission scan with a $^{57}$Co point source was performed for attenuation correction. Afterwards, the tail vein catheter was removed while a tourniquet was gently applied to the base of the tail. The resulting drop of blood was used to determine blood glucose concentration of dams. After the procedure, dams were allowed to wake up and afterwards were kept in their cages for 24 hours to achieve almost complete decay of $^{18}$F-FDG which has a half-life time of ~110 minutes [82]. On the next day, dams were injected with buprenorphine as described above, euthanized by $CO_2$ inhalation and the fetuses were subsequently removed and decapitated.

For $^{14}$C-mannitol clearance experiments, dams were relocated to the isotope laboratory of the CMMC and handled and anesthetized as described above. A similar procedure was performed as described by Sibley [83]. During the procedure, the jugular vein was exposed and injected with 100 µL of 3.5 µCi of $^{14}$C-mannitol. Roughly 3 minutes after injection, the animal was opened along the linea alba to expose the uterus and access the inferior vena cava from which blood was drawn 4 to 4.5 minutes after tracer injection. Subsequently, feto-placental units were collected, viable and resorbed fetuses counted and each decapitated fetus and placenta was weighed. Next, placentas were discarded and fetuses were minced in biosol at 56°C O/N. On the next day, 10 mL of scintillation liquid was added to 100 µL of maternal serum and to each dissolved fetus. Both were put in a Packard TriCarb 1900 TR Liquid Scintillation Analyzer for beta decay counting. Materno-fetal clearance ($K_{mf}$) expressed as µL per minute per gram of placenta was calculated from collected data on beta decay in maternal serum and minced fetuses.

### 3.1.2 mMR16-1 and IgG interventions

The antibody mMR16-1, a mousenized anti-IL-6R antibody, was kindly provided by Chugai Pharmaceutical Co. Ltd. (Japan), and used according to manufacturer's suggestions and agreement. HFD dams were injected intraperitoneally (i.p.) with concentrations of antibody as suggested by Chugai Pharmaceutical and as reported by Wu et al. [84] of 25 mg/kg bodyweight of mMR16-1 at E0.5, E7.5 and E14.5 or 10 mg/kg bodyweight of rat IgG isotype control (IgG) antibody to investigate the effect of IL-6 signaling blockade. Pregnant dams were sacrificed at E15.5 after injection of BrdU and buprenorphine, and organs were collected, as described above.

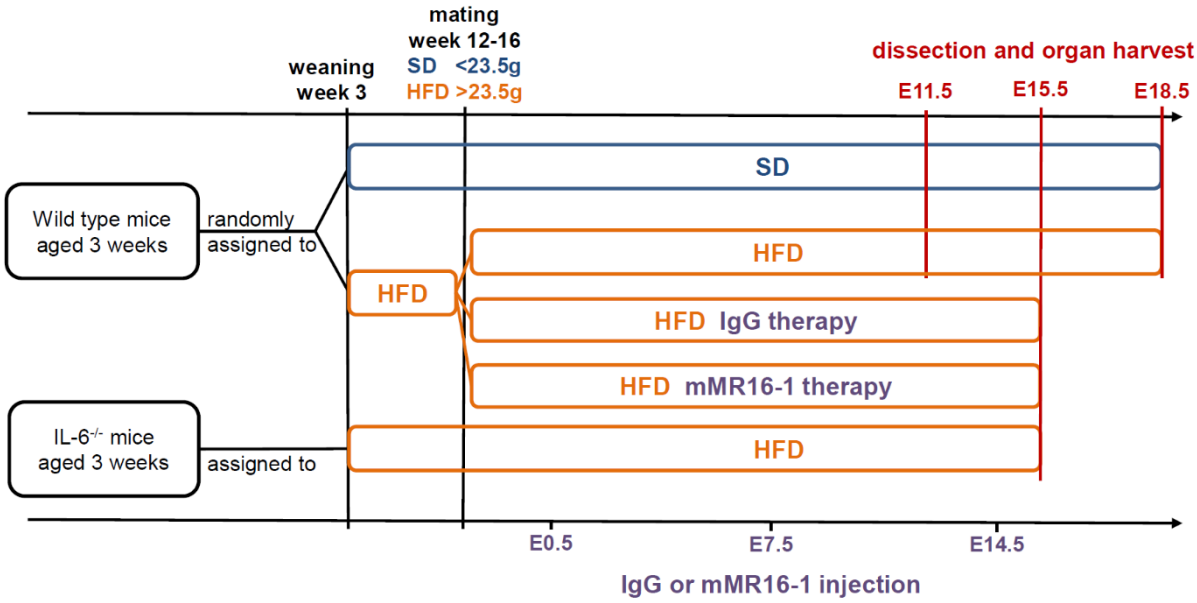


**Figure 3.1.1.1: Mouse model and interventions used in this work.** C57BL/6N wild type mice were randomly assigned to SD or HFD after weaning at the age of 3 weeks. Mice were mated at an age of 12 to 16 weeks. When obese (body weight > 23.5 g), HFD mice were mated and afterwards for several mice mMR16-1 therapy or control IgG therapy were conducted by injections on E0.5, E7.5 and E14.5. SD and HFD dams were dissected at E11.5, E15.5 and E18.5 to retrieve blood and organs (placentas, egWAT, etc.). Several SD and HFD dams were allowed to give birth to determine pregnancy duration. Further, mMR16-1, IgG and IL-$6^{-/-}$ mice were dissected only at E15.5. IL-$6^{-/-}$ mice received HFD after weaning and when obese, they were mated and were dissected only at E15.5 to collect blood and organs (placentas, egWAT, etc.).

### 3.2 Histochemical, immunohistochemical and immunofluorescence methods

The microscopic analysis of tissues and organs requires the segmentation of these biological specimens in micrometer-thin sections. The staining of such sections enables detection of structures and, when using epitope-specific antibodies, even the identification of many (macro-)molecules, such as proteins [85]. As mentioned above, organs and tissues gathered for this work were embedded either in Tissue-Tek®OCT or in paraffin after dissection from animals. Paraffin-embedded tissues were molded in blocks on a heated EG1140 H and, after hardening, were sectioned on a RM2 microtome at various thicknesses, i.e. 7 µm for stereology immunohistochemistry (IHC), 5 µm for other IHC, or 3 µm for immunofluorescence (IF). For stereology IHC [81], the tissue blocks were exhaustively sectioned and a random section between the first 40 sections was determined. This random section and the following 2 sections comprised one interval, and every 40$^{th}$ following section of this interval were also collected, e.g. sections 17, 18, and 19 (interval 1), then sections 57, 58, and 59 (interval 2), then sections 97, 98, and 99 (interval 3), and so on until the placenta was completely sectioned. One section from interval 1 and all 40$^{th}$ consecutive sections, e.g. sections 17, 57, 97, etc., were stained by hematoxylin and eosin. Another section from the first interval and all 40$^{th}$ consecutive sections, e.g. sections 18, 58, 98, etc., were stained by IHC with CD31 primary antibody. The use of IHC protocols permits the specific identification and localization of epitopes bound by a primary antibody. Staining signals originate after incubation with a secondary antibody conjugated with a horseradish peroxidase (HRP) that catalyzes

the specific reaction of DAB to a brown-colored staining product at the site of reaction which is thus specific to the primary antibody. Staining protocols for histochemical, IHC or IF of paraffin-embedded sections always comprised de-waxing in 3 changes of NeoClear® for 15 minutes, 1 change of each 100%, 96%, 80%, 70% ethanol and de-ionized water for 1 minute each. Subsequently, re-hydrated sections were either subjected to a) hematoxylin staining (histochemistry) or b) heat-induced epitope retrieval (HIER) for IHC and IF. For a) hematoxylin staining, sections were incubated in Mayer's hematoxylin for 5 minutes, rinsed in de-ionized water, blued under running tap water for 10 minutes and rinsed again in de-ionized water. Afterwards, eosin staining was performed in eosin G staining solution for 2 minutes. Slides were then rinsed in de-ionized water twice and de-hydrated in ascending concentrations of ethanol (70 – 100%) for 1 minute each. Lastly, slides were kept in 2 changes of NeoClear® for 5 minutes each and were mounted in NeoMount®. Sections that received b) HIER for 25 minutes in citrate buffer pH 6 were subsequently cooled for at least 30 minutes. Tissues on the slides were outlined with a hydrophobic pen, rinsed in PBS-T and blocked in urea-hydrogen peroxide (1 tablet per 5 mL) for 10 minutes. Urea-hydrogen peroxide was discarded and slides were then incubated with Sea Blocking buffer for 1 hour. Sea Blocking buffer was discarded and primary antibody (Table 3.1) was incubated O/N at 4°C. Next, sections were washed for 5 minutes in PBS-T, 3 changes, and ZytoChem Plus HRP One-Step Polymer anti-Mouse/Rabbit/Rat was incubated subsequently for 30 minutes at room temperature (R/T). Sections were then washed in PBS-T and treated with ImmPACT™ DAB substrate according to manufacturer instructions. Reactions were stopped by immersing sections in de-ionized water. Then, sections were counterstained with Mayer's hematoxylin for 2 minutes, rinsed in de-ionized water and put under running tap water for 10 minutes. After a rinse in de-ionized water, sections were de-hydrated in ascending concentrations of ethanol, kept in NeoClear® and mounted in NeoMount® as described above.

Table 3.1: Antibody dilutions used in this work for IHC and IF.

| Antibody | IHC/IF | Dilution (in antibody diluent) |
|---|---|---|
| BrdU | IF | 1:1000 |
| CD31 | IHC & IF | 1:300 |
| CD45 | IHC | 1:2000 |
| Cy3-conjugated | IF | 1:400 |
| DyLight488-conjugated | IF | 1:400 |
| E-cadherin | IHC & IF | 1:1000 (IHC), 1:100 (IF) |
| HRP-conjugated-goat anti-rabbit (Tyramide SuperBoost™) | IF | 1:500 |
| Laminin$\gamma$1 | IF | 1:100 |
| P-cadherin | IHC & IF | 1:1000 (IHC), 1:100 (IF) |
| VE-cadherin | IHC & IF | 1:1000 (IHC), 1:100 (IF) |
| $\beta$-catenin | IHC & IF | 1:200 (IHC), 1:100 (IF) |
| $\gamma$H2A.X | IF | 1:4000 |

IF was performed on sections close to the placental mid-line where the cord was present and sections were treated similarly to b) HIER. Briefly, after urea-hydrogen peroxide treatment, sections were incubated with 300 mM glycine in de-ionized water for 30 minutes before Sea blocking for 1 hour. Primary antibodies (Table 3.1) were incubated O/N at 4°C. Then, sections were washed 3 times in PBS-T for 5 minutes and the secondary antibody was applied for 1 hour, i.e. either a Cy3-conjugated, DyLight488-conjugated, or HRP-conjugated-goat anti-rabbit from Tyramide SuperBoost™ kit according to manufacturer instructions. Afterwards, sections were washed in PBS-T and Tyramide SuperBoost™ (Table 2.5) treated sections were further treated with working solution and stop solution. For multiplexing, Tyramide SuperBoost™ treated sections were again subjected to HIER, blocking, primary and secondary antibody incubation as described above. Note that multiplexing with primary antibodies of different host species, e.g. rabbit and mouse, was performed without the use of Tyramide SuperBoost™ secondary antibodies, but utilized a Cy3-cunjugated secondary antibody against rabbit and a DyLight488-conjugated secondary antibody against mouse or vice versa. Sections were subsequently washed in PBS-T and nuclear-counterstained with DAPI (1:1000 in antibody diluent). Lastly, sections were washed in PBS-T, rinsed in de-ionized water and mounted using Fluoromount™.

Since paraffin-embedding disposes tissues of lipids that were once inside tissues and cells, histochemical staining protocols for lipids, such as Oil Red O staining, are best performed on native tissue [85]. To this end, placentas were embedded in Tissue-Tek® OCT immediately after dissection, stored at -80°C and sectioned on a Cryostat CM3050 S. For Oil Red O, 5 µm thick non-consecutive sections were prepared, transferred on dry ice and fixed promptly in -20°C cold methanol for 1 minute. After a short rinse in de-ionized water, sections were treated with 60% (v/v) 2-propanol in de-ionized water for 5 minutes at R/T and were subsequently stained in Oil Red O staining solution for 20 minutes at R/T. Sections were then rinsed twice in de-ionized water and counterstained with Mayer's hematoxylin as described above before mounting with Fluoromount™. Sections were scanned on a Histoscan SCN400.

### 3.2.1 Quantitation of IHC and IF stained sections

The analysis and quantitation of IHC and IF stained tissue sections was performed by blinded investigators to avoid bias.

CD45-IHC stained placental and egWAT sections were counted as follows: three or five randomly chosen pictures of 343.43 µm by 258.59 µm from placental or egWAT sections, respectively, were used for CD45-positive cell counting. Cells were counted in ImageJ Fiji using the cell counter tool. Positive cell counts were normalized to the tissue area analyzed and expressed as positive cells per $mm^2$. Five sections from independent dams per group were stained and analyzed.

To quantify IF stained BrdU, γH2A.X, TUNEL-positive and EC nuclei in placental sections, scanned sections were divided in 10 equally sized frames and 3 frames were manually counted using the cell counter tool in ImageJ Fiji. The first frame that was counted originated close to the middle section of the Lz, the second frame lied on the distal end of the Lz and the third frame lied in between the other 2

frames, schematized in Figure 3.2.1.1. Total cell nuclei number per frame was automatically counted in the DAPI channel by Fiji using particle analysis. Positive cell counts were normalized to the total number of cell nuclei for CD31 stained EC and expressed as percentage of positive cells. Typically, 6 to 7 sections from independent dams per group were analyzed.

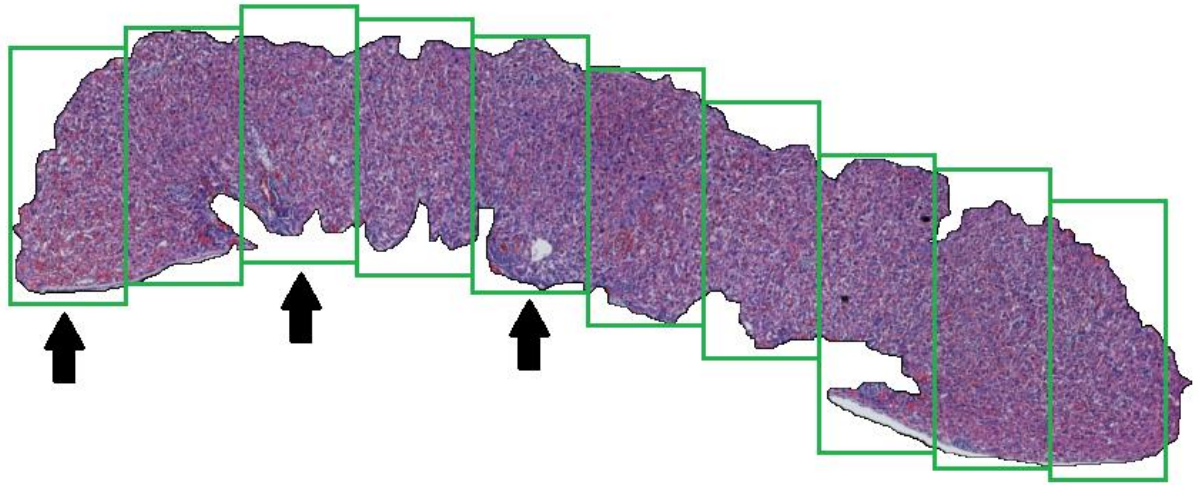

**Figure 3.2.1.1: Scheme of framing for cell counting analysis of placenta Lz.** This example of a hematoxylin and eosin stained placenta visualizes the frame segmentation by 10 equally sized green rectangles of the Lz, of which 3 were chosen for cell counting, indicated by black arrows. One frame is on the distal end, one frame is in the center of the Lz and the third lies between those other two. For better visualization, a hematoxylin and eosin stained placenta is shown, however the framing was applied in the same way on IF stained sections for cell counting.

### 3.2.2 Quantitation of Oil Red O sections

Analysis of scanned Oil Red O stained sections was done with QuPath. Using unstained and Oil Red O stained placental tissue regions virtually extracted from multiple sections, a random forest pixel classifier was trained to predict positive and negative pixels. The labyrinth zone was manually annotated in each section and afterwards the classifier was used to detect Oil Red O positive pixels. Subsequently, stain-positive area fraction per section was calculated and normalized to total placenta area. During the procedure, the investigator was blinded for sample affiliation.

## 3.3 Stereological analysis of the placenta

The three-dimensional (3D) properties of tissues and organs can be estimated by calculating these 3D-properties from 2D-histo sections [86]. To this end, placentas and adjacent tissue were stained as mentioned above. After sections were digitalized on a Histoscan SCN400, they were processed into 4096 by 4096 pixel tiles with a scale of 3.96 µm/pixel. Line and point grids were superimposed on these tiles and points falling on placental strata, i.e. labyrinth zone (Lz), junctional zone (Jz), decidua or chorionic plate, as well as fetal capillary profiles and intersections of a line with fetal capillaries (FC) or maternal blood sinuses (MBS) were counted in ImageJ Fiji (see Figure 4.2.2.2 and Figure 4.3.5.1).

Densities of volumes, surface area and others were calculated using the following equations published by Coan [24]:

$$V_{(Obj)} = t \times a_{(p)} \times \Sigma P \quad (1)$$

$$S_{(structure)} = (2 \times \Sigma I_{(structure)}/I_{(p)} \times \Sigma P_{(reference)}) \times V_{(reference)} \quad (2)$$

$$V_{v(struc,ref)} = P_{(struc)}/P_{(total)} \quad (3)$$

$$L_{V(cap)} = 2Q_A \quad (4)$$

$$d = 2[(V_{V(struc)}/L_{V(cap)})/\pi]^{1/2} \quad (5)$$

Where $V_{(Obj)}$ equals the assumed placental volume, t is the number of sections multiplied by their thickness, $a_{(p)}$ is the area attributed to a grid point, $\Sigma I_{(structure)}$ equals the sum of intersections of the line with the structure (MBS or FC), $\Sigma P_{(reference)}$ is the total number of points on the Lz, $I_{(p)}$ equals the length of the line associated with each grid point, $V_{v(struc,ref)}$ denotes the volume fraction of a placental stratum (e.g. Lz, Jz) within the placental reference space, $P_{(struc)}$ equals the number of points attributed to the stratum and $P_{(total)}$ is the number of points falling on the reference structure, i.e. the placenta, and the respective stratum, $Q_A$ represents the numerical density of capillaries per unit area of Lz, $L_{V(cap)}$ is the length density of fetal capillaries, and d represents the mean diameter of these capillaries. The calculated values were then multiplied by the absolute placental volume to generate absolute quantities. Values were further weight-averaged for each placenta [81].

### 3.4 Laser-capture microdissection and proteomics profiling

The placental halves embedded in Tissue-Tek® OCT were further used to generate 16 µm thick placental sections which were transferred onto PEN-Membrane slides for laser-capture microdissection (LCM). This procedure utilizes a LMD7000 microscope equipped with a laser that can be controlled to dissect specific fractions of a tissue section. To differentiate between placental Lz which was aimed to collect by LCM and other placental zones, sections were stained with toluidine blue. In brief, sections were first fixed in 70% (v/v) ethanol in de-ionized water supplemented with cOmplete EDTA-free Protease Inhibitor Cocktail at 4°C for 1 minute. Subsequently, sections were rinsed in de-ionized water and stained in toluidine blue for 1 minute followed by a rinse in de-ionized water and 70% (v/v) ethanol. Sections were then dried for at least 1 hour at R/T before LCM was performed [80]. The settings used on the LMD7000 for dissection can be found in Table 3.2. During LCM, between 8 and 12 mm² of dissected placental tissues were collected from 3 sections per placenta, 5 placentas per group, 1 placenta per dam. After collection, SP3 lysis was performed as described by Hughes [87]. In brief, SP3 buffer was added to each tube at a volume similar to the volume of collected placental tissue. Samples were then heated at 95°C for 10 minutes and chromatin degraded in a Diagenode Bioruptor for 10 minutes (cycle 30/30 seconds) at R/T. Afterwards, DTT was added to a final concentration of 5 mM, vortexed and incubated for 30 minutes at 55°C. Then, CAA was added to a final concentration of

40 mM, vortexed and incubated for 30 minutes in the dark at R/T. Samples were frozen at -20°C until mass spectrometry and proteomics data analysis by the staff of the CECAD Proteomics Facility.

Table 3.2: Settings on LMD7000 for LCM of placental sections.

| | |
|---|---|
| Power | 16 – 18 |
| Aperture | 20 |
| Velocity | 7 |
| Specimen Balance | 23 |
| Head Current | 100% |
| Pulse Frequency | 201 |

### 3.4.1 Mass Spectrometry

To analyze samples, Q Exactive Plus Orbitrap (Thermo Scientific) mass spectrometer coupled to an EASY nLC 1000 (Thermo Scientific) was used. Peptides were loaded with solvent A (0.1% (v/v) formic acid in de-ionized water) onto an in-house packed analytical column (50 cm — 75 µm I.D., filled with 2.7 µm Poroshell EC120 C18, Agilent). Chromatographical separation of peptides was done at a constant flow rate of 250 nL/minute with the following gradient: 3 – 5% solvent B (0.1% formic acid in 80% acetonitrile) within 1.0 minute, 5 – 30% solvent B within 119.0 minutes, 30 – 50% solvent B within 19.0 minutes, 50 – 95% solvent B within 1.0 minute, followed by washing and column equilibration. The mass spectrometer was set to data-dependent acquisition mode. The MS1 survey scan was acquired from 300 – 1750 m/z at a resolution of 70,000. Isolation of the top 10 most abundant peptides was done within a 2.1 Th window and peptides were subjected to HCD fragmentation at a normalized collision energy of 27%. A maximum injection time of 60 milliseconds was applied, as the AGC target was set to 5e5 charges. Product ions were detected at a resolution of 17,500 in the Orbitrap. Dynamic exclusion of precursors was set for 25.0 seconds [80].

### 3.4.2 Proteomics data analysis

Maxquant (version 1.5.3.8) with default parameters was utilized to process raw data from mass spectrometry. Briefly, MS2 spectra were searched against the Uniprot MOUSE.fasta database with a list of common contaminants included. False discovery rates (FDR) on protein and PSM level were estimated by the target-decoy approach to 1% (Protein FDR) and 1% (PSM FDR), respectively. A minimal peptide length of 7 amino acids was set and carbamidomethylation at cysteine residues was considered as a fixed modification. Oxidation (M) and Acetyl (Protein N-term) were included as variable modifications. The match-between runs option was enabled. LFQ quantification was enabled using default settings. Further analysis was carried out with Perseus (version 1.5.5.3). Briefly, LFQ values were log2-transformed, and proteins flagged as “potential contaminants”, “reverse” and “only identified by site” were removed from the data set. Only proteins which have been quantified in all samples were retained after filtering the data. A two-sample Student’s *t* test was used to determine statistically significant changes [80].

### 3.5 Electron microscopy

To obtain placentas for electron microscopy, pregnant dams were perfusion fixated at E15.5. First, dams were injected subcutaneously with 0.1 mg/kg bodyweight buprenorphine dissolved in sodium chloride 0.9% solution 30 minutes prior to perfusion. Then, perfusion was performed in deep isoflurane anesthesia as mentioned above under 3.1.1. The animal was opened along the linea alba, the uterus was carefully placed outside the belly to ensure perfusion of uterine vessels, and the heart was exposed by incision of the thorax and removal of several ribs. A cannula was carefully inserted into the left ventricle while pre-perfusion solution (Table 2.4) was running which was placed about 1.2 m above the animal. Once the cannula was placed, this solution ran for 2 minutes after which it was switched to formaldehyde Roti®-Histofix 4% for another 10 minutes. Successful fixation was determined by inspecting the liver, which appeared light brown, and a kidney, which appeared pale with dark stains. Next, uteri and feto-placental units were removed to collect placentas. These were cut in 2 mm by 2 mm by 2 mm sized tissue cubes from the center of the organ and transferred into EM fixation solution for 4 hours at 4°C. Afterwards, tissues were transferred to 10X D-PBS until epon-embedding by Mojgan Ghilav of the Research Group of Prof. Wilhelm Bloch, at the Department of Molecular and Cellular Sports Medicine, Institute of Cardiovascular Research and Sports Medicine, German Sport University Cologne, Cologne, Germany. Mrs. Ghilav also prepared semi- and ultra-thin sections for EM at the Department of Anatomy I, Faculty of Medicine and University Hospital Cologne, University of Cologne, Cologne, Germany, which was performed by Tim van Beers.

### 3.6 Protein isolation and detection

Approximately 25 mg of placental tissue, that was snap frozen in liquid nitrogen after dissection, was manually ground using a 1.5 mL-reaction tube mortar in modified RIPA buffer. Lysed tissues were kept on ice and were sonicated for 20 seconds at 50% energy and 3 × 10% cycle on a Sonopuls HD, then incubated on ice for 1 hour and subsequently centrifuged at 18,500 g for 5 minutes at 4°C. Supernatants were collected and protein concentration was determined using Pierce™ BCA Protein Assay kit according to manufacturer instructions on an Infinite M200 pro at 562 nm. For protein detection, 20 to 30 µg of protein was added to 5X western blot loading buffer and de-ionized water and separated on 8% to 12% acrylamide SDS-PAGE under reducing conditions, followed by transfer onto a nitrocellulose membrane by blotting for 2 hours at 1.3 mA/cm$^2$, and at R/T using Towbin buffer. After blotting, membranes were shortly rinsed in de-ionized water and stained for 2 minutes in Ponceau S solution. Afterwards, membranes were washed 3 times in TBST and were blocked with 2% BSA, 5% non-fat dry milk powder (w/v) in TBST for 1 hour on a shake plate at R/T. Next, membranes were incubated with primary antibodies for 30 minutes at R/T followed by incubation O/N at 4°C. On the next day, membranes were washed 3 times for 7 minutes in TBST and secondary antibodies against primary antibody species were applied for 1 hour at R/T. Membranes were washed in TBST and subsequently incubated for detection with ECL for 1 minute. Images were taken on a ChemiDoc XRS+. From those images, densitometric analysis was performed using ImageLab software.

### 3.7 Enzyme-linked immunosorbent assays of serum proteins

#### 3.7.1 IL-6 ELISA

The concentration of IL-6 in undiluted maternal serum from E15.5 was measured by IL-6 ELISA kit EZMIL6. Manufacturers' protocols were followed to perform IL-6 ELISA. Plates were read on an Infinite M200 pro at the respective wavelengths.

#### 3.7.2 Serum amyloid A2 (SAA2) ELISA

SAA2 concentration was measured in undiluted maternal serum, from E15.5 dams from which received i.p. injections of mMR16-1 or IgG, by mouse SAA2 ELISA kit in animals. The ELISA was performed according to manufacturer instructions and plates were read on an Infinite M200 pro at the respective wavelengths.

### 3.8 Genotyping

Table 3.3: Genotyping primers used in this work

| Name | Type | Sequence | Company |
|---|---|---|---|
| oIMR0212 | Primer (common) | 5'-TTCCATCCAGTTGCCTTCTTGG-3' | Eurofins Genomic |
| oIMR0213 | Primer (wild type reverse) | 5'-TTCTCATTTCCACGATTTCCCAG-3' | Eurofins Genomic |
| oIMR0214 | Primer (mutant reverse) | 5'-CCGGAGAACCTGCGTGCAATCC-3' | Eurofins Genomic |

#### 3.8.1 DNA extraction

Backcrossing of B6.129S2-IL6tm1Kopf/J IL-$6^{+/-}$ to BL/6N background with BL/6N IL-6 wild type mice required genotyping of offspring before weaning in order to select IL-$6^{+/-}$ offspring for subsequent backcrossing. To this end, ear tags from 3 week old mice were collected and lysed in 500 µL tail lysis buffer pH 8 supplemented with 5 µL Proteinase K per sample O/N at 55°C on a shake plate. Next, 500 µL of 2-propanol was added and incubated for 10 minutes at R/T after which samples were centrifuged at 20,000 g for 15 minutes at 4°C. Supernatant was removed and the DNA-pellets washed with 500 µL of 70% ethanol of -20°C before repeating centrifugation for 10 minutes. Again, supernatant was removed and the DNA-pellets were air-dried for 1 hour before adding 50 µL de-ionized water and vortexing thoroughly. Samples were kept at 4°C from that point on.

#### 3.8.2 PCR and agarose gel electrophoresis

First, an adequate amount of PCR mastermix was made with specific primers (Table 3.3). After mixing, 1 µL of extracted DNA was added to 19 µL PCR mix. Reaction tubes were placed in a PCR Cycler Biometra Tone and the protocol from Table 3.4 was applied.

Table 3.4: Steps in the PCR cycling program

| Step | | Time | Temperature |
|---|---|---|---|
| Denaturation | | 3 minutes | 94°C |
| 36 cycle | Denature | 30 seconds | 94°C |
| | Anneal | 1 minute | 62°C |
| | Extend | 1 minute | 72°C |
| Extension | | 10 minutes | 72°C |
| Cool and hold | | indefinitely | 4°C |

For gel electrophoresis, a 1.5% agarose gel was made with Midori Green. Then, samples were added and the electrophoresis was run at 110 V. The gel was removed and imaged on a BioDoc Analyze. An example of genotyping can be found in Appendix 6.1 (Figure 6.1.1).

### 3.9 Real-Time Quantitative Polymerase Chain Reaction (RT-qPCR)

#### 3.9.1 qPCR oligonucleotides

Table 3.5: Oligonucleotides used in this work. IL6 and TNFα primer have been published elsewhere [79, 88], MCP1 to CAT primer have been published elsewhere [79].

| Name | Type | Sequence | Company |
|---|---|---|---|
| E-cadherin (*CDH1*) | Forward primer | 5'-CAGTCATAGGGAGCTGTCTACCAAA-3' | Eurofins Genomics |
| | Reverse primer | 5'-GGGTACACGCTGGGAAACAT-3' | |
| | Taqman probe | 5'-CACCACCACCGCGACCCTGC-3' | |
| P-cadherin (*CDH3*) | Forward primer | 5'-GACATGGATGGAGAGGGCTCTA-3' | Eurofins Genomics |
| | Reverse primer | 5'-CTCATACTTCTGCGGCTCAAACT-3' | |
| | Taqman probe | 5'-CCTTGATGCCAACGATAACGCTCCG-3' | |
| VE-cadherin (*CDH5*) | Forward primer | 5'-TGGCCAAAGACCCTGACAAG-3' | Eurofins Genomics |
| | Reverse primer | 5'-TCGGAAGAATTGGCCTCTGT-3' | |
| | Taqman probe | 5'-CTCAGCGCAGCATCGGGTACTCCAT-3' | |
| β-catenin (*CTNNB1*) | Forward primer | 5'-GGACGTTCACAACCGGATTG-3' | Eurofins Genomics |
| | Reverse primer | 5'-GGACCCCTGCAGCTACTCTTT-3' | |
| | Taqman probe | 5'-CCATTGTTTGTGCAGTTGCTTTATTCTCCC-3' | |
| β-actin (*ACTB*) | Forward primer | 5'-TGACAGGATGCAGAAGGAGATTACT-3' | Eurofins Genomics |
| | Reverse primer | 5'-GCCACCGATCCACACAGAGT-3' | |
| | Taqman probe | 5'-ATCAAGATCATTGCTCCTCCTGAGCGC-3' | |
| HPRT (*HPRT1*) | Forward primer | 5'-TGGCCATCTGCCTAGTAAAGCT-3' | Eurofins Genomics |
| | Reverse primer | 5'-TAGGCTCATAGTGCAAATCAAAAGTC-3' | |
| | Taqman probe | 5'-TTTTTAGAAATGTCAGTTGCTGCGTCCCC-3' | |

| | | | |
|---|---|---|---|
| GAPDH | Forward primer | 5'-ATGTGTCCGTCGTGGATCTGA-3' | Eurofins Genomics |
| | Reverse primer | 5'-TGCCTGCTTCACCACCTTCT-3' | |
| | Taqman probe | 5'-CCGCCTGGAGAAACCTGCCAAGTATG-3' | |
| IL6 | Forward primer | 5'-ACAAAGCCAGAGTCCTTCAGAGA-3' | Eurofins Genomics |
| | Reverse primer | 5'-CACTCCTTCTGTGACTCCAGCTTA-3' | |
| | Taqman probe | 5'-AGTCCTTCCTACCCCAATTTCCAATGCTC-3' | |
| TNFα | Forward primer | 5'-GGCTGCCCCGACTACGT-3' | Eurofins Genomics |
| | Reverse primer | 5'-GACTTTCTCCTGGTATGAGATAGCAA-3' | |
| | Taqman probe | 5'-CCTCACCCACACCGTCAGCCG-3' | |
| MCP1 | Forward primer | 5'-GGCTCAGCCAGATGCAGTTAAC-3' | Eurofins Genomics |
| | Reverse primer | 5'-CTTGGTGACAAAAACTACAGCTTCTT-3' | |
| | Taqman probe | 5'-CCCCACTCACCTGCTGCTACTCATTCA-3' | |
| CXCL1 | Forward primer | 5'-AGACCATGGCTGGGATTCAC-3' | Eurofins Genomics |
| | Reverse primer | 5'-AGCCTCGCGACCATTCTTG-3' | |
| | Taqman probe | 5'-CTGCACCCAAACCGAAGTCATAGCCAC-3' | |
| CXCL10 | Forward primer | 5'-CATCCCTGCGAGCCTATCC-3' | Eurofins Genomics |
| | Reverse primer | 5'-CCCTTTTAGACCTTTTTTGGCTAA-3' | |
| | Taqman probe | 5'-CCCACGTGTTGAGATCATTGCCACG-3' | |
| IL1A | Forward primer | 5'-TGGCAACTCCTTCAGCAACA-3' | Eurofins Genomics |
| | Reverse primer | 5'-TCGGGAGGAGACGACTCTAAATA-3' | |
| | Taqman probe | 5'-TCAGATTCACAACTGTTCGTGAGCGCTC-3' | |
| IL1B | Forward primer | 5'-TGACAGTGATGAGAATGACCTGTTC-3' | Eurofins Genomics |
| | Reverse primer | 5'-GGACAGCCCAGGTCAAAGG-3' | |
| | Taqman probe | 5'-ACCCCAAAAGATGAAGGGCTGCTTCC-3' | |
| CYBA | Forward primer | 5'-CGTCTGGCCTGATTCTCATCA-3' | Eurofins Genomics |
| | Reverse primer | 5'-GATAGAGTAGGCGCCGAAATACC-3' | |
| | Taqman probe | 5'-CATCGTGGCTACTGCTGGACGTTTCAC-3' | |
| CYBB | Forward primer | 5'-CCCAACTGGGATAACGAGTTCA-3' | Eurofins Genomics |
| | Reverse primer | 5'-TCAGGGCCACACAGGAAAAC-3' | |
| | Taqman probe | 5'-ACCATTGCAAGTGAACACCCTAACACCACA-3' | |
| NCF1 | Forward primer | 5'-CACCTTCATTCGCCATATTGC-3' | Eurofins Genomics |
| | Reverse primer | 5'-ACAGGTCCTGCCACTTAACCA-3' | |
| | Taqman probe | 5'-CATCCCCAGCCAGCACTATGTGTACATGT-3' | |
| NCF2 | Forward primer | 5'-CCGATATTCCACCACCTCCTAA-3' | Eurofins Genomics |
| | Reverse primer | 5'-CATAGGCACGCTGAGCTTCA-3' | |
| | Taqman probe | 5'-TCACCAGGTCACAAGCAAAAAGAGCCC-3' | |
| NOX4 | Forward primer | 5'-GAAGGTCCCTAGCAGGAGAACA-3' | Eurofins Genomics |
| | Reverse primer | 5'-ACTGAAAAGTTGAGGGCATTCAC-3' | |
| | Taqman probe | 5'-TCTCAGGTGTGCATGTAGCCGCCC-3' | |
| GPX | Forward primer | 5'-GACACCAGGAGAATGGCAAGA-3' | Eurofins Genomics |
| | Reverse primer | 5'-TTCTCACCATTCACTTCGCACTT-3' | |
| | Taqman probe | 5'-TGAATTCCCTCAAGTACGTCCGACCTGG-3' | |

| | | | |
|---|---|---|---|
| SOD | Forward primer | 5'-GTACCAGTGCAGGACCTCATTTTA-3' | Eurofins Genomics |
| | Reverse primer | 5'-GTCTCCAACATGCCTCTCTTCAT-3' | |
| | Taqman probe | 5'-CTCACTCTAAGAAACATGGTGGCCCGG-3' | |
| CAT | Forward primer | 5'-CCATCCTTTATCCATAGCCAGAA-3' | Eurofins Genomics |
| | Reverse primer | 5'-GAATCCCTCGGTCACTGAACAA-3' | |
| | Taqman probe | 5'-TCGTCCCGAGTCTCTCCATCAGGTTTCT-3' | |

### 3.9.2 RNA isolation

Approximately 100 mg of snap frozen tissue, stored at -80°C, was added to 1.5 mL TRI Reagent® and homogenized in a Mixer mill MM 400 at 30 Hz for 30 seconds. Depending on tissue rigidity, homogenization was repeated up to 4 times. Then, lysates were incubated for 5 minutes at R/T before adding 300 µL of chloroform, vortexing and incubating again for 3 minutes. Subsequently, samples were centrifuged at 13,680 g for 15 minutes at 4°C to achieve phase-separation of RNA, DNA and debris. The topmost phase containing RNA was transferred to a fresh tube and added with 750 µL 2-propanol and mixed. Samples were then incubated on ice for 20 minutes and subsequently centrifuged at 21,000 g at 4°C for 15 minutes. Afterwards, supernatant was removed and the remaining RNA pellet washed 2 times with 75% ethanol with centrifugation in between at 21,000 g at 4°C for 5 minutes. The supernatant was removed and the pellet was air-dried after which DEPC-$H_2O$ was added to resuspend the pellet and stored at -80°C. RNA purity and concentration were determined by spectrophotometry on an Infinite M200 pro. RNA has an absorption maximum at an optical density (OD) of 260 nm which was used to determine RNA concentration, while protein OD of 280 nm was used to calculate RNA purity by dividing $OD_{260}/OD_{280}$. If this ratio is between 1.8 and 2.0, the purity was high and RNA was used for generating cDNA.

### 3.9.3 Generating cDNA stocks

RNA was reverse transcribed to double-stranded cDNA from 0.5 µg RNA dissolved in DEPC-$H_2O$. The resulting amount of cDNA stocks proved sufficient for the estimated number of qPCR assays required. RNA samples were first treated according to manufacturer's instruction with RQ1 DNAse (1u/µL) plus RQ1 DNAse buffer for 15 minutes at R/T after which reactions were stopped with RQ1 DNAse stop solution and incubation for 15 minutes at 65°C. Next, oligo-dT and random primer in DEPC-$H_2O$ were added and heated to 70°C and incubated for 5 minutes before cool-down on ice for 1 minute. As a consequence, oligo-dT primers bind to the poly-A tail at the 3'-end of RNA molecules and random primers further bind at several random locations on the RNA strand. Then, reverse transcription was achieved by adding DNA polymerase, reaction buffer, dNTP mix, RNasin® and DEPC-$H_2O$ and incubating for 1 hour at 37°C. At the end, the reaction was stopped by incubating samples on ice for 1 minute. Resulting cDNA stocks were kept at -20°C.

### 3.9.4 RT-qPCR assays

RT-qPCR assays utilizing cDNA stocks (2.5 µL for Platinum® or 1 µL for SyBR®) and oligonucleotide primers (Table 3.5) were prepared with Platinum® qPCR SuperMix-UDG with ROX or SYBR® Green Master Mix. qPCR plates were run on a Taqman 7500 using TAMRA quencher and FAM reporter. The delta-delta Ct method was used to calculate gene expression fold changes for each assay [89]. For normalization, housekeeping genes *ACTB*, *HPRT1* and *GAPDH* were used. Graphs in the result section show results after normalization to the housekeeping gene that was most homogeneously expressed in both tested groups. Normalized data were similar among housekeeping genes (data not shown).

Table 3.6: Platinum ® Taqman temperature and cycling.

| Step | Cycles | Stage | Time | Temperature |
|---|---|---|---|---|
| Step 1 | | Holding stage | 2 minutes | 50°C |
| Step 1 | | Holding stage | 10 minutes | 95°C |
| Step 1 | 40 cycles | Cycling stage | 15 seconds | 95°C |
| Step 2 | | Cycling stage | 1 minute | 60°C |

Table 3.7: SyBR® temperature and cycling.

| Step | Cycles | Stage | Time | Temperature |
|---|---|---|---|---|
| Step 1 | | Holding stage | 2 minutes | 95°C |
| Step 1 | 40 cycles | Cycling stage | 15 seconds | 95°C |
| Step 2 | | Cycling stage | 1 minute | 60°C |
| Step 1 | | Melt curve stage | 15 seconds | 95°C |

### 3.9.5 Lipid peroxidation assay

A marker for lipid oxidation and thus oxidative stress, malondialdehyde (MDA), was detected utilizing the Lipid Peroxidation (MDA) assay kit. In brief, 10 mg of placental tissue were homogenized in MDA lysis buffer and processed further according to manufacturer's instructions. Basically, the assay measures the production of a colorimetric product from the reaction of MDA with TBA and this reaction product can be quantitated by spectrophotometry at an absorbance maximum of 532 nm, measured on Infinite 200 pro.

## 3.10 Cell culture studies

Culturing of cells was done in humid incubators at 37°C and 5% $CO_2$. For handling, cells were transferred to a cell culture hood with laminar flow which was decontaminated with ethanol and UV-light on a daily basis to provide as sterile working conditions as possible. Media were supplemented with PenStrep to avoid bacterial contamination, and mycoplasma contamination tests of culture media were

regularly performed. All solutions from non-sterile source added to cell cultures were either autoclaved or sterile-filtered prior to use.

### 3.10.1 Cell culture medium

Table 3.8: Cell culture media purchased and used in this work.

| Medium | Company |
|---|---|
| DMEM/F12, HEPES #11039-021 | Gibco®, Carlsbad, California, USA |
| Endothelial cell medium #1001 | ScienCell, Carlsbad, California, USA |

### 3.10.2 Cell lines

Table 3.9: Commercial cell lines used in this work.

| Cell line | Company |
|---|---|
| BeWo, ACC-No. 458 | Deutsche Sammlung von Mikroorganismen und Zellkulturen (DSMZ), Braunschweig, Germany |
| HPVEC, #7100 | ScienCell, Carlsbad, California, USA |

### 3.10.3 Maintenance of cell lines

Human trophoblast-derived choriocarcinoma cells (BeWo) were purchased from DSMZ and cultured according to manufacturer instructions. Briefly, cells were thawed carefully in a 37°C water bath until completely thawed and then transferred to 9 mL fresh DMEM/F-12 HEPES medium. This medium was supplemented with 1% (v/v) PenStrep and 10% (v/v) FBS. Cells in medium were centrifuged at 125 g for 3 minutes, supernatant was removed and cells were resuspended in 1 mL medium before plating in flasks. Typically, every 48 hours, the cell medium was changed and cells were split shortly before reaching 100% confluence by removing the medium, washing with D-PBS and incubating with trypsin-EDTA for 3 to 5 minutes at 37°C. Fresh medium with FBS and PenStrep was subsequently added to block trypsin-EDTA. Cells in suspension were centrifuged at 125 g for 3 minutes to remove supernatant and 1 mL of fresh medium was added to resuspend. Either 1/4 or 1/5 of cell suspension were then plated in 75 $cm^2$ flasks filled with approximately 10 mL of fresh medium.

Human placental vein endothelial cells (HPVEC), which are primary placenta cells from one placenta/lot, were purchased from ScienCell and cultured in accordance with manufacturer instructions. In brief, cells were received at passage one, thawed and then plated in flasks filled with 10 mL fresh endothelial cell medium supplemented with 1% (v/v) endothelial cell growth supplements, 5% (v/v) FBS and 1% (v/v) PenStrep. Flasks were coated with 0.2% (v/v) gelatin in de-ionized water on the day before plating cells. To this end, gelatin was diluted with de-ionized water to 0.2% and 7.5 mL gelatin solution was incubated in a 75 $cm^2$ flask for 1 hour. When cells were seeded, the medium was changed 16 hours after first plating to remove residual DMSO. From there, medium was changed every 48 hours and cells were

split before reaching confluence similar as described above, however, 1/2 of cell suspension was plated per 75 cm² flask. After 8 passages, HPVEC were not further split or used for assays, since they are primary cells.

### 3.10.4 Stimulation of cells

The influence of cytokines or fatty acids on cell behavior and protein expression was studied by applying cell medium supplemented with either a dissolved fatty acid or hyperIL-6 (description below) to cells in culture. Fatty acids were purchased as sodium palmitate (PA), sodium oleate (OA) and linoleic acid sodium salt (LA) and were first dissolved in de-ionized water to a final concentration of 50 mM and mixed in a heated shaker at 70°C. For cell stimulation, fatty acids were further diluted in cell medium supplemented with 5% (w/v) protease-free and fatty acid-free BSA to a final concentration of 2.5 mM. To enhance dissolution, these 2.5 mM stocks were heated to 40°C for 15 minutes on a shake plate.

Stimulation of cells with IL-6 was done with a fusion protein of IL-6 and its soluble IL-6R. The bioactive fusion protein hyperIL-6 is constructed by recombinant human IL-6 (Val30 – Met212) which is ligated to a small glycine and serine-rich peptide chain with the sequence 'GGGSGGGSGGGS' to the IL-6 receptor-alpha (Leu20 – Asp358) [90]. HyperIL-6 was received at a concentration of 500 µg/mL and was diluted 1:100 in culture medium to generate a stock solution before further diluting to the required final concentrations.

### 3.10.5 Cell culture for protein detection

Cells were seeded in 6-well plates at a density of 300,000 cells per well. To achieve this density, cells were counted in a Neubauer chamber after splitting. After seeding in wells, cells were maintained in medium O/N, approximately 16 hours. Then, medium was removed and cells were either stimulated with a) medium plus FBS plus PenStrep or b) medium plus FBS plus PenStrep with 5% (w/v) protease-free and fatty acid-free BSA or c) various concentrations of fatty acids (PA, OA or LA) dissolved in medium as described above or d) medium plus FBS plus PenStrep with hyperIL-6. To assess phosphorylation of Stat3 after hyperIL-6 stimulation, cells were incubated for 15 minutes with hyperIL-6 in medium at 37°C. Stimulation with fatty acids was performed for 24 hours at 37°C. After stimulation, medium was removed and cells were put on ice after adding 1 mL of 4°C cold PBS. Cells were collected in D-PBS, centrifuged at 125 g for 3 minutes, washed in D-PBS twice and supernatant was removed. Pellets were then frozen and stored at -80°C. After four repetitions per stimulation, frozen pellets were thawed on ice and 40 µL modified RIPA buffer was added, vortexed and incubated on ice for 1 hour. Next, samples were centrifuged at 18,500 g for 5 minutes at 4°C and supernatant was transferred to fresh tubes. Supernatant was used in a Pierce™ BCA Protein Assay to determine protein abundance in duplicate and for protein detection, 20 µg of protein were used as described above (section 3.6).

### 3.10.6 Permeability assay

BeWo cells were split and seeded in inserts with a pore size of 0.4 µm at a density of 50,000 cells/insert in a 24-well plate filled with 800 µL medium per well and 300 µL medium per insert. Typically, medium was replaced after 48 hours and cells took 48 to 72 hours to reach confluence which was confirmed by staining cells with CellStain® and inspection under a microscope. When confluent, medium was removed and cells were treated with fatty acids for 24 hours. Afterwards, medium was carefully removed from inserts and inserts were transferred to a fresh 24-well plate filled with 800 µL plain DMEM/F12 medium (without FBS, PenStrep). Subsequently, 300 µL of Streptavidin-HRP diluted 1:20 in plain medium was added to each insert and incubated for 30 minutes at 37°C. Next, inserts were removed and 30 µL from each underlying well was transferred on a 96-well plate in triplicates. Then, 50 µL of TMB substrate solution was added to each well and incubated for 20 minutes at R/T on a shake plate. Reaction was stopped by applying 25 µL of 2N $H_2SO_4$ to each well and absorption was subsequently measured at 450 nm on an Infinite M200 pro.

### 3.10.7 AdipoRed assay

The intracellular accumulation of triglycerides can be quantified by AdipoRed assays. To this end, 15,000 cells per well were plated in 96-well plates and allowed to sit O/N, approximately 16 hours. Then, medium was removed and 100 µL medium plus fatty acids was added as described above and incubated for 8 hours. After incubation, medium with fatty acids was removed, cells were rinsed in D-PBS and 100 µL of AdipoRed staining solution was added to each well and incubated for 10 minutes at 37°C. Immediately afterwards, fluorescence was read with excitation/emission 485/572 nm on a GloMax® Multi Detection System.

### 3.10.8 Tube formation assay

The formation of vessel structures, so called tubes, is a characteristic of several cells and cell lines, like HPVEC. In order to assess their tube formation capacity and changes in tube formation due to stimulation with hyperIL-6, HPVEC were subjected to this assay. A µ-slide was coated with 10 µL 4°C cold, growth factor-reduced matrigel and incubated for 45 minutes to 1 hour at 37°C. Afterwards, 5,000 HPVEC per well were seeded directly in stimulation (10 ng/mL or 50 ng/mL hyperIL-6) or control medium (without hyperIL-6). The seeded µ-slide was placed in an incubator for 1 hour at 37°C after which it was transferred to a pre-heated confocal Zeiss Meta 510 microscope equipped with an incubator chamber set to 37°C and 5% $CO_2$. After 12 hours of incubation with stimulants or control medium, images of the wells were taken to manually count closed tubes using ImageJ Fiji. The number of such tubes was then normalized to the total analyzed area.

### 3.10.9 Caspase-GLO® 3/7 apoptosis assay

HPVEC apoptosis was detected by a commercial Caspase-GLO® 3/7 assay. After coating a 96-well plate with 0.2% gelatin, 15,000 cells per well were seeded and allowed to attach for 12 hours.

Afterwards, cells were stimulated without, with 10 ng/mL or 50 ng/mL hyperIL-6 for 12 hours. Subsequently, Caspase-GLO® 3/7 assay was used to detect caspase activity following manufacturer's instructions.

### 3.10.10 Cell proliferation assay with BrdU

Proliferation of HPVEC was determined by cell proliferation ELISA with BrdU from commercial source. To this end, a 96-well plate was coated with 0.2% gelatin and 10,000 cells/well were seeded and cultured for 12 hours. Afterwards, cells were stimulated without, with 10 ng/mL or 50 ng/mL hyperIL-6 for 12 hours before removing stimulants and added fresh stimulation medium with BrdU and incubating for 24 hours. BrdU incorporation in HPVEC was measured according to manufacturer's instructions.

### 3.10.11 Cell senescence by beta-galactosidase assay

Senescence of HPVEC was assessed by seeding 10,000 cell per well in a gelatin-coated 96-well plate after which cells were allowed to attach for 12 hours. Next, cells were stimulated with, i.e. 10 ng/mL or 50 ng/mL of hyperIL-6, or without hyperIL-6 for 48 hours. Afterwards, the senescence-associated beta-galactosidase activity was determined as previously published [91]. In brief, after incubation with stimulants for 48 hours, cells were washed twice with D-PBS and fixed in 2% formaldehyde plus 0.2% glutaraldehyde in D-PBS solution. Next, cells were washed twice with D-PBS and fresh beta-gal staining solution was added and incubated O/N at 37°C. On the next day, cells were washed with D-PBS and transferred to a BX43F microscope to scan wells and take images (DP80 dual CCD camera and cellSens Dimension V1.8 software). Using ImageJ Fiji, blue-colored beta-gal positive cells were counted and relative senescence rate was calculated.

## 3.11 Statistical analyses

Statistical analyses were performed with GraphPad Prism software. D'Agostino and Pearson test was used to determine normality distribution of the data. Sets of normally distributed data were analyzed by two-tailed Student's *t* test or one-way ANOVA followed by Tukey's multiple comparison test (indicated in figure description) and non-normally distributed data were analyzed by two-tailed Mann-Whitney test (indicated in figure description). Significant difference was determined by a $p$ value of $<0.05$. Graphs of data calculated or published before May 2019 are shown as mean ± SEM independent of normal distribution or non-normal distribution. Later, after consulting a statistician, graphs of data are shown as mean ± SEM if normally distributed and as median ± interquartile range if non-normally distributed. Due to the large dataset in proteomics profiling, Student's *t* test $p$ values were post-tested by the method of Benjamini-Hochberg correction [92] and significant difference after correction was determined by a $q$ value of $<0.05$. Further details are shown in the figure descriptions.

# 4. Results

### 4.1 The pre-delivery inflammatory reaction is mitigated by MO in C57BL/6N mice

Note: This part of the results section, i.e. “The pre-delivery inflammatory reaction is mitigated by MO in C57BL/6N mice”, was published in the Journal of Reproductive Immunology in the article “Maternal obesity attenuates predelivery inflammatory reaction in C57BL/6N mice” [79]. Sarah Appel, Merle Schulze-Edinghausen and Tobias Kretschmer contributed equally to this work with the help of several others:

Animal handling and tissue collections was performed by Ruth Janoschek, Inga Bae-Gartz, Marion Handwerk and Sarah Appel. The qPCR assays were prepared and performed by Merle Schulze-Edinghausen, Tobias Kretschmer and Maria Wohlfarth, while data calculation was done by Merle Schulze-Edinghausen and Sarah Appel. Histological stainings (IHC for CD45) were performed by Tobias Kretschmer, while picture processing for cell counting was done by Merle Schulze-Edinghausen and Tobias Kretschmer. Lipid peroxidation assay was performed by Merle Schulze-Edinghausen and Maria Wohlfarth. Malte Heykants performed multiplex cytokine assays. Statistical analyses were performed by Merle Schulze-Edinghausen, Sarah Appel and Tobias Kretschmer. The project was supervised and supported by technical input and advice by Kai-Dietrich Nüsken, Eva Hucklenbruch-Rother, Esther Mahabir, Jörg Dötsch and Sarah Appel.

#### 4.1.1 Inflammation, leukocyte infiltration and oxidative stress in placental tissue and egWAT

Two time-points of murine gestation, E15.5 which represents the beginning of the third trimester of pregnancy and E18.5 which represents the end of the third trimester shortly before parturition, were investigated on placental and egWAT level. While SD dams usually gave birth around E19, HFD dams took about an extra day before giving birth (Figure 4.1.1.2 D). Gene expression of IL-6 and TNFα, two pro-inflammatory cytokines, was significantly increased in placentas of SD dams on E18.5 compared to E15.5. MCP1 and the murine IL-8 homologue CXCL1 were not significantly altered and CXCL10, IL-1α and IL-1β were down-regulated without reaching statistical significance (Figure 4.1.1.1 B). On E18.5 in placentas of obese dams, TNFα was significantly up-regulated compared to E15.5 and IL-6, MCP1, and IL-1β were unaltered in expression. CXCL1, CXCL10 and IL-1α on the other hand appeared down-regulated, but without reaching statistical significance (Figure 4.1.1.1 C). Concomitantly, with an increase in IL-6 and TNFα gene expression at E18.5 compared to E15.5 in SD dams, there was significant infiltration of leukocytes (CD45-positive) in the Lz. This increase in leukocytes towards the end of pregnancy was not observed in HFD dams (Figure 4.1.1.1 A). Further, in both, SD and HFD placentas, lipid peroxidation, a marker for oxidative stress, as assessed by MDA assay was significantly increased at E18.5 compared to E15.5, however MDA level were also significantly higher in HFD placentas at E18.5 compared to SD (Figure 4.1.1.1 D). Anti-oxidative genes GPX and CAT were significantly down-regulated at E18.5 compared to E15.5 in SD placentas, whereas pro-oxidative stress genes remained largely unaltered (Figure 4.1.1.1 E).

The pro-oxidative genes CYBB, NCF1 and NCF2 were significantly up-regulated in placentas of obese dams at E18.5 compared to E15.5 and the anti-oxidative CAT gene expression was significantly reduced (Figure 4.1.1.1 F).

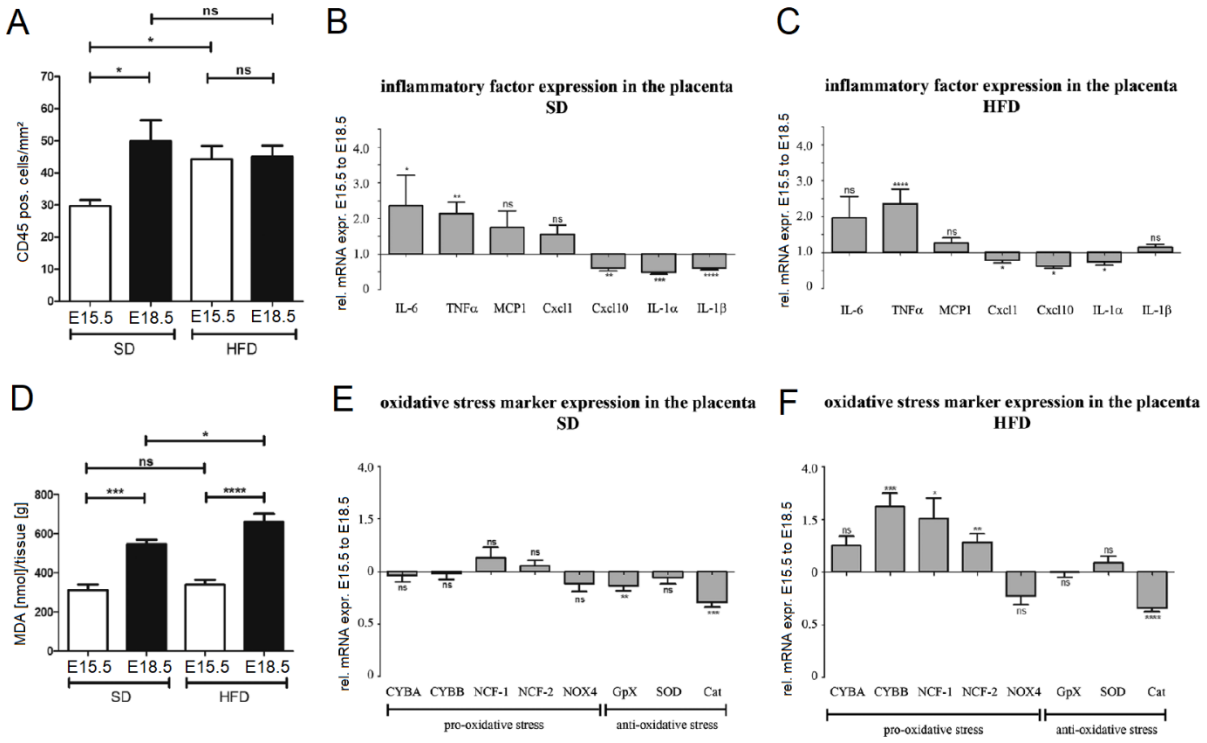


**Figure 4.1.1.1: Inflammation, leukocyte infiltration and oxidative stress measurements in placentas at E15.5 and E18.5.** (A) Quantitation of CD45-positive leukocytes in the Lz of the placenta of obese and lean dams at E15.5 and E18.5, *n* = 5 placentas for both groups and both gestations days. (B) Gene expression measurement by qPCR of pro-inflammatory factors in placentas of SD dams normalized to ACTB at E15.5 and E18.5. Expression was set to 1 for E15.5 and the fold change on E18.5 relative to E15.5 is shown. For SD at E15.5 *n* = 16 placentas from 5 dams, at E18.5 *n* = 25 placentas from 5 dams. (C) Gene expression measurement by qPCR of pro-inflammatory factors in placentas of HFD dams normalized to ACTB at E15.5 and E18.5. Expression was set to 1 for E15.5 and the fold change on E18.5 relative to E15.5 is shown. For HFD at E15.5 *n* = 21 placentas from 5 dams, at E18.5 *n* = 25 placentas from 5 dams. (D) Lipid peroxidation assay to determine oxidative stress level as assessed by change in MDA in placentas of SD and HFD dams at E15.5 and E18.5. For SD *n* = 11 placentas from 11 dams of E15.5 and *n* = 9 placentas from 9 dams of E18.5. For HFD *n* = 10 placentas from 10 dams of E15.5 and *n* = 10 placentas from 10 dams of E18.5. (E) Gene expression measurement by qPCR of oxidative stress markers in placentas of SD dams normalized to ACTB at E15.5 and E18.5. Expression was set to 1 for E15.5 and the fold change on E18.5 relative to E15.5 is shown. For SD at E15.5 *n* = 21 placentas from 5 dams, at E18.5 *n* = 25 placentas from 5 dams. (F) Gene expression measurement by qPCR of oxidative stress markers in placentas of HFD dams normalized to ACTB at E15.5 and E18.5. Expression was set to 1 for E15.5 and the fold change on E18.5 relative to E15.5 is shown. For HFD at E15.5 *n* = 21 placentas from 5 dams, at E18.5 *n* = 25 placentas from 5 dams. *ns* = not significant; * $p$ <0.05, ** $p$ <0.01, *** $p$ <0.001, **** $p$ <0.0001, calculated by two-tailed Student's *t* test (for normally distributed data) or a Mann-Whitney test (for non-normally distributed data). Graphs show mean ± SEM. Figure was published in Appel, Schulze-Edinghausen, Kretschmer et al. [79] Figure 1 and was modified.

We further investigated inflammatory markers in the egWAT of both diet groups and gestation days, since we hypothesized that the egWAT might produce higher amounts of inflammatory markers that could affect uterine tissues due to its proximity to these tissues. Significantly elevated expression of pro-inflammatory genes IL-6, TNFα, CXCL1, CXCL10, MCP1 and IL-1β were measured in egWAT of SD dams at E18.5 compared to E15.5 (Figure 4.1.1.2 B). By contrast, these genes remained unaltered in egWAT of obese dams (Figure 4.1.1.2 C). Additionally, the amount of leukocytes was not significantly altered in egWAT in either diet group at E15.5 or E18.5 (Figure 4.1.1.2 A).

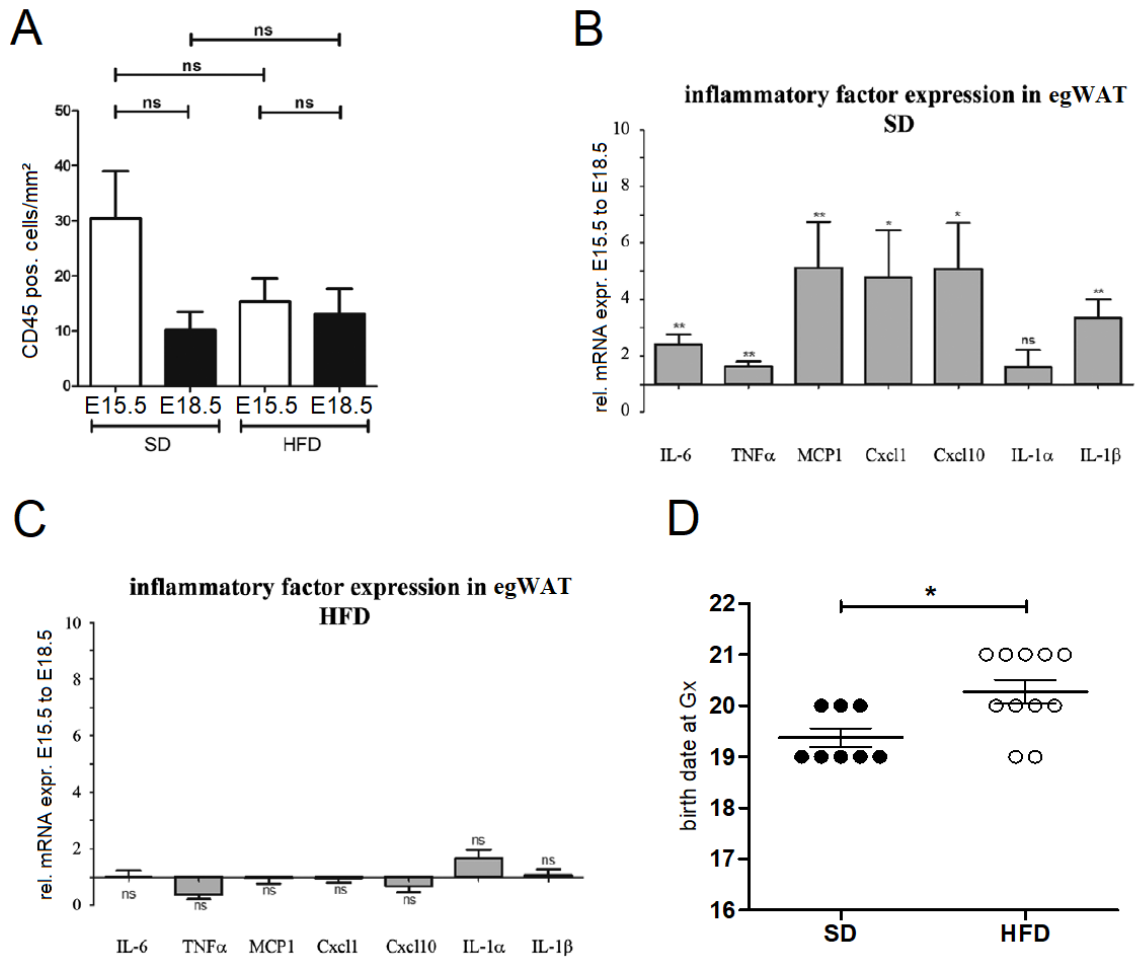


**Figure 4.1.1.2: Leukocyte infiltration, inflammatory factor expression in egWAT at E15.5 and E18.5, and duration of gestation.** (A) Quantitation of CD45-positive leukocytes in the egWAT of SD and HFD dams at E15.5 and E18.5, *n* = 5 egWAT for both groups and both gestation days. (B) Gene expression measurement by qPCR of pro-inflammatory factors in egWAT of SD dams normalized to ACTB at E15.5 and E18.5. Expression was set to 1 for E15.5 and the fold change on E18.5 relative to E15.5 is shown. For SD at E15.5 *n* = 8, at E18.5 *n* = 5. (C) Gene expression measurement by qPCR of pro-inflammatory factors in egWAT of HFD dams normalized to ACTB at E15.5 and E18.5. Expression was set to 1 for E15.5 and the fold change on E18.5 relative to E15.5 is shown. For SD at E15.5 *n* = 8, at E18.5 *n* = 8. (D) Duration of gestation expressed as the "birth date at Gx" in SD and HFD dams. *n* = 8 for SD and *n* = 11 for HFD. *ns* = not significant; * *p* <0.05, ** *p* <0.01, calculated by two-tailed Student's *t* test (for normally distributed data) or a Mann-Whitney test (for non-normally distributed data). Graphs show mean ± SEM. Figure was published in Appel, Schulze-Edinghausen, Kretschmer et al. [79] Figure 1 and was modified.

## 4.2 MO affects EC homeostasis and causes elevated IL-6 serum level which could cause EC senescence

Note: This part of the results section, i.e. “MO affects EC homeostasis and causes elevated IL-6 serum level which could cause EC senescence”, was recently published in parts in Nutrients in the article “Effect of Maternal Obesity in Mice on IL-6 Levels and Placental Endothelial Cell Homeostasis” [81]. This work was made possible with the help of several others:

Animal handling and tissue collections was performed by Eva-Maria Turnwald, Ruth Janoschek, Inga Bae-Gartz, Marion Handwerk, Sarah Appel and Tobias Kretschmer. The qPCR assays were prepared and performed by Merle Schulze-Edinghausen and Maria Wohlfarth, while data calculation was done by Sarah Appel and Tobias Kretschmer. Protein isolation and detection were performed by Maria Wohlfarth, densitometric analysis was contributed by Sarah Appel and Tobias Kretschmer. Histological stainings (IHC) were performed by Merle Schulze-Edinghausen and Tobias Kretschmer (IHC, IF and Stereology), while picture processing for stereology was done by Peter Zentis and analysis of IF and stereology sections was conducted by Tobias Kretschmer. The IL-6 ELISA on serum samples was conducted by Merle Schulze-Edinghausen. Cell culture assays and analyses (apoptosis, BrdU, senescence-associated beta-galactosidase and tube formation assay) were performed by Merle Schulze-Edinghausen and Tobias Kretschmer (tube formation assay). Statistical analyses were performed by Merle Schulze-Edinghausen, Sarah Appel and Tobias Kretschmer. The project was supervised and supported by technical input and advice by Astrid Schauss, Eva Hucklenbruch-Rother, Jörg Dötsch and Sarah Appel.

The significant reduction of fetal weight (0.3786 ± 0.004382 g in HFD vs. 0.4482 ± 0.008337 g in SD, $p < 0.0001$) in HFD offspring of this animal cohort (project A057) at E15.5 was previously reported by Appel et al. [93]. In this work, fetal IUGR was also observed (Figure 4.4.1.1 B, Figure 4.6.1.1 B). In the work of Kretschmer et al. [81], the aim was to elucidate if a defective vascularization of the placenta under MO might contribute to the observed IUGR phenotype.

### 4.2.1 Significant reduction in EC marker expression in placentas under MO

Gene activity (mRNA expression) and protein level of EC markers in whole placental lysates of E15.5 were determined to study the effect of MO on vascularization of the placenta (Figure 4.2.1.1). The qPCR assays revealed significant down-regulation of the EC markers CD31, vWF and Tie-1 in placentas of HFD dams. Expression level were normalized to ACTB and HPRT. Data is shown for normalization to HRPT (Figure 4.2.1.1 A). For normalization to ACTB, similar results were obtained (data not shown). The marker CD31 is primarily found in the Lz of placentas which harbors the transfer zone for nutrient and gas exchange (Figure 4.2.1.1 B). Additionally, CD31 protein level was significantly lower ($p$ 0.03) in whole placental lysates from HFD dams. Interestingly, a similar, significant reduction ($p$ 0.0006) in CD31 protein level was observed in placentas of dams of project A046 (Figure 4.2.1.1 F). Hence, data indicates an effect of MO on ECs of the transfer zone.

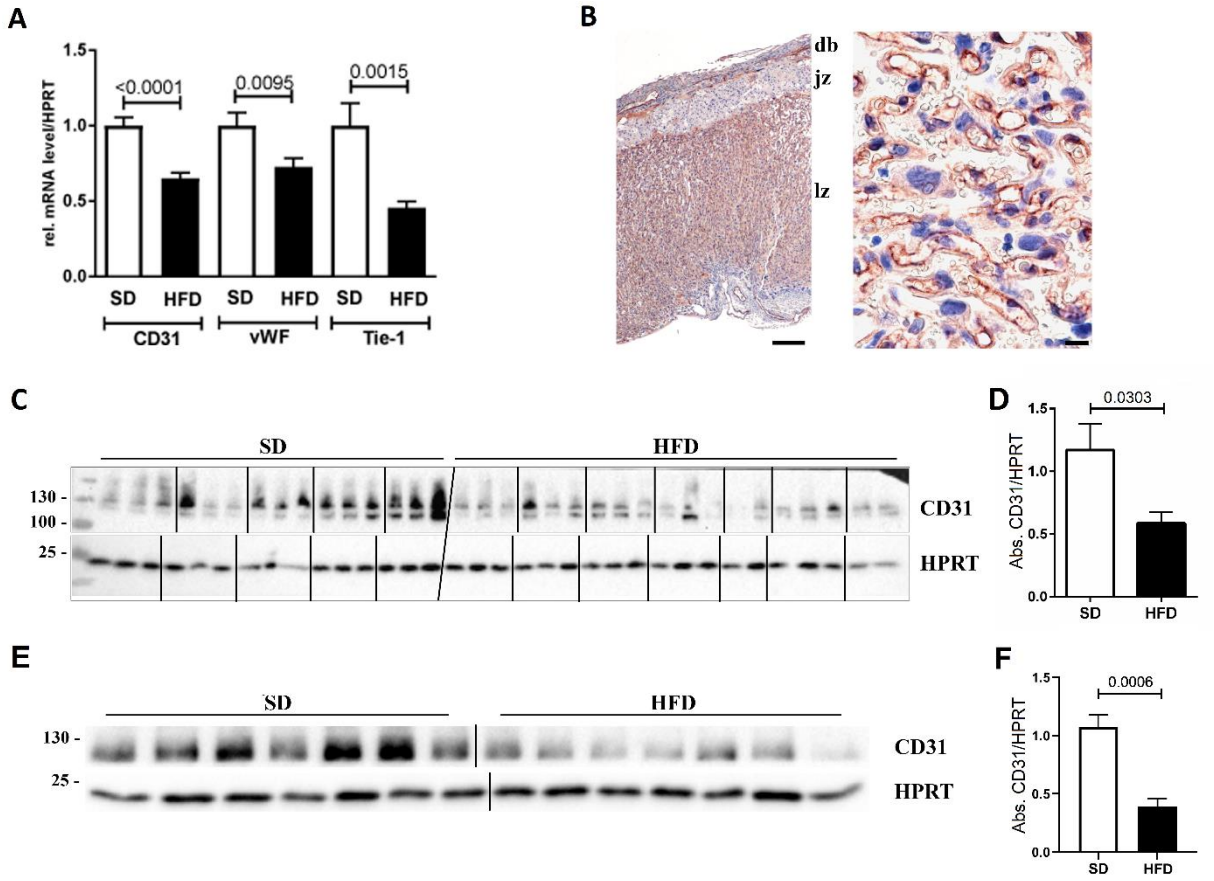


**Figure 4.2.1.1: EC marker level under MO.** (A) Gene expression in placentas of SD and HFD of vascular EC markers CD31, vWF and Tie-1 detected by qPCR and normalized to HPRT; *n* = 21 placentas from 5 dams in SD, *n* = 21 placentas from 6 dams in HFD group. The *p* value is indicated above graphs and was calculated by Mann-Whitney test. (B) Representative images showing placental sections stained for CD31 by IHC. Left panel (scale bar: 200 µm) shows the 3 main zones, Lz, Jz and Db, and CD31 to be primarily expressed in fetal capillaries in the Lz as detailed in the right panel (scale bar: 10 µm). (C) Western blot detection of CD31 in SD and HFD placentas (project A057). HPRT was detected as loading control. *n* = 15 placentas from 5 dams for SD and *n* = 19 placentas from seven dams for HFD. (D) Densitometric analysis of CD31 signal from western blot in (C) normalized to HPRT. (E) Western blot detection of CD31 in SD and HFD placentas (project A046). HPRT was detected as loading control. *n* = 7 placentas, 1 per dam for both SD and HFD. (F) Densitometric analysis of CD31 signal from western blot in (E) normalized to HPRT. All graphs show mean ± SEM. The *p* value is displayed above the graph, calculated by Mann-Whitney test. Figure was published in Kretschmer et al. [81], Figure 1 and was modified.

### 4.2.2 Disturbed EC homeostasis and placental vascular morphology

Assessing EC homeostasis, i.e. EC proliferation, apoptosis and senescence, was done by means of IF staining for BrdU-positive (proliferation), TUNEL-positive (apoptosis) and γH2A.X-positive (senescence) EC which were detected specifically by co-staining for the EC marker CD31 (Figure 4.2.2.1 A – C). The stainings were performed on sections close to the placental midline and quantitation by cell counting of scanned sections in ImageJ Fiji revealed the number of positively stained EC. No difference in BrdU-positive or TUNEL-positive cell count was observed in the Lz for HFD placentas compared to controls (Figure 4.2.2.1 D & E). However, the amount of γH2A.X-positive EC was significantly larger in placentas under MO compared to controls (*p* 0.0262, Figure 4.2.2.1 F). This indicates elevated level of senescence in EC as assessed by γH2A.X-positive staining.

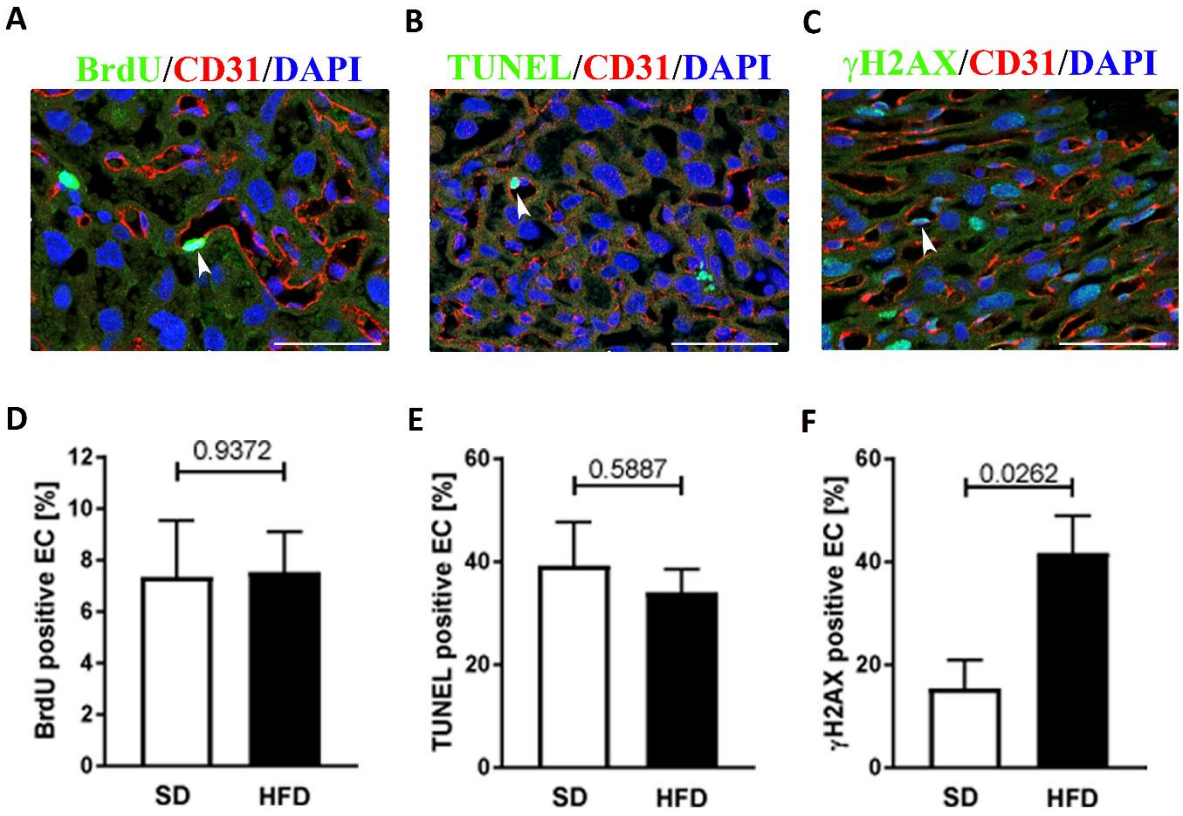


**Figure 4.2.2.1: Placental EC homeostasis under maternal obesity.** (A – C) Representative images of placental Lz with IF stainings for proliferation marker BrdU (A, green), apoptosis by TUNEL (B, green) and senescence/DNA-damage marker γH2A.X (C, green). Co-staining was performed for CD31 (red) and nuclei by DAPI (blue). Scale bar = 50 µm. (D – F) Quantitation of IF-positively stained EC nuclei by BrdU (D, *n* = 6 placentas, 1 placenta per dam for both groups SD & HFD), by TUNEL (E, *n* = 6 placentas, 1 per dam for both SD & HFD) and by γH2A.X (F, *n* = 7 placentas, 1 per dam for both SD & HFD). Graphs show mean ± SEM. The *p* value is denoted above graphs in the figure, calculated using Mann-Whitney test. Figure was published in Kretschmer et al. [81], Figure 2 and was modified.

Vascularization and vessel morphology of the Lz was studied by stereological means and to this end, placental section were stained by IHC against CD31 after exhaustive sectioning (Figure 4.2.2.2 A & B). Quantitation of FC surface area revealed a significant reduction (*p* 0.038) in placentas under MO concomitant with a significantly decreased total capillary length (*p* 0.002) and a tendency towards an increased capillary diameter (*p* 0.072) in those placentas compared to controls (Figure 4.2.2.2 C – E). These results strongly suggest an impaired vascularization of the placentas in obese dams.

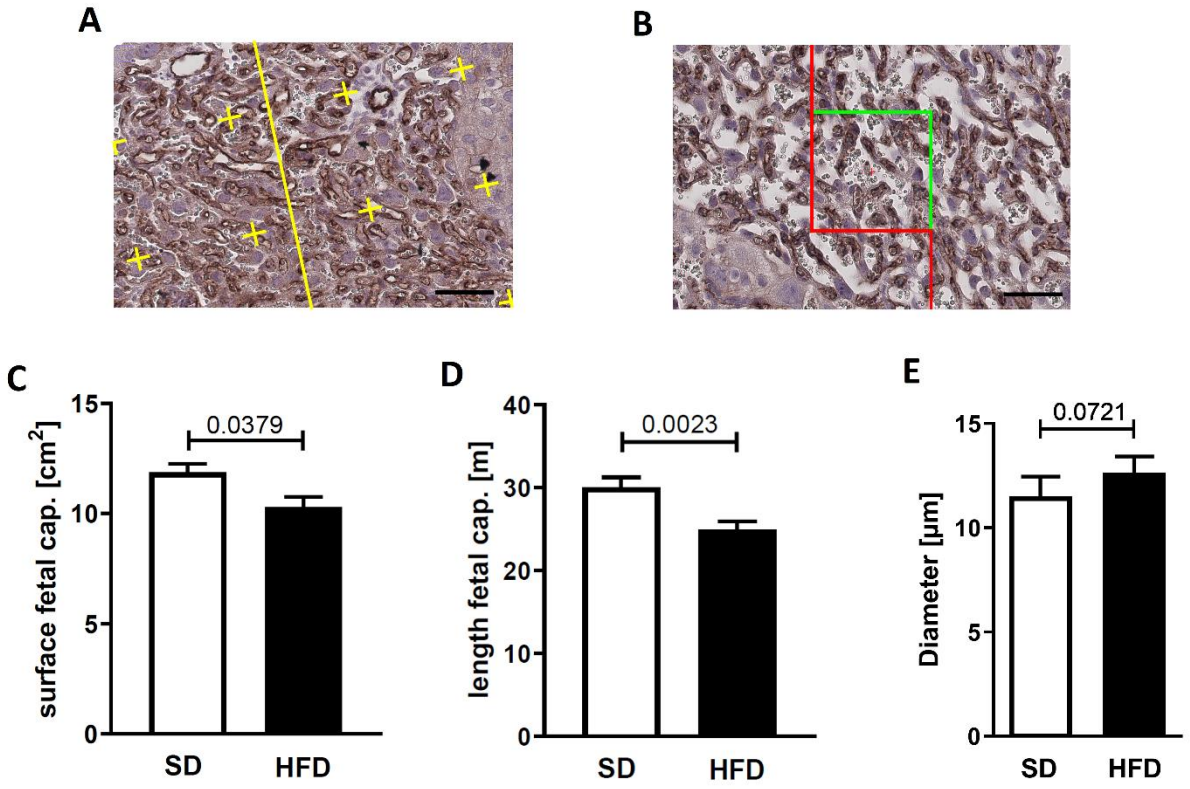


**Figure 4.2.2.2: Vascular morphology assessed by stereology under MO.** (A) Representative image showing the Lz in a SD placenta stained with antibodies against CD31 and DAB. A grid for stereological analysis of fetal capillary surface area was superimposed on the image. Scale bar = 50 µm. (B) Representative image showing the Lz in a SD placenta stained similar to (B) for CD31. A grid was superimposed on the image to assess fetal capillary length and diameter. Scale bar = 50 µm. (C – E) Quantitation of fetal capillary surface area (C), fetal capillary length (D) and fetal capillary diameter (E) after stereological analyses. Graphs show mean ± SEM. For SD *n* = 8 placentas from 8 dams, for HFD *n* = 7 placentas from 7 dams, the *p* values are denoted above graphs in the figure, calculated using Mann-Whitney test. Figure was published in Kretschmer et al. [81], Figure 2 and was modified.

### 4.2.3 Change in level of IL-6 inflammatory marker

We hypothesized that IL-6 can influence EC homeostasis in placentas of our obese mouse model and, as a consequence, determined IL-6 level in the serum of dams at E15.5. Serum IL-6 level was significantly elevated (*p* 0.048) in dams at E15.5 under MO by a margin of nearly 4-fold (Figure 4.2.3.1 A). Conversely, qPCR assays showed no difference in IL-6 gene expression (*p* 0.286) in placentas of obese dams (Figure 4.2.3.1 B). In addition, detection of IL-6 mRNA in egWAT revealed a 3-fold increase compared to control dams that was not statistically significant (*p* 0.204, Figure 4.2.3.1 D). However, weight of the egWAT pad dissected from obese dams was significantly elevated (*p* <0.0001, Figure 4.2.3.1 C) and IL-6 protein level detected in egWAT were increased about 2.5-fold (Figure 4.2.3.1 E & F), but again without falling below the border of statistical significance (*p* 0.057). Nonetheless, these results suggest that the placenta is not the source of IL-6 production released in the serum and increased IL-6 serum level could rather originate from augmented fat pads in obese dams.

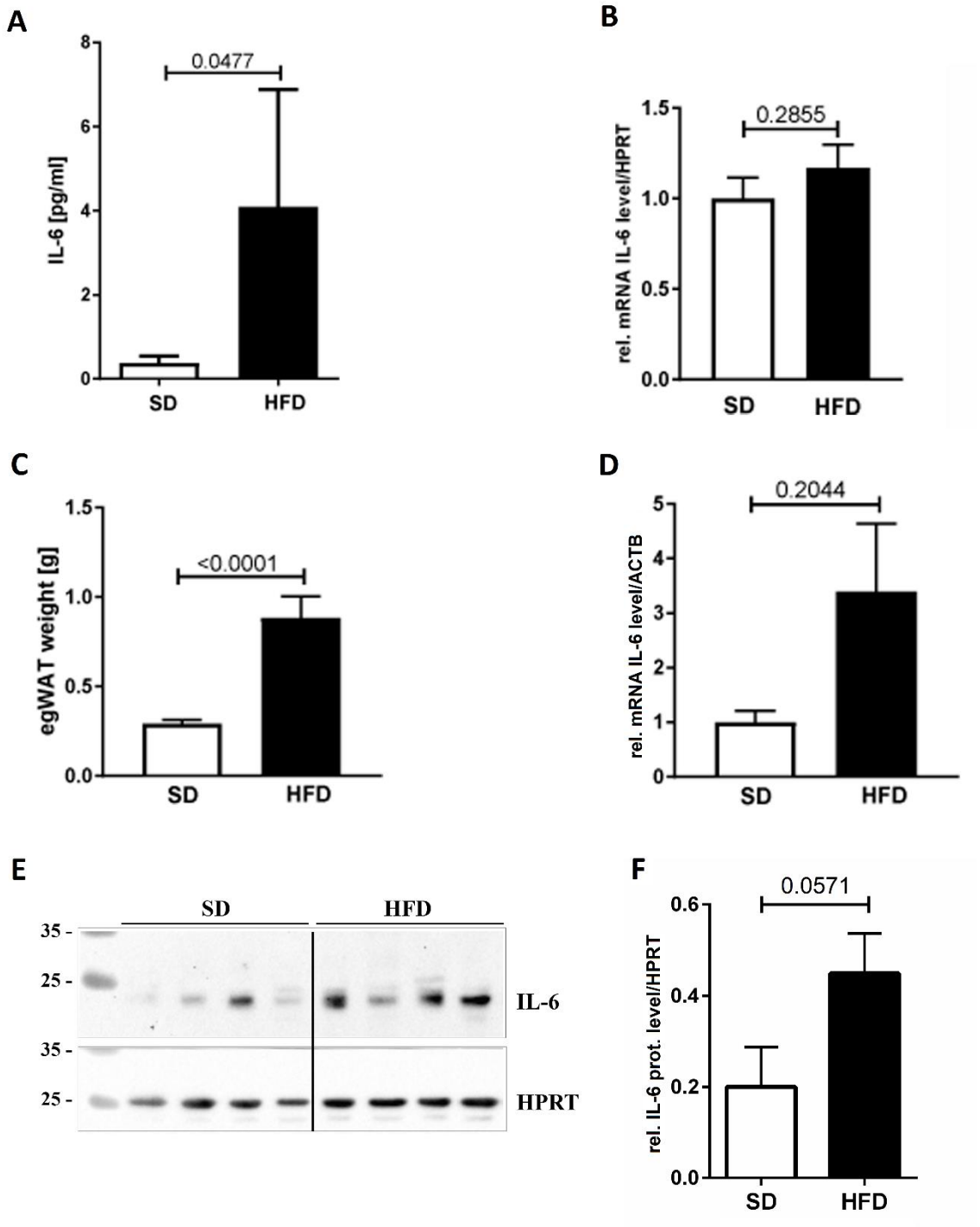


**Figure 4.2.3.1: Interleukin-6 expression level in serum, placentas and egWAT under MO.** (A) Serum level of IL-6 determined by ELISA in SD (*n* = 9) and HFD (*n* = 10) dams. (B) IL-6 gene expression in placental lysates (*n* = 16 from 4 dams in SD and *n* = 25 from 7 dams in HFD) analyzed by qPCR and normalized to HPRT. (C) Weight of dissected egWAT pad, *n* = 12 for SD and *n* = 14 for HFD. (D) IL-6 gene expression in egWAT, *n* = 8 for SD and HFD, analyzed by qPCR and normalized to ACTB. (E) Western blot for the detection of IL-6 and HPRT as loading control in *n* = 4 samples of egWAT for SD and HFD. (F) Densitometric analysis of relative IL-6 protein level from (E) normalized to HPRT. Graphs show mean ± SEM. The *p* value is denoted above graphs in the figure, calculated using Mann-Whitney test. Figure was published in Kretschmer et al. [81], Figure 3 and was modified.

### 4.2.4 Effect of IL-6 stimulation on placental EC homeostasis

It has been stated that serum IL-6 is able to pass over the placental barrier and to reach fetal ECs in the transfer zone [94, 95]. Furthermore, it was noted that IL-6 also is capable of causing EC activation and apoptosis [69], which led us to test the hypothesis that IL-6 can affect placental EC homeostasis (proliferation, apoptosis and/or senescence) and tube formation capacity *in vitro*. To this end, human placenta vein endothelial cells (HPVEC) were treated with various concentrations (without IL-6, with 10 ng/mL or 50 ng/mL) of IL-6 (i.e. hyperIL-6, a bioactive fusion protein of IL-6 and the IL-6R, see Methods 3.10.4). To verify the activity of IL-6 in HPVEC cultures, p-Stat3 level as a well-known target of IL-6 signaling was assessed, and we found p-Stat3 level to be clearly increased upon IL-6 stimulation (Figure 4.2.4.1 A). The effect of IL-6 stimulation of HPVEC on proliferation was determined by BrdU assay (Figure 4.2.4.1 B). For quantitation of apoptosis, the Caspase-GLO® 3/7 assay was used and senescence was estimated by quantifying senescence-associated beta-galactosidase activity (Figure 4.2.4.1 C & D). Neither BrdU, nor Caspase-GLO® 3/7 assays showed significant differences after treatment with IL-6, indicating no effect of IL-6 on EC proliferation and apoptosis. Conversely, IL-6 showed a concentration-dependent effect (10 ng/mL, $p$ 0.057; 50 ng/mL, $p$ 0.029) on senescence of EC deduced from significantly elevated senescence-associated beta-galactosidase activity (Figure 4.2.4.1 D). No clear effect was detected for tube formation capacity after IL-6 stimulation (Figure 4.2.4.1 E).

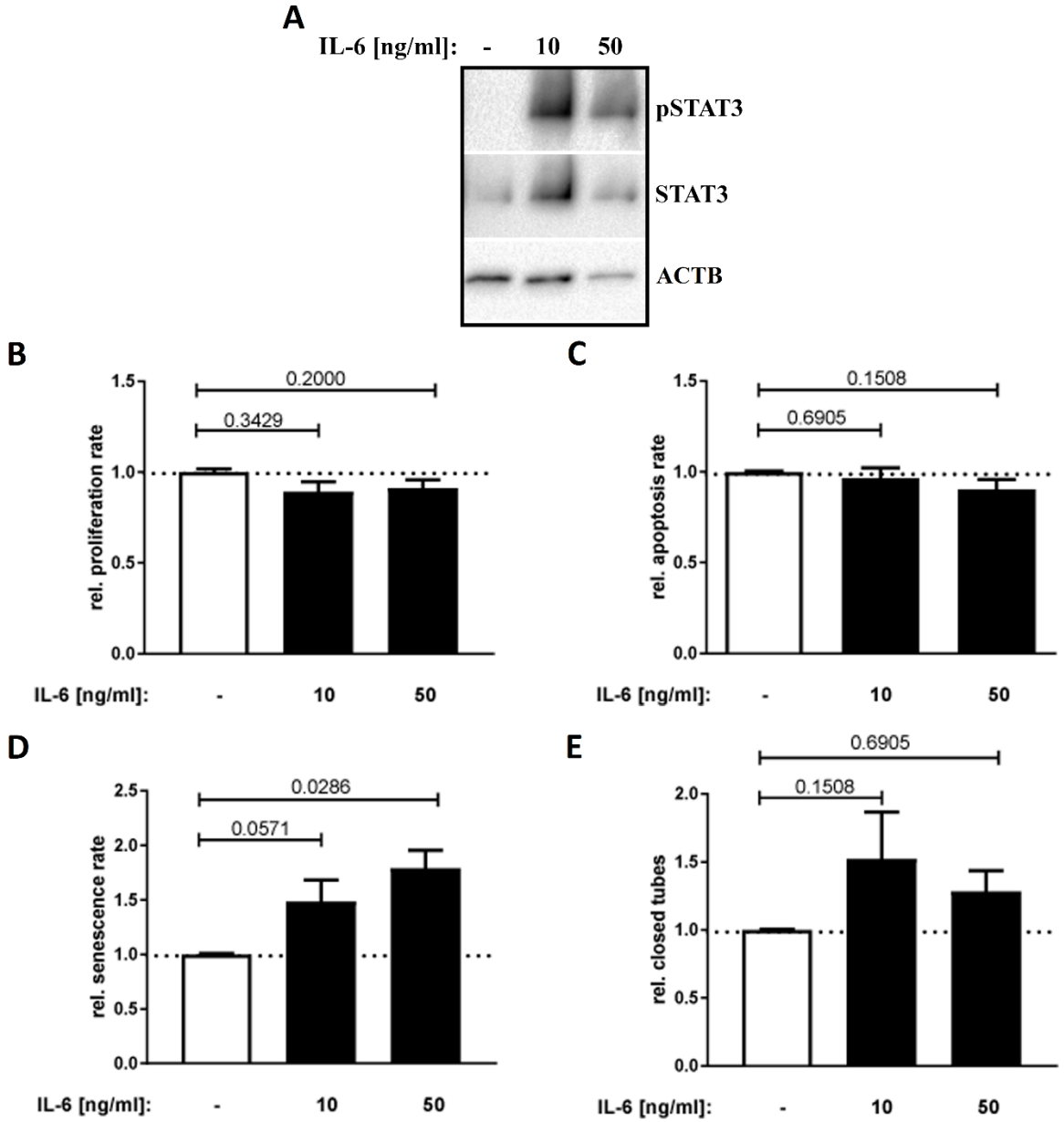


**Figure 4.2.4.1: The effect of IL-6 stimulation on HPVEC.** (A) Analysis of HPVEC after 15 minute-stimulation without (-), with 10 ng/mL or 50 ng/mL of IL-6 by western blot. The level of p-Stat3, total Stat3 and ACTB were detected. (B) Relative proliferation rates were measured with a BrdU assay after HPVEC were stimulated with similar concentrations as in (A) and *n* = 6 replicates. (C) Relative apoptosis rates were assessed by Caspase-GLO® 3/7 assay after HPVEC were stimulated similarly to (A) and *n* = 5 replicates. (D) Relative senescence rates were determined with senescence-associated beta-galactosidase activity assays after HPVEC were stimulated similarly to (A) and *n* = 5 replicates. (E) Tube formation capacity was determined after HPVEC were stimulated similarly to (A) and *n* = 5 replicates. Graphs show mean ± SEM. The *p* value is denoted above graphs in the figure, calculated using Mann-Whitney test. Figure was published in Kretschmer et al. [81], Figure 4 and was modified.

### 4.2.5 No difference in expression of markers for proliferation, apoptosis and senescence, but significant reduction in p-Stat3 in placentas of obese dams

Since increased EC senescence and reduced EC marker expression due to MO were found in placentas, molecular marker expression for proliferation, apoptosis and senescence were also assessed

in whole placental lysates (Figure 4.2.5.1). Results of western blots and densitometric analyses showed no difference for cyclin D1, PCNA (proliferation), γH2A.X (senescence) or cleaved-caspase 3 and PARP (apoptosis) expression between placentas of obese and controls dams. However, p-Stat3 was found to be significantly reduced in placentas of obese dams.

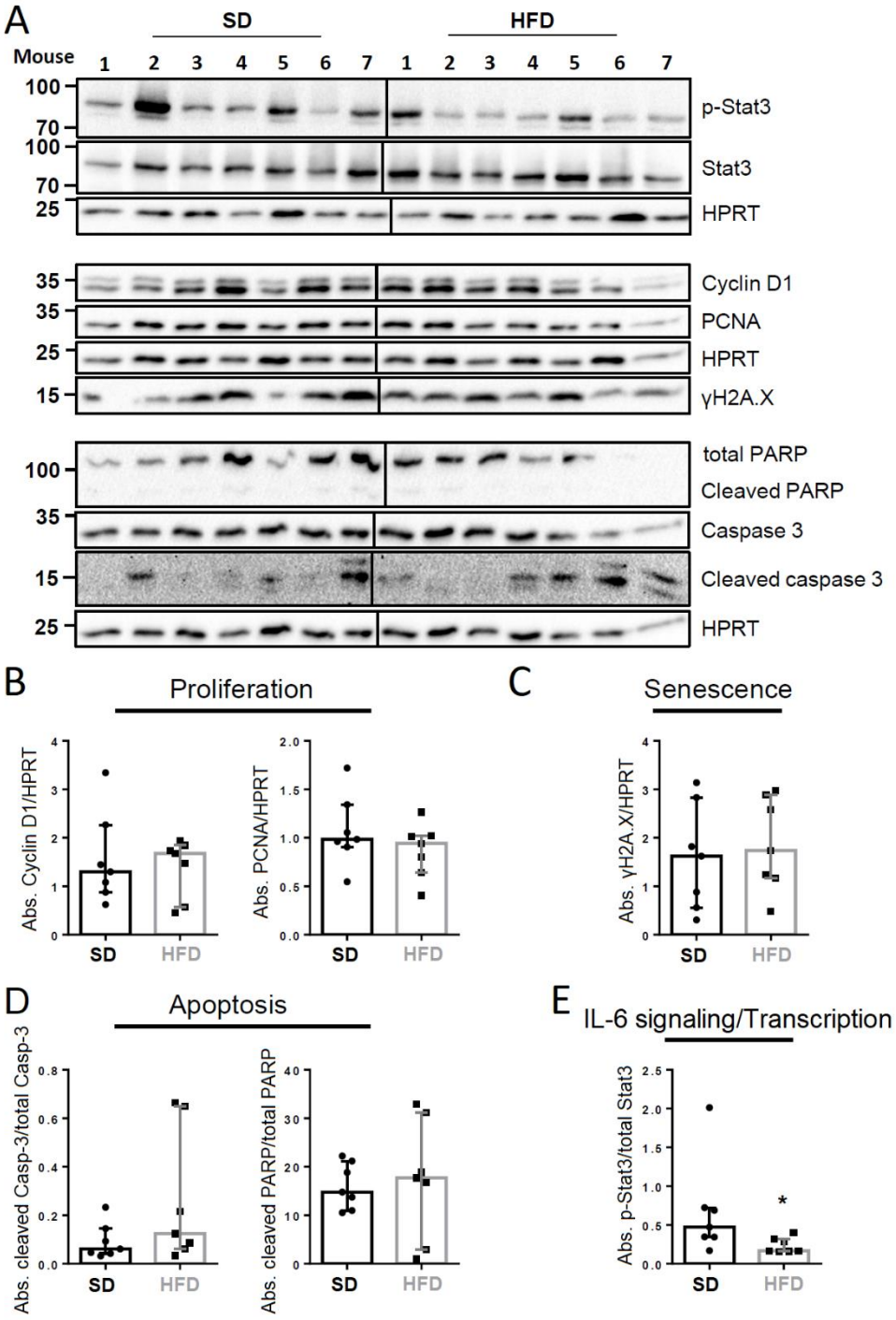


(*Figure caption on the next page*)

**Figure 4.2.5.1: Level of markers for proliferation, senescence, apoptosis and IL-6 signaling/transcription in placentas at E15.5.** (A) Western blotting of placental lysates (SD and HFD: *n* = 7 placentas, 1 per dam) showed p-Stat3, total Stat3, Cyclin D1, PCNA, γH2A.X, PARP, Caspase 3, cleaved caspase 3 and HPRT (loading control) protein level. (B) Densitometric analyses of western blots of proliferation markers Cyclin D1 and PCNA normalized to HPRT. (C) Densitometric analyses of western blots of the senescence marker γH2A.X normalized to HPRT. (D) Densitometric analyses of western blots of apoptosis markers cleaved caspase 3 normalized to total caspase 3 and cleaved PARP (~89 kDA) normalized to total PARP (~116 kDA). (E) Densitometric analyses of western blots of p-Stat3 normalized to total Stat3. Graphs show median ± interquartile range and * $p$ <0.05, calculated using Mann-Whitney test.

## 4.3 MO impairs trophoblast differentiation, disrupts basement membrane integrity and affects cell-cell interactions

Note: This part of the results section, i.e. “MO impairs trophoblast differentiation, disrupts basement membrane integrity and affects cell-cell interactions”, was recently in parts submitted for publication to Biology of Reproduction in the article “Maternal, high fat diet-induced obesity affects trophoblast differentiation and placental function in mice”. The prospective first author is Tobias Kretschmer and the work presented was made possible through the assistance of several others:

Animal handling and tissue collections was performed by Eva-Maria Turnwald, Marion Handwerk, Sarah Appel and Tobias Kretschmer. LCM procedure and protein extraction was conducted by Tobias Kretschmer. Quantitation after SP3 lysis was done by the staff of the Cologne Proteomics Facility (CECAD), supervised and statistically analyzed by Christian K. Frese. The qPCR assays were prepared and performed by Maria Wohlfarth, while data calculation was done by Tobias Kretschmer. Protein isolation, detection and densitometric analysis were performed by Tobias Kretschmer. Placenta collection by perfusion fixation was conducted by Marion Handwerk and Tobias Kretschmer, while tissue embedding and sectioning was done by Mojgan Ghilav. Electron microscopy was performed by Tim van Beers and Wilhelm Bloch and observations were interpreted by Wilhelm Bloch and Tobias Kretschmer. Histological stainings (IHC, IF, Oil Red O and Stereology) were performed by Tobias Kretschmer, while picture processing and scripting for Oil Red O and stereology was done by Peter Zentis and analysis of Oil Red O and stereology sections was conducted by Tobias Kretschmer. Cell culture assays and analyses (AdipoRed and permeability assays) were performed by Tobias Kretschmer. Data collection and statistical analyses were performed by Peter Zentis and Tobias Kretschmer. The project was supervised and supported by technical input and advice from Inga-Bae Gartz, Eva Hucklenbruch-Rother, Jörg Dötsch and Sarah Appel.

### 4.3.1 The proteomics profile of the Lz is altered regarding cell adhesion and AJ markers in obese dams

LCM was used on cryo-preserved tissue sections of placentas to specifically dissect and collect the Lz for the analysis of its proteome profile. Studying the proteomics profile of the Lz permits detection of a high number of proteins and can drive a hypothesis-generating approach. In placentas of obese and control dams, proteomics profiling revealed two distinct component clusters for each group SD and HFD (Figure 4.3.1.1 A) and 1619 proteins were detected. Among these, 126 proteins were significantly

different in expression between both groups. For the 126 proteins, *q* value was below 0.05 and the Log2 difference was ≤ -0.454 (< 0.73-fold) and ≥ 0.406 (> 1.33-fold) (Appendix 6.2, Table 6.1). These detected proteins were put into String database (version 11) and a network of protein clusters was generated in which functional pathways and the confidence of protein interactions can be displayed [96].

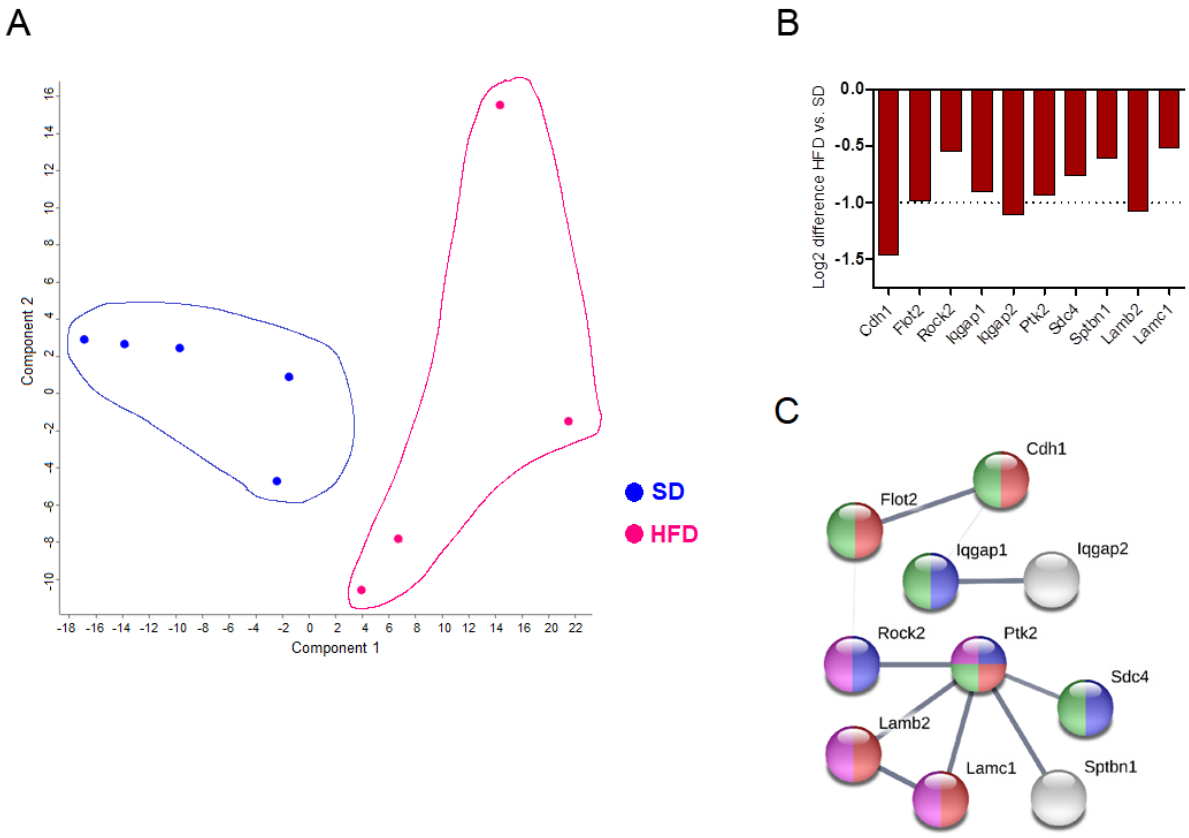


**Figure 4.3.1.1: Proteomics profiling revealed altered protein level and clustering under MO.** (A) Clustering and principal component analysis revealed two different clusters for control (blue, *n* = 5 placentas, 1 placenta per dam) and obese (magenta, *n* = 4 placentas, 1 placenta per dam) dams. (B) Protein quantitation by proteomics profiling of markers for adhesion and cell junction in the Lz from obese compared to control dams. To represent halving in expression level, a dotted line was added at a Log2 difference of -1.0. Graphs show mean values. (C) String database-generated network of protein interactions in which red-colored nodes (Cdh1, Flot2, Ptk2, Lamb2, and Lamc1) are markers of cell adhesion processes, green-colored nodes (Cdh1, Flot2, Iqgap1, Ptk2, and Sdc4) are related to adherens junctions, blue-colored nodes (Iqgap1, Rock2, Ptk2, and Sdc4) are related to the regulation of cell junction assembly, and magenta-colored nodes (Ptk2, Rock2, Lamb2, and Lamc1) are proteins of the KEGG pathway of focal adhesion. The graphic was made in String v11 with the thin lines between nodes representing a low interaction and low confidence score (0.150) and the thick lines between nodes representing a medium to high interaction and confidence score (>0.400) [96]. All proteins denoted in this figure were significantly altered as determined by Student's *t* test and Benjamini-Hochberg correction [92] with a *q* value <0.05. Figure is in revision for publication in Kretschmer et al. Biology of Reproduction 2020, Fig. 1 and was modified.

From the list of 126 significantly altered proteins, 78 proteins were categorized as *protein binding* by String database, 60 proteins were involved in *cellular component organization*, 13 were related to *cell*

*junctions*, and 4 proteins were related to *focal adhesion*. Among the set of 126 proteins detected in the Lz, E-cadherin was found to be the most prominent of the down-regulated cell junction and cell adhesion-related proteins (Figure 4.3.1.1 B). According to String database, E-cadherin could share protein-interactions with Ptk2, Flot2 and Iqgap1 which are also down-regulated junction and adhesion-related proteins. Furthermore, two subunits of the major basement membrane protein laminin, i.e. Lamb2 and Lamc1, were also found to be significantly decreased in expression (Figure 4.3.1.1 B & C). These results suggest altered cell-cell and cell-basement membrane adhesion in placentas of obese dams as a consequence of down-regulation of these proteins.

### 4.3.2 Localization of AJ markers in the Lz

IHC and IF were used to identify the localization of AJ markers within the Lz and Jz. First, staining for β-catenin revealed its intracellular expression in cells of the Lz and Jz. In the Jz, β-catenin was particularly present in larger trophoblasts and the staining pattern suggests accumulation primarily at the cell membrane boundary and thus the site of cadherin-catenin interaction (Figure 4.3.2.1 A & B). Besides, in SynT of the Lz and fetal ECs, β-catenin was also observed (Figure 4.3.2.1 C). In the Lz, both E-cadherin and P-cadherin were found (Figure 4.3.2.1 D & G), while in the Jz only P-cadherin was weakly stained by IHC and IF (Figure 4.3.2.1 G – I). The transition from Jz to Lz could be well-observed by E-cadherin staining which indicates that this cadherin is exclusively and most prominently expressed in the Lz (Figure 4.3.2.1 D – F). Using confocal microscopy, the localization of E-cadherin towards the SynT cell boundary where cell junctions between SynT layer I and II are present could be highlighted (Figure 4.3.2.1 E). Towards the fetal endothelium, there were yellow artifacts of signal overlay. On the other hand, P-cadherin expression seemed limited to the apical face of SynT (Figure 4.3.2.1 H). VE-cadherin expression was not clearly possible to denote from IHC and IF stains and green staining artifacts were observed in fetal blood vessels (Figure 4.3.2.1 J – L). These observations were similar in placentas from obese and control dams.

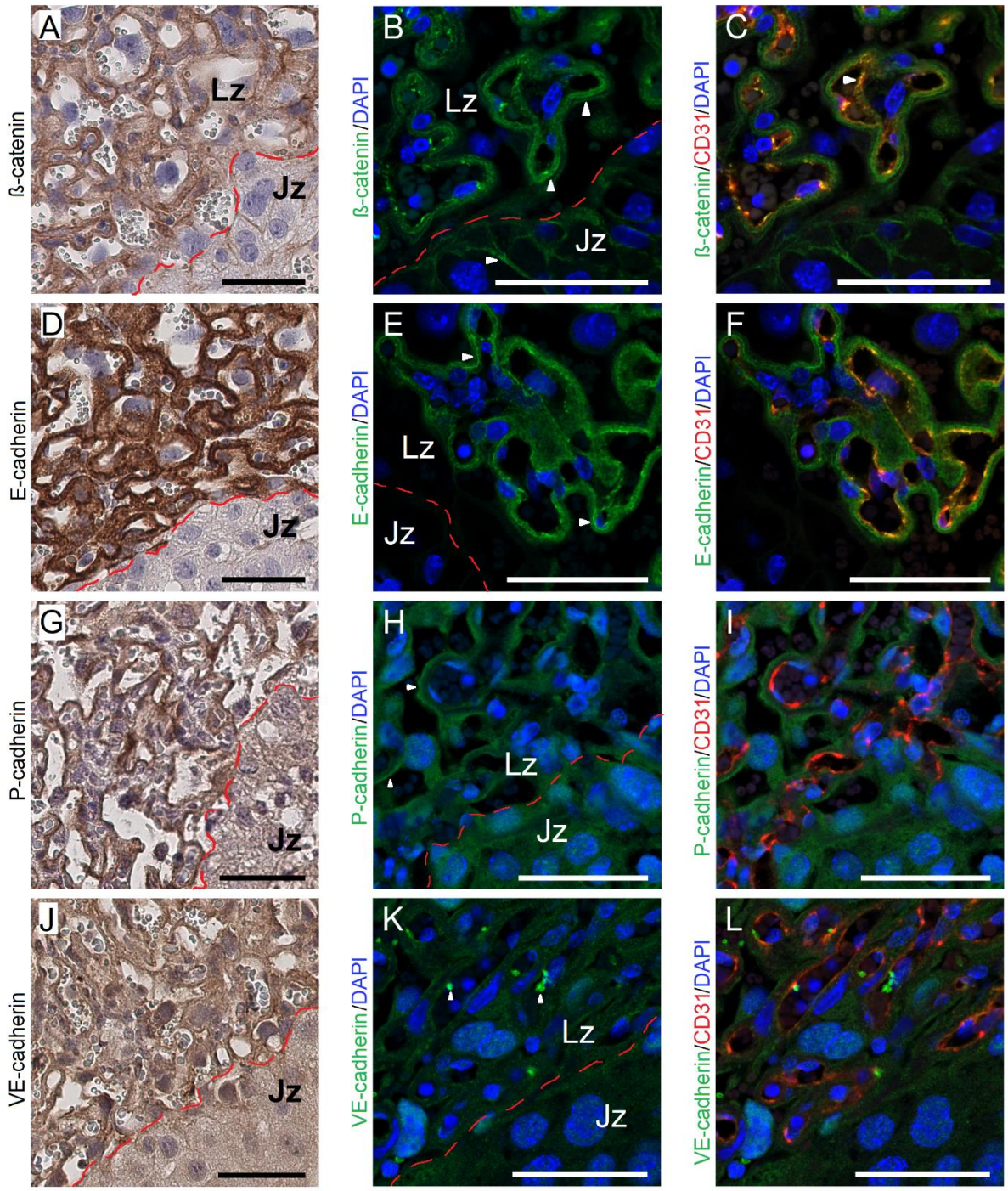


**Figure 4.3.2.1: AJ marker localization in murine placentas by IF and IHC.** Representative images are derived from control placentas since HFD had no influence on staining patterns. (A, D, G, J) IHC showed localization of β-catenin (A), E-cadherin (D), P-cadherin (G) and VE-cadherin (J) and dotted lines in these panels A, D, G and J denote the transition from Lz to Jz. (B, C, E, F, H, I, K, L) IF staining showed β-catenin (B & C, green) in SynT (B, vertical arrow heads) and in trophoblasts of the Jz (B, horizontal arrow head) and co-localization to fetal capillary CD31-positive (red) ECs (C, arrow head). SynT in the transfer zone were E-cadherin-positive (E & F, green) highlighting SynT cell boundaries (E, arrow heads) with minor yellow artifacts (F) towards the endothelial side. P-cadherin was localized towards maternal blood sinuses (H & I, green), probably in MTB (H, arrow heads). VE-cadherin staining was very poor with green dotted artifacts (K, arrow heads) and indicated no specific IF signal and no clear IHC staining pattern (J – L). Scale bars: 50 µm. Figure is in revision for publication in Kretschmer et al. Biology of Reproduction 2020, Fig. 2A and was modified.

### 4.3.3 Significant reduction of AJ markers expression under MO at E15.5

Next, the integrity of AJ was examined by protein quantitation of AJ markers in whole placental lysates. We previously reported down-regulation of β-catenin in placentas of obese dams at E15.5 [93], however in this work, total β-catenin was down-regulated without reaching statistical significance (*p* 0.053) in whole placenta lysates. The β-catenin phosphorylated at tyrosine 654 (phosphorylated Y654-β-catenin) is a marker for reduced E-cadherin to catenin-binding and is observed at ~88 kDa by a fade band in our western blots (Figure 4.3.3.1 A) together with a second band at ~92 kDa which is the size of total β-catenin. Western blot with an antibody specific to total β-catenin confirmed that the 92 kDa band detected by the phosphorylated Y654-β-catenin-antibody belongs to total β-catenin. The data showed a trend towards up-regulation in placentas of obese dams of phosphorylated Y654-β-catenin, again with a certain degree of variability in expression level (Figure 4.3.3.1 A & B). Among the cadherins, E-cadherin was found significantly reduced, P-cadherin and VE-cadherin showed no clear change in expression level compared to controls, but displayed high variability in expression level. Similar to observations from western blotting, proteomics profiling specifically of the Lz also showed a significant reduction in E-cadherin and a strong tendency for β-catenin down-regulation (Log2 difference -1.2 in obese vs. control, *q* 0.059). On mRNA level, no difference in E-cadherin and VE-cadherin expression level were measured in whole placental samples, however, β-catenin expression was strongly reduced (*p* 0.016) when normalized to any of the two housekeeping genes (HPRT and ACTB) in placentas from obese dams. P-cadherin expression was only significantly reduced when normalized to ACTB (*p* 0.031), but not HPRT (Figure 4.3.3.1 C).

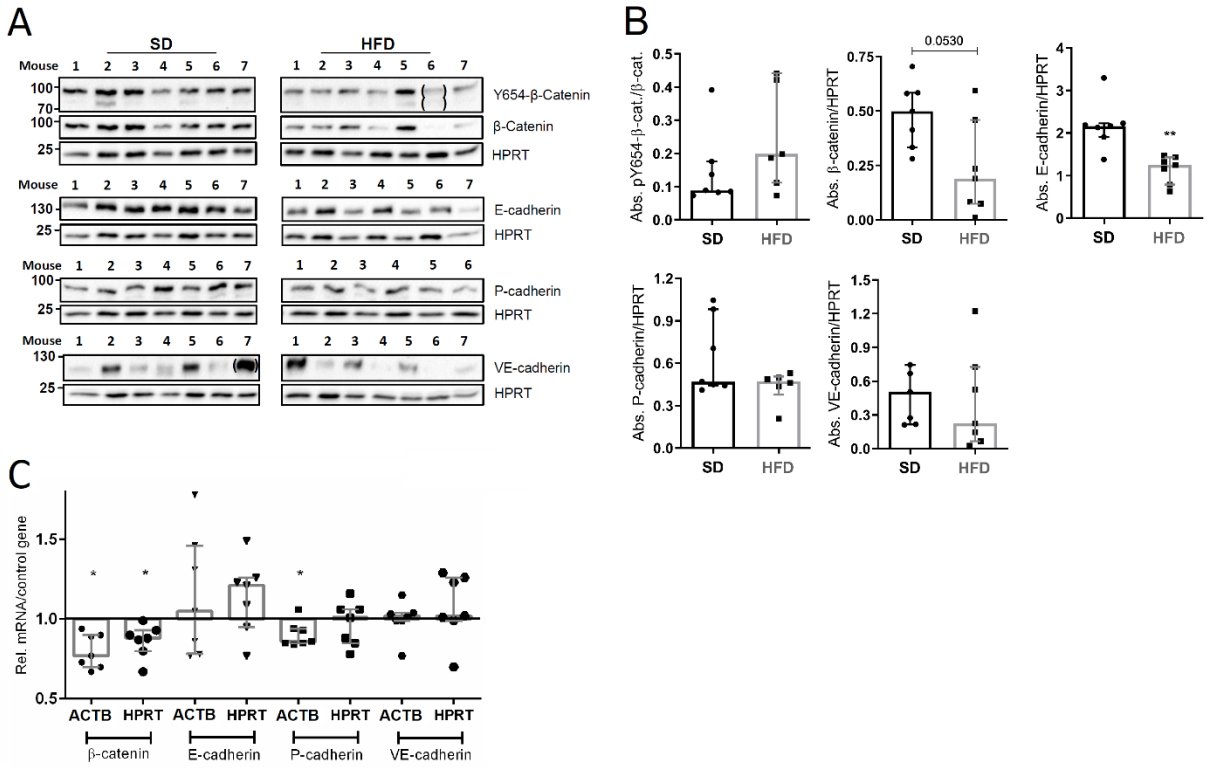


(*Figure caption on the next page*).

**Figure 4.3.3.1: Level of AJ markers on protein and mRNA level in placentas at E15.5.** (A) Western blotting of whole placental lysates (SD and HFD: *n* = 7 placentas, 1 per dam) showed phosphorylated Y654-β-catenin (lower band at ~88 kDa), total β-catenin (~92 kDa), E-cadherin, P-cadherin, VE-cadherin and HPRT (loading control) level. (B) Densitometric analyses of western blots of phosphorylated Y654-β-catenin, total β-catenin, E-cadherin, P-cadherin, VE-cadherin normalized to HPRT. Two outliers were excluded from graph, i.e. phosphorylated Y654-β-catenin (~88 kDa band, HFD mouse 6) and VE-cadherin (SD mouse 7) indicated by brackets "( )". Graphs show median ± interquartile range and * *p* value <0.05, ** *p* <0.01, or *p* value is shown above graph. (C) Analyses of gene expression of AJ markers in placentas by qPCR. Normalization was performed with housekeepings HPRT and ACTB and relative expression level of HFD normalized to SD (line at 1.0) are shown in graphs. *n* = 7 placentas, 1 per dam, for SD and HFD. Graphs show median ± interquartile range and * *p* <0.05, calculated using Mann-Whitney test. Figure is in revision for publication in Kretschmer et al. Biology of Reproduction 2020, Fig. 2B, C and D, and was modified.

### 4.3.4 MO affects cell homeostasis and cell junctions in the transfer zone and causes lipid accumulation in the Lz

By means of electron microscopy, we aimed to examine ultrastructure and cell junctions in the transfer zone of placentas. Control placentas (Figure 4.3.4.1 A – C) displayed a regular phenotype of the transfer zone with SynT layer I and II. Both layers shared an undulated cell boundary and had intact cell-cell contacts and AJ showing syncytial fusion. Fetal ECs showed ordinary paracellular clefts with AJ and tight junctions as well as desmosomes which were identified by higher electron density. Additionally, the BM was found regular in thickness and a few segments displayed small deposits of ECM material. In SynT, lipid and lipoprotein deposits were rarely seen and their extent was rather small. As a consequence, the SynT developed normally and fused which was also evident from SynT II to BM contact which was continuous showing no detachments. In stark contrast to controls, placentas from obese dams (Figure 4.3.4.1 D – F) displayed major lipid and lipoprotein deposition which could be intracellular and extracellular of SynT. The BM was disrupted with excessive lipid and ECM accumulation also showing detachment of ECs on one side and SynT on the other side. Besides, both ECs and trophoblasts appeared condensed frequently and with irregular nuclei, while the SynT II seemed loose from the BM on its basal side. Furthermore, the SynT showed a defective differentiation by the absence of a defined cell boundary in electron density which was observed in control placentas. Although ECs and SynT showed damaged connection to the BM, there were no apoptotic cells visible. On some trophoblasts, entangled membrane deposits and lipoprotein structures were observed in placentas of obese dams, but not in control dams.

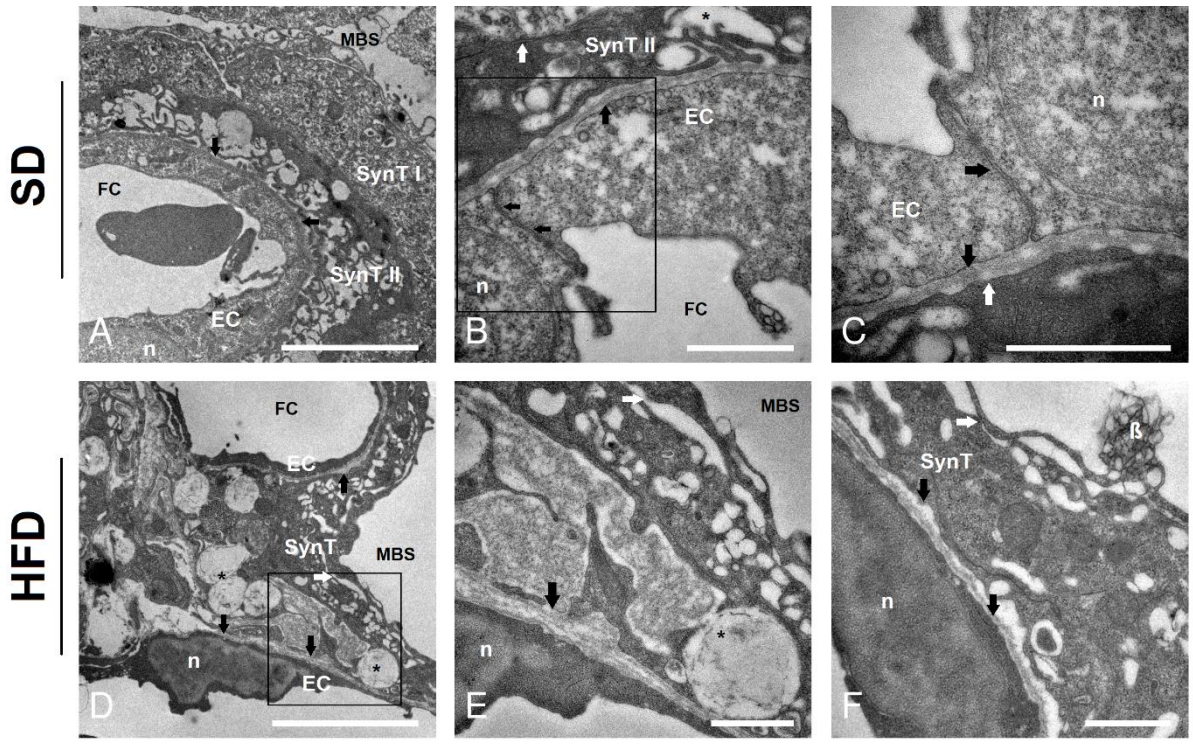


**Figure 4.3.4.1: Ultrastructure of the maternal transfer zone of SD and HFD placentas.** (A – C) The phenotype of control placentas shows the materno-fetal transfer zone with a fetal capillary (FC), endothelial cell (EC) and nucleus (n) in addition to the basement membrane (BM, black arrows in A, vertical black arrows in B & C). The condensed syncytiotrophoblast layer II (SynT II) and the fused SynT I were observed. The SynT I faces towards maternal blood sinus (MBS) on one side and the SynT II on the other side (horizontal white arrow in B). EC showed paracellular cleft with cell junctions (horizontal black arrows in B & C), i.e. with AJ and electron dense desmosomes. The separating BM between EC and SynT II sporadically showed extracellular matrix deposition (ECM, vertical black arrows in B & C). In (B), a small deposit of lipids can be seen (*). (C) A close-up of the framed area in (B). (D – F) The ultrastructure in HFD placentas. The BM was disrupted and enriched in ECM deposits (vertical black arrows) and ECs and their nuclei appeared condensed. The SynT accumulated high amounts of lipids and lipoproteins (*) and seemed undifferentiated and unfused, therefore a second SynT layer could not be observed. The connection of ECs and SynT to the BM was disrupted and discontinuous (vertical black arrows in E & F). Cell junctions of SynT were barely present (horizontal white arrows in E & F) and entangled cell debris (ß) was observed towards the MBS on SynT surface (F). The frame in (D) shows the close-up in (E). In total, 5 different placentas per group, 1 per dam, were analyzed and representative images are shown. Scale bar: A & D 5 µm; B, C, E & F 1 µm. Figure is in revision for publication in Kretschmer et al. Biology of Reproduction 2020, Fig. 3 A – F and was modified.

Since extensive lipid deposition was observed in placentas of obese compared to control dams, lipid accumulation in the transfer zone was determined by a semi-quantitative approach using Oil Red O staining of placental sections. Sections were stained (Figure 4.3.4.2 A – D) and analyzed by pixel quantitation which showed a significant increase in Oil Red O-positive area fraction (*p* 0.004, Figure 4.3.4.2 E) and thus, a significantly augmented lipid accumulation in the transfer zone of placentas of obese dams compared to controls. Red-stained lipid droplets were found in or between SynT which indicates a similar pattern of staining to the pattern of deposition observed under electron microscopy (Figure 4.3.4.1 A & D).

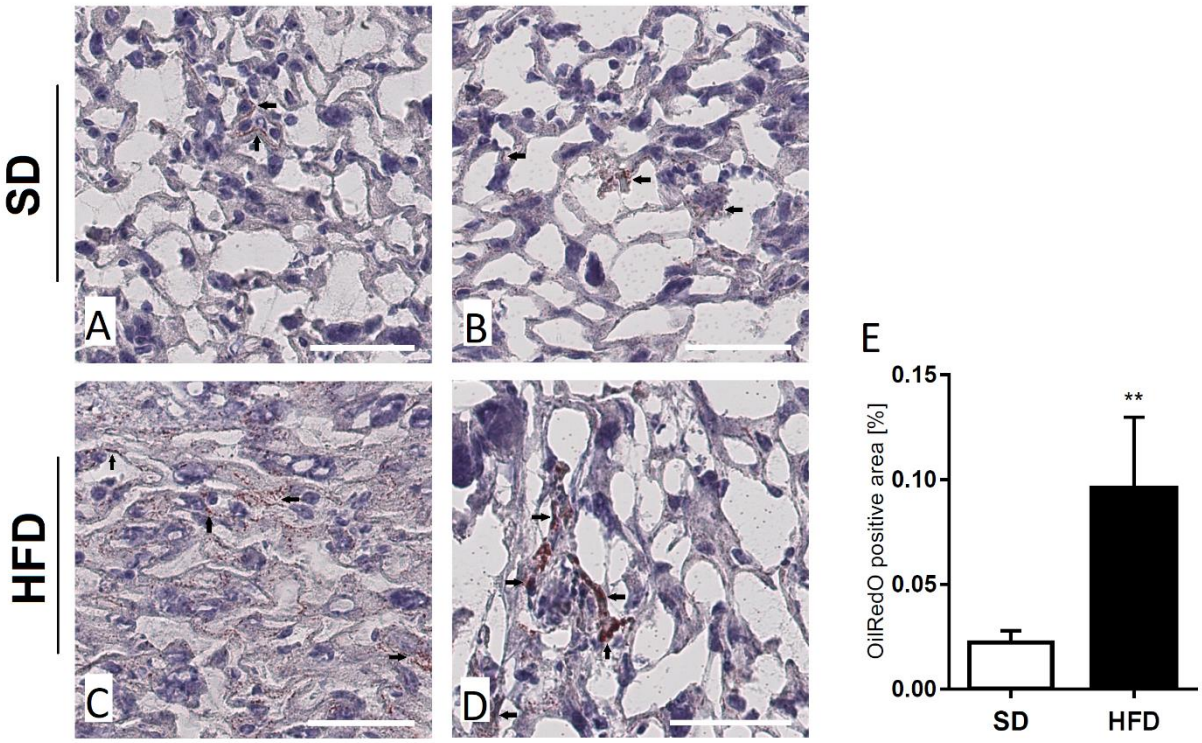


**Figure 4.3.4.2: Lipid quantitation by Oil Red O staining of placental Lz.** (A & B) In the Lz of SD placentas, small clusters of Oil Red O stained lipid deposits (arrows) were observed mostly in trophoblasts of the syncytium (A). (C & D) In HFD Lz, the staining pattern was more intense and deposits of lipids appeared larger than in SD, similar to what was observed under EM (arrows in D). Each panel shows a different placenta, in total 5 placentas from 5 dams for SD and 6 placentas from 6 dams for HFD were analyzed. (E) Semi-quantitation of Oil Red O-positive pixel area fraction in the Lz of SD and HFD placentas ($n$ = 5 placentas for SD and $n$ = 6 placentas for HFD, 1 placenta per dam). Graph shows mean ± SEM, ** $p$ <0.01, calculated using Student's $t$ test. Figure is in revision for publication in Kretschmer et al. Biology of Reproduction 2020, Fig. 3 G – K and was modified.

### 4.3.5 MO affects placental morphology and impairs Lz development

We previously reported that vascularization of the placenta was severely affected by MO, as assessed by stereology [81]. Further stereological assessment showed that total placental volume was significantly increased ($p$ 0.029, Figure 4.3.5.1 A) in placentas from obese dams and Lz:total placental volume ratio was strongly decreased ($p$ 0.021, Figure 4.3.5.1 C) under MO. However, there was no difference in the volume fraction of the Lz between control and obese dams, while there was a trend towards reduction of the Lz:Jz ratio ($p$ 0.150, Figure 4.3.5.1 B). Therefore, the relations between the exchange zone for nutrients and oxygen, the Lz, total placental volume and probably Jz volume are disturbed which implies an impaired development of the Lz under MO.

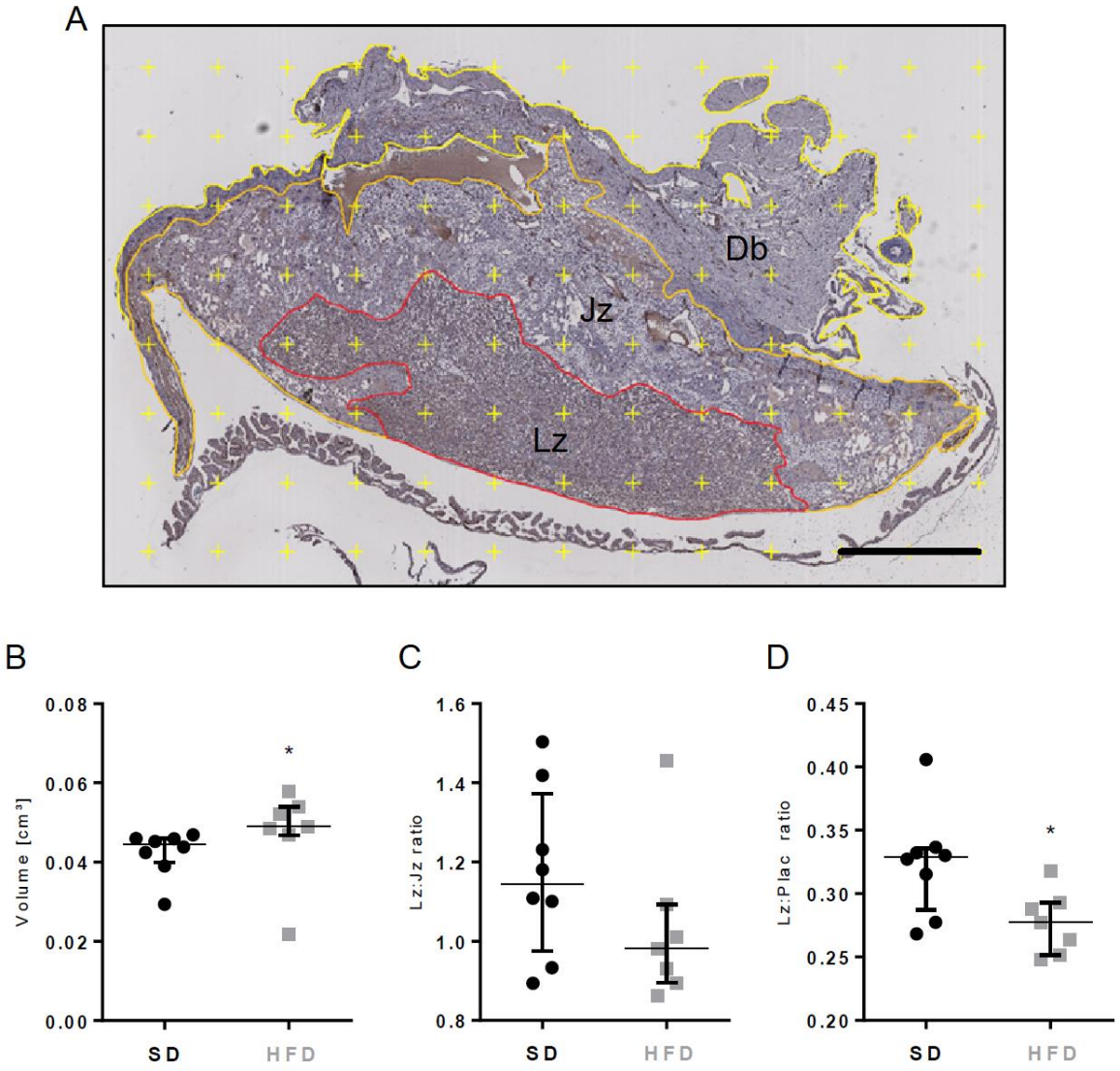


**Figure 4.3.5.1: Stereological assessment of placentas from SD and HFD dams.** (A) Representative image of a total placenta stained with CD31-IHC to show the different placental zones (Lz = red outline, Jz = orange outline, Db = yellow outline). The yellow crosses represent an area of 250,000 µm². Scale bar: 1 mm. (B) Lz to Jz volume ratio and (C) Lz to total placenta volume ratio were determined in SD (*n* = 8 placentas from 8 dams) and HFD (*n* = 7 placentas from 7 dams). Ratios are shown in arbitrary units. Graphs display median ± interquartile range, * *p* <0.05, calculated using Mann-Whitney test. Figure is in revision for publication in Kretschmer et al. Biology of Reproduction 2020, Fig. 4 D – F and was modified.

### 4.3.6 Fatty acid stimulation of BeWo cells reduces β-catenin protein level and affects lipid accumulation and cell layer permeability

The HFD used in this study contains high amounts of fatty acids compared to the SD. Among these fatty acids are palmitic acid (PA), oleic acid (OA) and linoleic acid (LA) and these fatty acids were therefore used in cell culture studies with trophoblast-like BeWo cells. We aimed to determine the effect of PA, OA and LA on protein level of AJ markers, intracellular lipid accumulation and cell layer permeability (Figure 4.3.6.1). PA, OA and LA were used at two different concentrations, however, none had an effect on E-cadherin protein level. Conversely, stimulation with 1000 µM of LA significantly decreased total

β-catenin protein level (*p* 0.029) and also significantly increased the relative cell layer permeability (*p* 0.029). On the other hand, a significant decrease (*p* 0.029) in cell layer permeability was found after stimulation with 500 µM OA. Furthermore, when BeWo cells were stimulated with OA at a concentration of 1000 µM, a tendency towards increased lipid accumulation was observed, however, other fatty acids had no such effect. Therefore, isolated LA at high concentrations can affect intracellular β-catenin level and BeWo cell layer permeability.

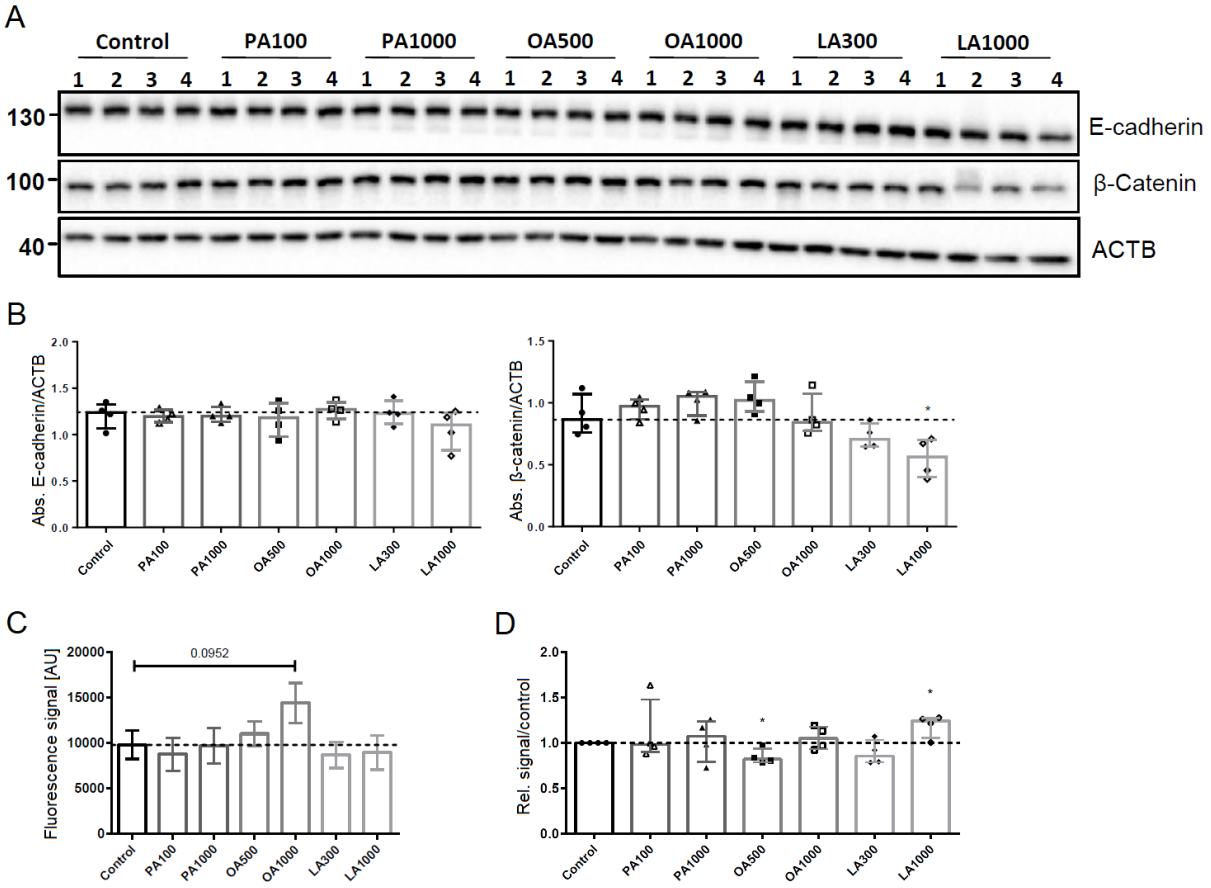


**Figure 4.3.6.1: Effects of stimulation with fatty acids on AJ marker protein level, cellular lipid accumulation and cell layer permeability in BeWo cells.** (A) Western blot after 24 hours stimulation of BeWo cells with various fatty acids (PA, OA, LA) at concentrations between 100 µM and 1000 µM (as indicated in the graphs). (B) Results of densitometric analyses of western blots for proteins E-cadherin and β-catenin normalized to ACTB. Bar graphs show median ± interquartile range, * *p* <0.05, calculated using Mann-Whitney test, *n* = 4 replicates (1 – 4 as indicated). (C) Results of AdipoRed assays showing relative lipid accumulation after 8 hours of stimulation with fatty acids at above-mentioned concentrations in BeWo cells. Bar graphs show fluorescence signal [AU], *n* = 5 replicates as mean ± SEM, and the *p* value for control versus OA 1000 µM is indicated above the graph, calculated using Mann-Whitney test. (D) Relative cell layer permeability normalized to control after 24 hours of stimulation with fatty acids. Bar graphs show median ± interquartile range, * *p* <0.05, calculated using Mann-Whitney test, *n* = 4 replicates. Figure is in revision for publication in Kretschmer et al. Biology of Reproduction 2020, Fig. 5 and was adapted.

IF staining for E-cadherin after stimulation of BeWo cells with either fatty acid (PA, OA or LA) or control revealed no major differences in staining patterns (data not shown). In these examples, E-cadherin was localized to the cell boundary and in several cells, it was also observed diffusely in the cytoplasm.

### 4.4 Passive transfer is significantly increased across the placental barrier, but glucose transport and metabolization rate seem unaltered under MO

Note: The part under 4.4.1 of the results section, i.e. “Materno-fetal transfer capacity is significantly increased under MO”, was recently in parts submitted for publication to Biology of Reproduction in the article “Maternal, high fat diet-induced obesity affects trophoblast differentiation and placental function in mice”. The prospective first author is Tobias Kretschmer and the work presented was made possible through the assistance of several others:

Animal handling for *in vivo* studies were performed by Marion Handwerk, Sarah Appel, Heike Endepols and Tobias Kretschmer. Placenta and fetus collection after isoflurane anesthesia was conducted by Marion Handwerk and Tobias Kretschmer. Positron emission tomography (PET) was conducted by Heike Endepols. Data collection and statistical analyses were performed by Heike Endepols and Tobias Kretschmer. The project was supervised and supported by Heike Endepols, Jörg Dötsch and Sarah Appel.

#### 4.4.1 Materno-fetal transfer capacity is significantly increased under MO

Since AJ marker level were reduced in mice *in vivo* under MO and in BeWo cells *in vitro* after fatty acids stimulation, together with ultrastructural defects in the Lz and reduced cell layer permeability *in vitro* after stimulation with LA, we aimed to determine materno-fetal transfer capacity *in vivo* by means of $^{14}$C-mannitol administration and liquid scintillation. $^{14}$C-mannitol is an inert radio-labeled tracer that crosses the placenta and reaches the fetal circulation without depending on active transporters and was therefore used as a marker of Lz integrity. Materno-fetal clearance ($K_{mf}$) was determined after accumulation of the non-metabolizable tracer $^{14}$C-mannitol in fetal lysates and liquid scintillation. The $K_{mf}$ significantly increased in offspring of obese dams compared to controls ($K_{mf}$ 166.4 *vs* 113.5, Effect size -52.93, CI -82.92 to -19.93, *p* 0.002) by a margin of 46.6% ± 14.6% (Figure 4.4.1.1 A). Additionally, fetal weight was recorded and significantly decreased by 8.5% ± 2.5% in offspring of obese dams (0.362 g *vs* 0.396 g, Effect size 0.0336g, CI 0.0136 to 0.0536, *p* 0.001, Figure 4.4.1.1 B), however, placental weight was unaltered (Figure 4.4.1.1 C). MO is thus associated with increased materno-fetal transfer capacity while offspring develop a growth restriction *in utero* as shown before in cohort A057 [93].

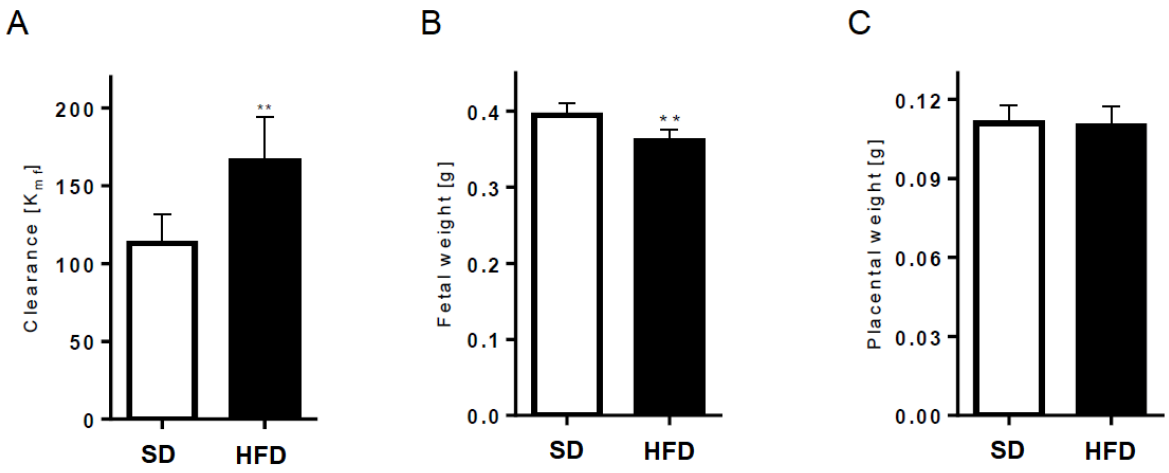


**Figure 4.4.1.1: Materno-fetal clearance, fetal and placental weight under MO.** (A) Materno-fetal transfer capacity (clearance) across the placental barrier of radiolabeled $^{14}$C-mannitol in SD and HFD dams. *n* = 39 fetuses from 5 dams for SD and *n* = 41 fetuses from 5 dams for HFD. (B) Fetal weight in SD and HFD offspring, *n* = 34 fetuses from 5 dams for SD and *n* = 42 fetuses from 5 dams for HFD. (C) Placental weight of SD and HFD placentas, *n* equals *n* under (B). Graphs show mean ± confidence interval, ** *p* <0.01, calculated using Student's *t* test. Figure is in revision for publication in Kretschmer et al. Biology of Reproduction 2020, Fig. 4 A – C and was modified.

### 4.4.2 Glucose transport and metabolization rate are probably unaltered under MO

The radio-labelled glucose analogue $^{18}$F-FDG was used to study glucose metabolization in control and obese dams and also to assess glucose transfer to fetuses via the placenta. PET was used to detect $^{18}$F-FDG accumulation in maternal and fetal tissue and the signal in fetal tissues was normalized to the injected dose corrected for body weight (SUVbw). The Patlak-approach with a lumped constant of 0.6 was used to calculate the glucose metabolization rate (GMR). Analyses of PET scans revealed the highest signal of $^{18}$F-FDG in fetal heart-liver area (Figure 4.4.2.1 A & B). Time-activity curve showed that directly after $^{18}$F-FDG injection, the signal in the aorta went to a maximum and subsequently plummeted. At the same time, the signals in fetal tissue and maternal spinal cord increased up until the end of the measurement at 60 minutes (Appendix 6.3, Figure 6.2.1). Based on these values, time-activity-curve rations (TAC ratios) were calculated with the signal from fetal tissue normalized to the signal from maternal spinal cord. The resulting TAC ratios showed no difference between obese and control dams (Figure 4.4.2.1 C). There was no significant difference in the data for relative $^{18}$F-FDG signal in fetal tissue when displayed as SUVbw (*p* 0.222, Figure 4.4.2.1 D). However, maternal blood glucose concentration significantly correlated with the signal in fetal tissue in control dams (*p* 0.021, R 0.83), but not in obese dams (*p* 0.25, R -0.63, Figure 4.4.2.1 E). These results indicate that net transfer of glucose across the placenta to fetal tissues is similar in obese and control dams. However, the positive correlation between maternal blood glucose and glucose supply to fetal tissues is absent in obese dams which indicates a disturbed regulation in glucose supply in obese dams.

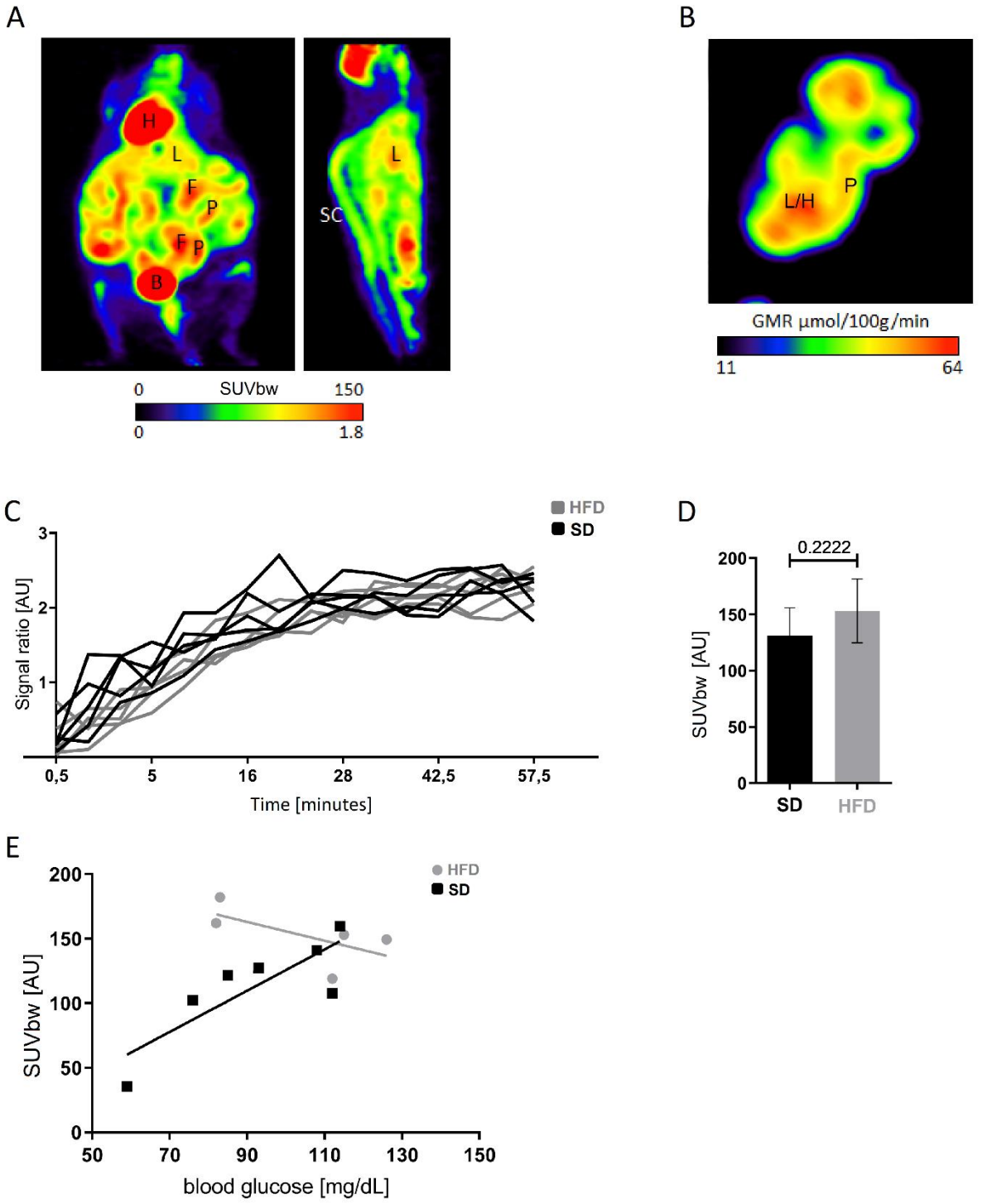


**Figure 4.4.2.1: $^{18}$F-FDG PET studies in SD and HFD dams.** (A) PET scan of an obese dam 60 minutes after $^{18}$F-FDG injection. Heart (H) and bladder (B) accumulated most of $^{18}$F-FDG, however, fetuses (F) and placentas (P) also accumulated $^{18}$F-FDG. The aorta of dams was used to normalize signals for Patlak analysis and calculate glucose metabolization rate (GMR). (B) PET scan image showed localization of $^{18}$F-FDG to the fetal heart-liver area and placentas. (C) Based on normalization of the injected dose (SUVbw) of $^{18}$F-FDG, TAC ratios were calculated for each dam over a course of 57.5 minutes (arbitrary units, AU). *n* = 5 dams for both SD and HFD. (D) Quantitation of $^{18}$F-FDG signal in fetal tissues normalized to SUVbw in SD and HFD dams. *n* = 5 dams for both SD and HFD. Bar graphs show mean ± SEM. The *p* value is indicated above graphs, calculated using Mann-Whitney test. (E) Linear regression of the $^{18}$F-FDG signal in fetal tissues normalized to the injected dose depending on maternal blood glucose in SD (black) and HFD (gray) dams. *n* = 7 dams for SD and *n* = 5 HFD. SD (black) *p* 0.021, R 0.83; HFD (gray) *p* 0.25, R -0.63, calculated using linear regression analysis.

### 4.5 Dynamics in AJ and EC marker expression during placental development

Results in this section, i.e. “Dynamics in AJ and EC marker expression during placental development”, have not been published or submitted by the time of writing this thesis. The work described hereafter was made possible with the help of several others:

Animal handling and tissue collection were performed by Eva-Maria Turnwald, Marion Handwerk, Sarah Appel and Tobias Kretschmer. Protein isolation, detection and densitometric analysis were performed by Tobias Kretschmer. Data collection and statistical analyses were performed by Tobias Kretschmer. The work was supervised and supported by Jörg Dötsch and Sarah Appel.

#### 4.5.1 Vascular and AJ marker dynamics in placentas of SD and HFD dams from E11.5 to E18.5

The placenta is a temporary organ which needs to develop in close concert with the embryo and adapt to its demands by a dynamic expression pattern of various markers and other factors. Under 4.3.1 and 4.3.3, it was reported that under MO at E15.5, various markers of the AJ are differentially expressed compared to control placentas. To assess the course of AJ marker and CD31 level from mid-gestation to shortly before term, E11.5, E15.5 and E18.5 placentas were analyzed by western blot (Figure 4.5.1.1). In placentas of obese dams, CD31 level was highest at E11.5 and declined gradually until E18.5 where it was significantly reduced ($p$ 0.026) compared to E11.5. In control placentas, there was a trend of down-regulation from E11.5 to E18.5 ($p$ 0.093) and further, a significant decrease between E15.5 and E18.5 which was not observed in placentas of obese dams. Moreover, VE-cadherin level significantly plummeted from E11.5 to E15.5 under both HFD and SD (both $p$ 0.002). Again, a further significant drop in expression can be seen in control placentas from E15.5 to E18.5 ($p$ 0.015) which was absent under MO, however a trend was still observed. Similarly, Y654-phospho-β-catenin level decreased significantly from E11.5 to E15.5 (SD $p$ 0.009, HFD $p$ 0.015) onto E18.5 in both HFD ($p$ 0.026) and SD ($p$ 0.002) placentas. Total β-catenin level did not change significantly from E11.5 to 16 or E18.5 under MO, but dropped significantly in SD placentas from E15.5 to E18.5 ($p$ 0.004). Conversely, E-cadherin level was lowest at E11.5 in placentas of both groups and significantly increased between E11.5 and E15.5 (both $p$ 0.002) prevailing on this level until E18.5 (both $p$ 0.002). The expression dynamics of P-cadherin were opposite under HFD compared to SD in that the level gradually and significantly increased ($p$ 0.041) from E11.5 to E18.5 in HFD placentas, but declined significantly ($p$ 0.041) from E11.5 to E18.5 in SD placentas. This suggests that especially towards the end of pregnancy, AJ dynamics are significantly altered under MO.

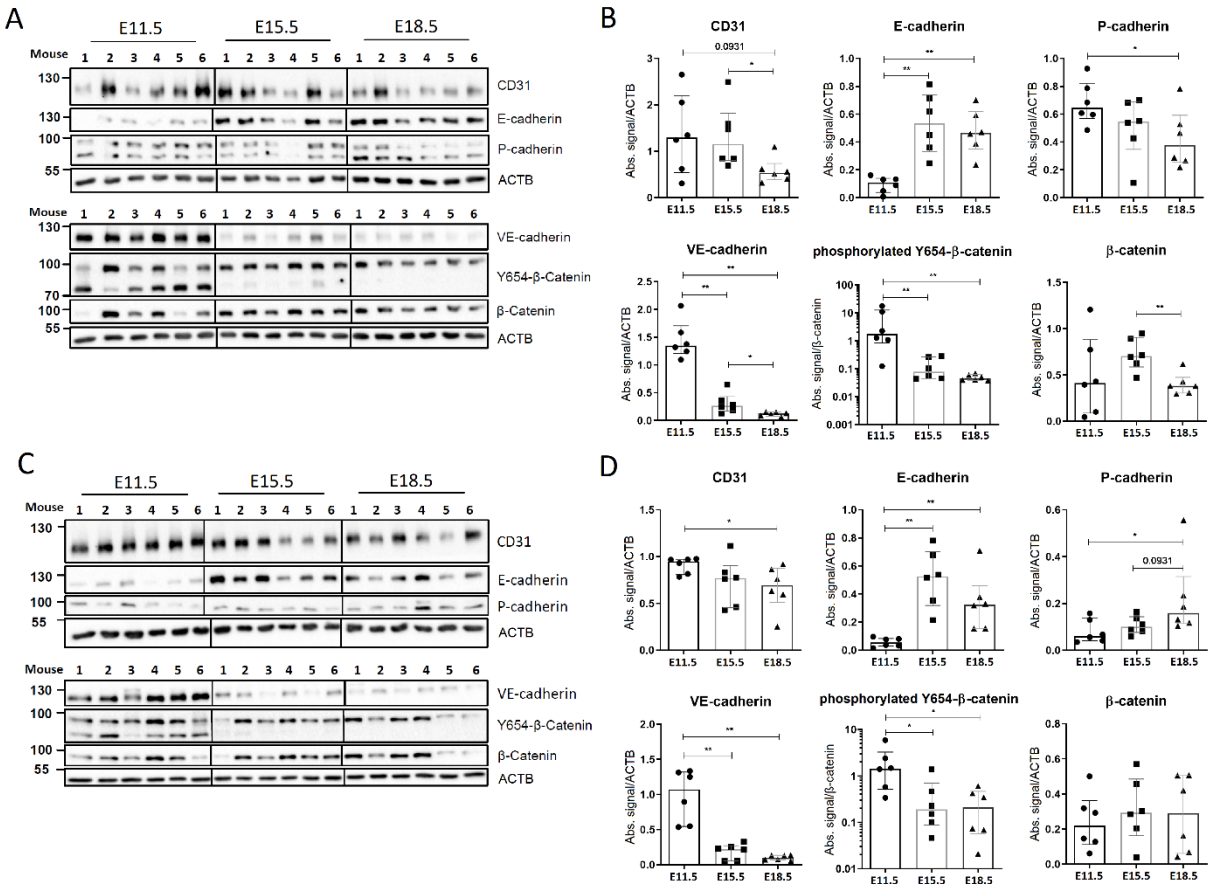


**Figure 4.5.1.1: Protein level dynamics of EC and AJ markers from E11.5, E15.5 and E18.5 in SD and HFD placentas.** (A) Western blotting of SD placental lysates (*n* = 6 placentas, 1 per dam) showing CD31, E-cadherin, P-cadherin, VE-cadherin, phosphorylated Y654-β-catenin, total β-catenin and ACTB (loading control) level. (B) Densitometric analyses of SD western blots of CD31, E-cadherin, P-cadherin, VE-cadherin, phosphorylated Y654-β-catenin and total β-catenin normalized to ACTB. Graphs show median ± interquartile range and * *p* value <0.05, ** *p* value <0.01, or *p* value is shown above graph. (C) Western blotting of HFD placental lysates (*n* = 6 placentas, 1 per dam) displaying CD31, E-cadherin, P-cadherin, VE-cadherin, phosphorylated Y654-β-catenin, total β-catenin and ACTB (loading control) level. (D) Densitometric analyses of HFD western blots of CD31, E-cadherin, P-cadherin, VE-cadherin, phosphorylated Y654-β-catenin and total β-catenin normalized to ACTB. Graphs show median ± interquartile range and * *p* <0.05, ** *p* <0.01, or *p* value is shown above graph, calculated using Mann-Whitney test.

### 4.5.2 AJ marker level at E11.5 and at E18.5 in SD and HFD dams

Under 4.3.1 and 4.3.3, it was demonstrated that MO led to a decrease in AJ marker E-cadherin and a tendency towards down-regulation of β-catenin at E15.5. Therefore, we tested whether MO also influences AJ marker expression earlier (E11.5) and later (E18.5) during gestation. At E11.5, AJ marker and vascular marker CD31 expression were similar in placentas of obese and control dams (Figure 4.5.2.1 A & B).

Interestingly, at E18.5 the AJ marker E-cadherin and total β-catenin expression were significantly down-regulated in placentas of obese dams (Figure 4.5.2.1 C & D), which was also reported previously [93]. Furthermore, in those placentas, there was a tendency towards decreased EC marker CD31 expression. On the contrary, P-cadherin expression was significantly increased in placentas of obese dams at E18.5

compared to controls whereas there was no difference between both groups at E11.5. Taken together, these results suggest that under MO, placental development is marginally affected until E11.5 regarding vascularization and cell junction integrity. However, at the end of pregnancy, there are major differences in vascular and AJ marker expression which could translate to placental function under MO.

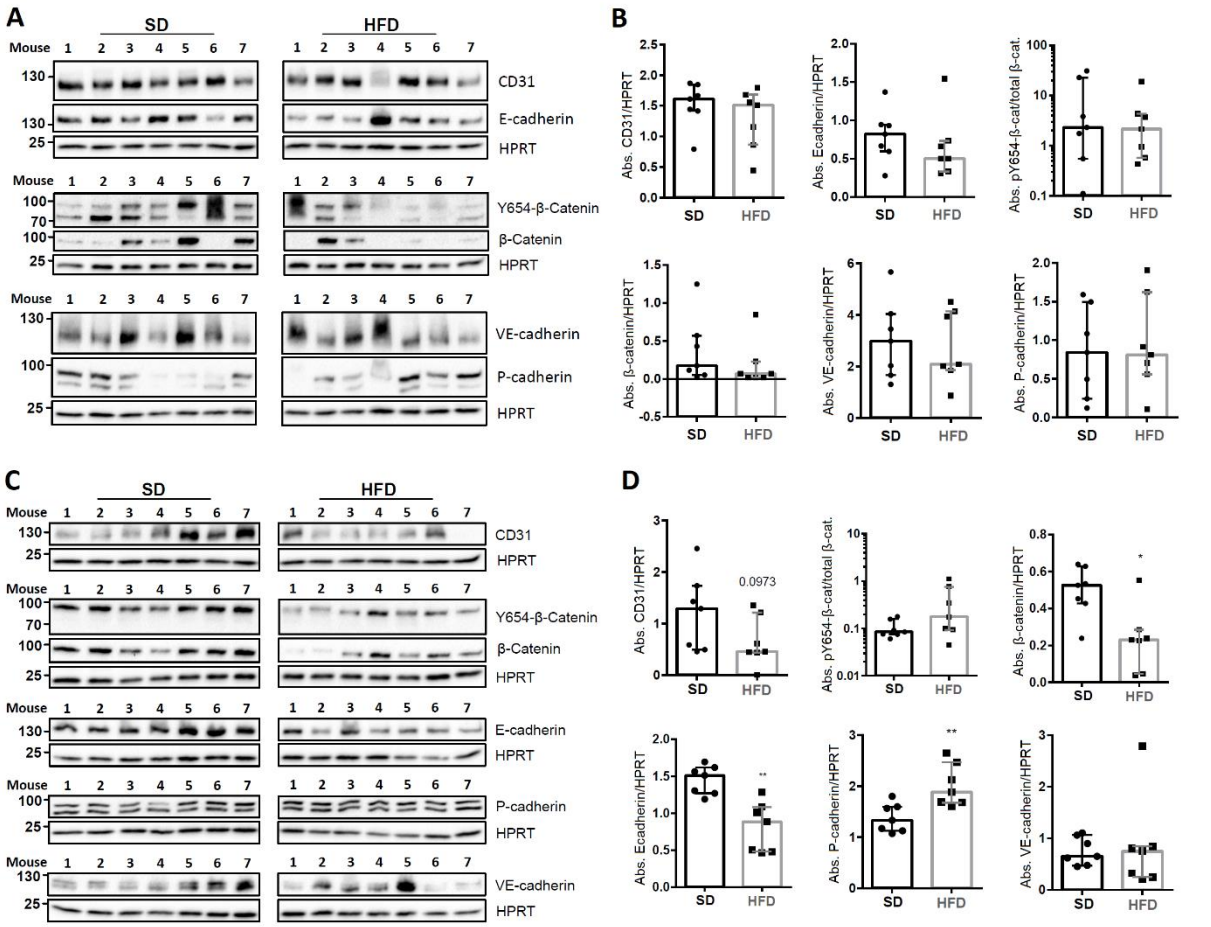


**Figure 4.5.2.1: Protein level of CD31 and AJ marker at E11.5 and E18.5 in SD and HFD placentas.** (A) Western blotting of whole placenta lysates from E11.5 (SD and HFD: *n* = 7 placentas, 1 per dam) showing CD31, E-cadherin, phosphorylated Y654-β-catenin, total β-catenin, VE-cadherin, P-cadherin and HPRT (loading control) level. (B) Densitometric analyses of western blots from (A) of phosphorylated Y654-β-catenin, total β-catenin, CD31, E-cadherin, P-cadherin, VE-cadherin normalized to HPRT. (C) Western blotting of whole placenta lysates from E18.5 (SD and HFD: *n* = 7 placentas, 1 per dam) showing CD31, phosphorylated Y654-β-catenin, total β-catenin, E-cadherin, P-cadherin, VE-cadherin and HPRT (loading control) level. (D) Densitometric analyses of western blots from (C) of phosphorylated Y654-β-catenin, total β-catenin, CD31, E-cadherin, P-cadherin, VE-cadherin normalized to HPRT. Graphs show median ± interquartile range and * $p$ <0.05, ** $p$ <0.01, or $p$ value is shown above graph, calculated using Mann-Whitney test.

## 4.6 Anti-IL-6R antibody therapy under MO causes similar maternal and fetal phenotype to HFD, but further increases placental IL-6 level and affects placental AJ and vascular marker expression

Results in this section, i.e. “Anti-IL-6R antibody therapy under MO causes similar maternal and fetal phenotype to HFD, but further increases placental IL-6 level and affects placental AJ and vascular marker expression”, have not been published or submitted by the time of writing this thesis. The work described hereafter was made possible with the help of several others:

Animal handling and tissue collection were performed by Marion Handwerk and Tobias Kretschmer. Protein isolation, detection, densitometric analysis and ELISA were performed by Tobias Kretschmer. Data collection and statistical analyses were performed by Tobias Kretschmer. The work was supervised and supported by Jörg Dötsch and Sarah Appel.

### 4.6.1 mMR16-1 or IgG antibody therapy under MO causes similar phenotype as HFD alone in dams and offspring, but only mMR16-1 significantly increases placental IL-6 level

We recently demonstrated that IL-6 serum level are increased in obese dams concomitant with EC damage and placental dysfunction [81]. Hence, we aimed to investigate effects of IL-6 signaling blockade by anti-IL6R therapy with mMR16-1 or IL-6 knock-out on placental vascular and AJ markers. Several of the dams that received HFD *ad libitum* after weaning and were obese at the time of mating (data not shown), were randomly selected after mating for IL-6 antibody therapy, i.e. IgG or mMR16-1. HFD dams without antibody therapy served as control together with IL-6$^{-/-}$ that also received HFD after weaning and were obese at the time of mating (data not shown).

For the mMR16-1 therapy, obese dams were treated over a period of 16 days of gestation with 3 injections of mMR16-1 on E0.5, E7.5 and E14.5 (see Methods section 3.1.2). As control, obese dams received an IgG antibody as described for mMR16-1. Similar to dams which received HFD without antibody therapy, IgG treated HFD dams had significantly more egWAT at section on E15.5 than SD dams. HFD dams that received mMR16-1 had about the same weight of egWAT as IgG and HFD without antibody therapy (not significant, but with a strong trend compared to SD, Figure 4.6.1.1 A). However, fetal weight was significantly reduced in both mMR16-1 and IgG treated dams compared to SD controls (Figure 4.6.1.1 B), as shown for HFD alone. Litter size alive and embryo resorption rate were unaltered, however there was a tendency towards increased resorption rates in HFD dams without antibody therapy compared to SD (Figure 4.6.1.1 C & D). In a small group ($n$ = 4 dams) of IL-6$^{-/-}$ mice, however, there was no resorption of embryos observed at all, whereas litter size was similar compared to SD, HFD, mMR16-1 and IgG dams. Fetal weight of IL-6$^{-/-}$ offspring was significantly reduced and dams of this group also showed a drastic increase in egWAT weight similar to HFD wild type dams and compared to SD dams. These results show that HFD, independent of interventions with mMR16-1, IgG antibodies or IL-6$^{-/-}$, has the strongest impact on maternal and fetal phenotypes. Also, similar to HFD alone, offspring of IL-6$^{-/-}$, mMR16-1 and IgG treated dams developed an IUGR (Figure 4.6.1.1 B).

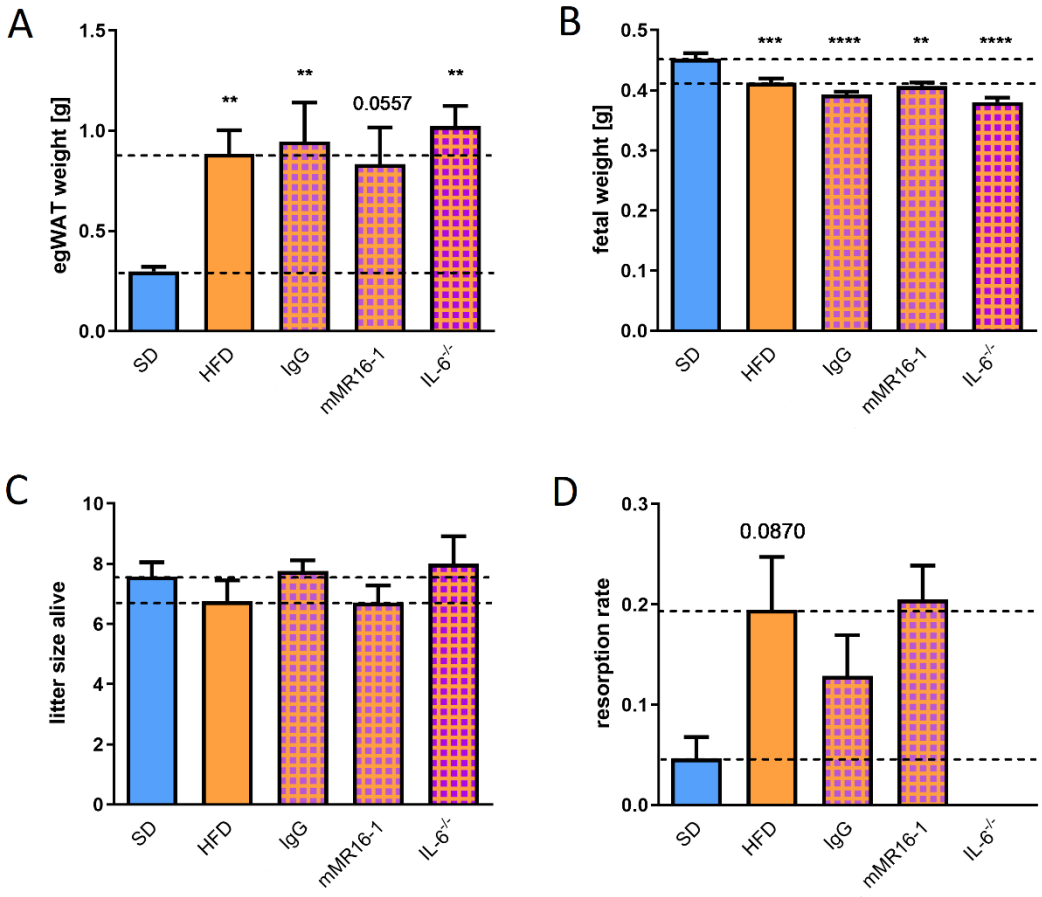


**Figure 4.6.1.1: Phenotypic data of dams and offspring from SD, HFD, mMR16-1 and IgG antibody-treated and IL-6$^{-/-}$ animals at E15.5.** (A) Weight of egWAT pads at section. SD *n* = 13, HFD *n* = 15, IgG *n* = 6, mMR16-1 *n* = 5, IL-6-/- *n* = 4. (B) Fetal weight at E15.5. SD *n* = 97 (13 dams), HFD *n* = 115 (15 dams), IgG *n* = 61 (8 dams), mMR16-1 *n* = 47 (7 dams), IL-6-/- *n* = 27 (4 dams). (C) Number of alive litters per dam at E15.5. SD *n* = 14, HFD *n* = 20, IgG *n* = 8, mMR16-1 *n* = 7, IL-6-/- *n* = 4. (D) Ratio of resorptions per dam observed at E15.5. SD *n* = 14, HFD *n* = 20, IgG *n* = 8, mMR16-1 *n* = 7, IL-6-/- *n* = 4. All graphs show mean ± SEM, * *p* <0.05, ** *p* <0.01, *** *p* <0.001, **** *p* <0.0001, or *p* value is shown above graph, calculated using one-way ANOVA followed by Tukey's multiple comparisons test. Dotted lines show either SD or HFD values for better orientation.

SAA2 level were measured by ELISA in maternal serum of antibody-injected dams to assess successful IL-6 signaling blockade in mMR16-1 treated dams. Median SAA2 level was higher in mMR16-1 injected dams compared to IgG controls (*p* 0.063). From both groups about half of the dams had low level (<500 pg/mL) while the other half had higher level (>1500 pg/mL) of serum SAA2 (Figure 4.6.1.2 A) indicating no uniform response to either antibody therapy regarding SAA2 expression and/or no blockade of SAA2 by mMR16-1.

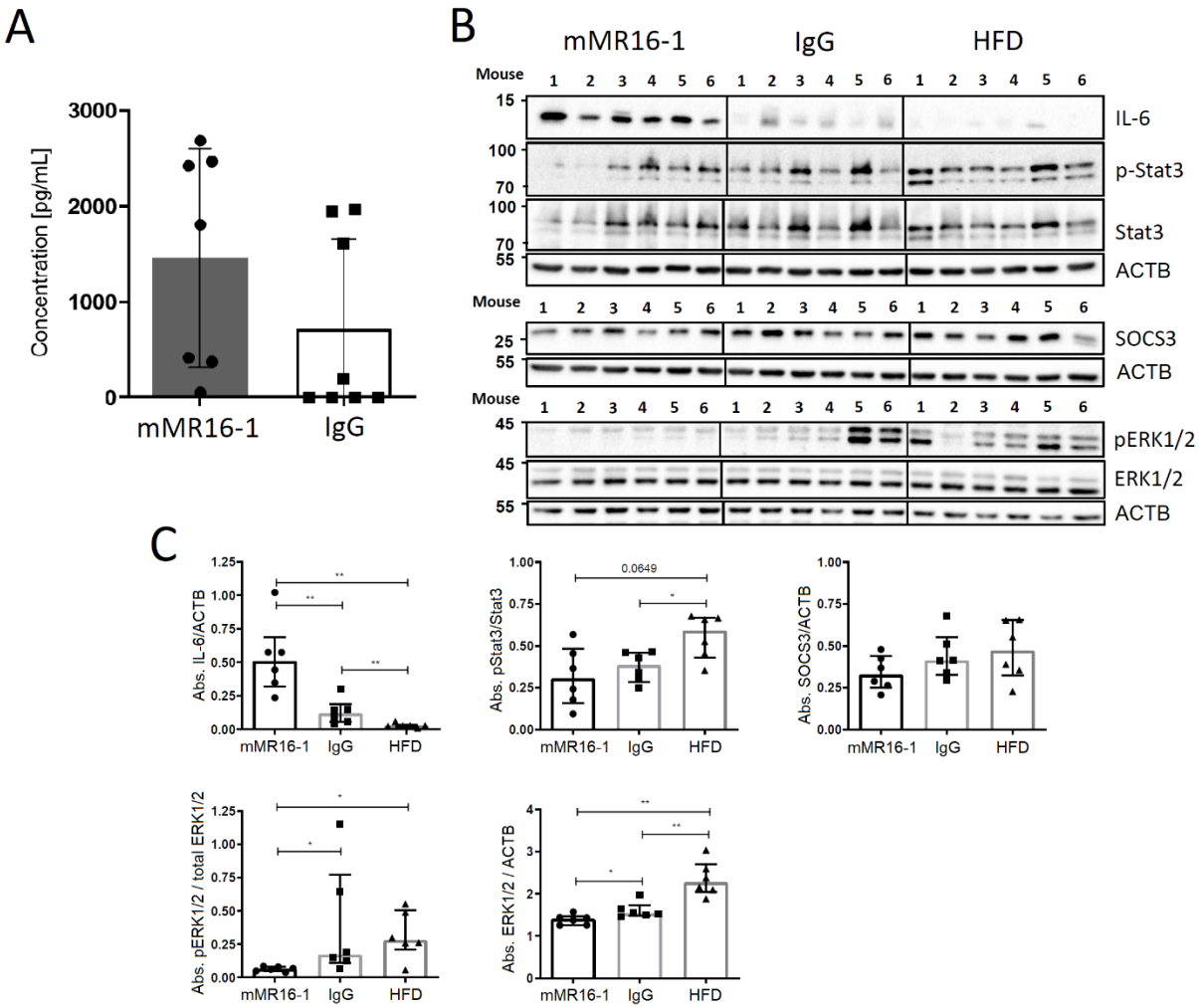


**Figure 4.6.1.2: SAA2 concentration and placental IL-6 signaling-related protein level in mMR16-1, IgG and HFD dams.** (A) SAA2 level in mMR16-1 and IgG treated dams at E15.5. For mMR16-1 *n* = 7 serums samples from 7 dams, for IgG *n* = 8 serums samples from 8 dams were used for the analysis. Graphs show median ± interquartile range and *p* value was calculated using Mann-Whitney test. (B) Western blot of IL-6, p-Stat3, total Stat3, SOCS3, pErk1/2, total ERK1/2 and ACTB (loading control) in placentas of mMR16-1, IgG and HFD dams (*n* = 6 dams per group, 1 placenta per dam). (C) Densitometric analyses of protein level from western blots of IL-6, SOCS3 and total ERK1/2 normalized to ACTB, as well as p-Stat3 normalized to total Stat3 and pErk1/2 normalized to total ERK1/2. Graphs show median ± interquartile range and * $p$ <0.05, ** $p$ <0.01, or $p$ value is shown above graph, calculated using Mann-Whitney test.

Next, IL-6 protein level were analyzed in placentas of mMR16-1, IgG and HFD control dams together with down-stream signaling molecules of the IL-6 signaling pathway (Figure 4.6.1.2 B &C), i.e. p-Stat3 and SOCS3. The expression of IL-6 in placentas of mMR16-1 injected dams was significantly increased compared to IgG ($p$ 0.004) and HFD control ($p$ 0.002) dams. Furthermore, IL-6 was also significantly increased ($p$ 0.009) in IgG compared to HFD placentas. SOCS3 protein level remained unaltered while p-Stat3 level were significantly reduced in placentas of IgG dams ($p$ 0.041) and also in mMR16-1 without reaching statistical significance ($p$ 0.065) compared to placentas from HFD dams. Expression of pErk1/2 was also significantly decreased in placentas of mMR16-1 treated dams compared to IgG ($p$ 0.015) and HFD ($p$ 0.026) dams. Total ERK1/2 level were reduced in mMR16-1 placentas compared to IgG ($p$ 0.026) and HFD ($p$ 0.002), as well as in IgG placentas compared to HFD ($p$ 0.004). These results suggest that mMR16-1 therapy over gestation increases IL-6 protein level in placentas and that either antibody therapy, mMR16-1 or IgG, might have an effect on growth and differentiation compared to HFD alone. However, classical readout marker SOCS3 for IL-6 feedback signaling was unaltered after antibody therapy over gestation.

### 4.6.2 Vascular and AJ markers are significantly reduced in placentas after mMR16-1 administration

Next, AJ and EC marker protein level were determined in placentas of mMR16-1, IgG and HFD dams. CD31 level was significantly decreased in mMR16-1 ($p$ 0.026) and IgG ($p$ 0.041) treated dams compared to HFD dams. Furthermore, P-cadherin and VE-cadherin level were significantly reduced ($p$ 0.026) in placentas of mMR16-1 treated dams compared to HFD. Protein level of E-cadherin and β-catenin remained unaltered in both mMR16-1 and IgG treated dams compared to HFD (Figure 4.6.2.1). Taken together, placental vascular development may be altered in dams which were administrated either mMR16-1 or IgG antibodies as seen by reduced level of CD31 and VE-cadherin whereas AJ marker level were unaffected.

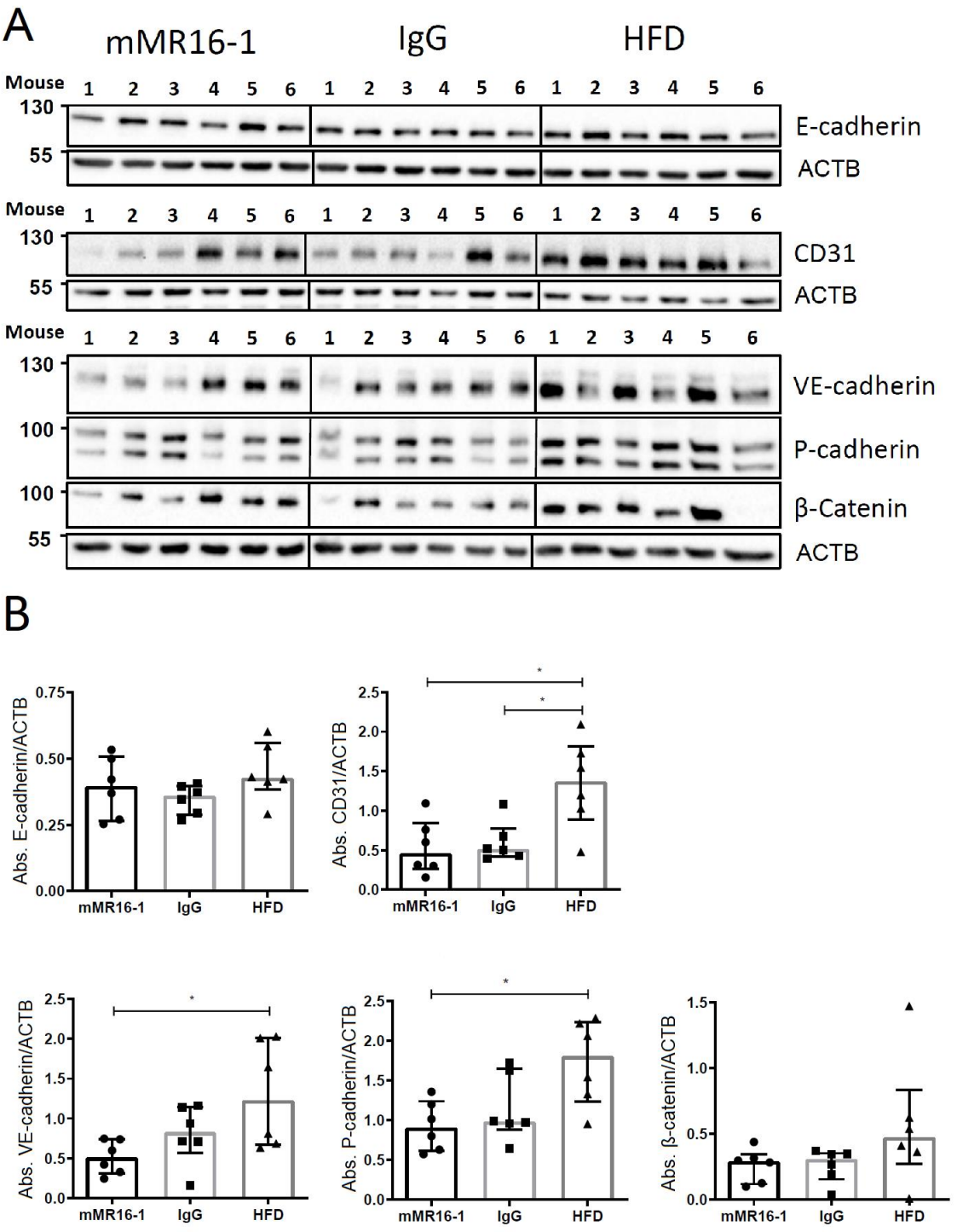


**Figure 4.6.2.1: Placental EC and AJ marker level in mMR16-1, IgG and HFD dams at E15.5.** (A) Western blots of CD31, E-cadherin, P-cadherin, VE-cadherin, β-catenin and ACTB (loading control) in placentas of mMR16-1, IgG and HFD dams ($n$ = 6 dams per group, 1 placenta per dam). (B) Densitometric analyses of protein level from western blots of CD31, E-cadherin, P-cadherin, VE-cadherin and β-catenin normalized to ACTB. Graphs show median ± interquartile range and * $p$ <0.05 calculated using Mann-Whitney test.

# 5. Discussion

### 5.1 Novel insights into maternal and fetal phenotypes under HFD-induced MO

In this work, we induced an obese phenotype in C57BL/6N mice by feeding a HFD from week 3 of age, through adolescence and pregnancy until pregnancy was terminated at various gestation days, E11.5, E15.5 and E18.5. Even though feeding this diet rich in fatty acids and calories from fat makes our mouse model primarily a HFD-model, this HFD has been shown to induce obesity [93] and can cause a compromised glucose tolerance, increased serum leptin and insulin level [77, 97] in these mice, which we believe could largely be attributed to its composition. These effects show that we basically generated a diet-induced obesity mouse model by HFD nutrition which accompanies the translational character and several co-morbidities of obesity from mice to human. These crucial aspects have led to an acceptance of HFD in animal models to induce overweight and obesity, study their pathophysiologic effects (also during pregnancy) and extrapolate from these effects to humans [98-101]. Hence, in this work, HFD dams were synonymously referred to as obese dams. The HFD used in this work comprised a significant amount of fatty acids, i.e. saturated and mono-unsaturated fatty acids from palm oil (about 4.5%) and animal lard (about 30.5%), of C-16:x and C-18:x carbon chain length (Appendix 6.4, Table 6.2). The total metabolizable energy from these fatty acids together with the remainder of shorter and longer chain fatty acids sums up to about 60% [81]. There have been other diets discussed in literature to induce obesity, and these may more closely reflect the “western-style” type of diet that is rich in sugar and saturated fatty acids, preferably consumed by humans. However, results from animal studies with western diets and HFD displayed comparable effects, for example on dam weight and fetal weight [97, 102-104]. In this work, *ad libitum* consumption of HFD led to a significantly higher weight-gain compared to control mice that received a SD for the same period of time, and typically the HFD dams reached 24 to 26 g bodyweight by week 12 of age, compared to 20 to 22 g for SD dams [93]. Hence, mating of HFD and SD dams took place from week 12 to week 16 of age with already obese HFD dams. At section day, HFD dams displayed significantly heavier egWAT “fat pads” which were on average more than 2-times heavier than in control dams and showed the obese phenotype persisted through pregnancy under HFD. Furthermore, offspring of HFD dams in this study developed an IUGR which was signified by lower embryo weight at E15.5 compared to offspring from SD dams. Towards the end of pregnancy, at E18.5, fetal weight was restored to a similar weight average in HFD and SD dams, indicating a catch-up growth during the third trimester of pregnancy under HFD which was mainly attributed to glucose stores of the placenta [93]. Conversely, in studies of human pregnancy of overweight and obese women, offspring had a higher risk of developing fetal macrosomia termed large for gestational age which was related to maternal body mass index (BMI) and gestational weight-gain [38, 105, 106]. Therefore, it seems more likely that in mice, HFD impacts on placental function and early fetal development rather than causing oversupply in mice offspring which would lead to overgrowth. Indeed, placental insufficiency and dysfunction are associated with fetal growth restriction in humans [107, 108], suggesting a primary role of the placenta in developing IUGR. Moreover, offspring of HFD dams displayed pathological effects early in life regarding body weight, egWAT and serum levels of insulin, indicating long-term effects and programming in offspring for obesity-associated pathologies [77].

### 5.2 Pre-delivery inflammatory events are altered in obese dams

Investigations on inflammatory events revealed that there is a significant increase in CD45-positive immune cell (leukocyte) infiltration, as well as an increased inflammatory marker expression in placentas of lean dams shortly before birth. While the increase in inflammatory marker expression was also present in placentas of obese dams, leukocyte infiltration was absent. However, there could be other relevant immune cells infiltrating the placenta which are not detected by CD45 staining, which suggests that further investigations are necessary to elucidate immune cell infiltration in placentas of normal and obese dams. Concomitant with the increase in CD45-positive immune cell infiltration in SD placentas was a lower anti-oxidative stress gene expression (of glutathione peroxidase and catalase) and an increase in oxidative stress, measured by lipid peroxidation, before parturition. This could be relevant to initiate birth and shedding of the placenta towards the end of pregnancy. In placentas of obese dams however, oxidative stress seemed enhanced compared to control dams at E18.5 since lipid peroxidation and pro-oxidative stress markers of the respiratory chain were elevated and occurred simultaneously to decreased catalase gene expression. Augmented oxidative stress can cause pre-mature aging and a decline in function of the placenta, which has been shown in placentas of obese women, together with an exaggerated inflammatory environment during pregnancy [36, 109]. Thus, increased oxidative stress in obese dams could harm placental function and might influence the immune cell infiltration observed in lean dams to initiate birth and placenta shedding.

We also studied egWAT in lean and obese dams at E15.5 and E18.5 since its functional unit, the adipocyte, produces inflammatory cytokines and chemokines that can reach the circulation [110]. Additionally, it was reported that low grade inflammation in adipose tissue of dams is linked to a physiological increase in adipose tissue during pregnancy [111]. We could show that on E18.5 (data not shown) and on E15.5, obese dams had significantly heavier egWAT than lean mice. In lean mice, pro-inflammatory gene expression of a variety of genes (IL-6, TNFα, IL-1β, CXCL1 and 10 and MCP1) was significantly increased in egWAT towards the end of pregnancy (E18.5) compared to E15.5. This increase was not observed in egWAT of obese dams. These results indicate that the egWAT could play a role in the inflammatory response shortly before parturition in lean dams whereas in obese dams this response seems hampered. We could even speculate that there is a link between the endocrine roles of adipose tissue described by Coelho et al. [112] and the absence of leukocyte infiltration in the placenta and a rise in inflammatory markers in egWAT before parturition. However, further studies are required to decipher the mechanisms of egWAT and placenta interplay before birth.

Lastly, the deficient leukocyte infiltration and slight change in pro-inflammatory gene expression in placentas of obese dams was accompanied by an attenuated inflammatory response in egWAT and an increase in the duration of gestation by about 1 day. Overall, our data suggest that these processes are relevant to initiate birth at about E19 in dams. Indeed, in human studies it was reported that obese women had prolonged pregnancy and that inflammation seems relevant at the end of pregnancy to initiate parturition [113, 114], however the mechanism remains unclear.

### 5.3 Impact of MO on placental EC homeostasis and vascularization

Maternal BMI is associated with the risk for several pathologies during pregnancy and obesity has been reported to affect vascular function and vascular EC homeostasis [115, 116]. Both of these factors have direct implications for placental development and function, since the placenta forms around maternal blood vessel-invading trophoblasts, is a highly vascularized organ and provides the main interface for fetal supply via nutrient and waste exchange from maternal and fetal blood, respectively [7]. Studies in rodents have shown that HFD has direct effects on placental function and outcome of pregnancy and influences vascularization and hemodynamics in the placenta. These adverse effects include placental vasculopathy and EC damage in mice [44], altered placental labyrinth size in rats [117], and reduced placental blood flow in primates [62]. Moreover, stereological analysis showed compromised placental size and morphology in high-fat high-sugar treated mice [104] which led us to believe that placental vascularization and morphology could be altered significantly in our model of maternal obesity. Indeed, our stereological analyses of placental vascularization in SD and HFD dams at E15.5 provide evidence for a disturbed vascular development of the placenta under MO, and both gene expression as well as western blot analyses showed a significant reduction of vascular marker level. One of these vascular markers down-regulated on the mRNA-level is Tie-1, an EC specific receptor tyrosine kinase, which has been implicated in the maturation of vessels and angiogenesis, the *de novo* formation of blood vessels [118]. Furthermore, in inflammatory diseases like rheumatoid arthritis and atherosclerosis, Tie-1 was reported to be up-regulated. Overexpression of Tie-1 is probably capable to induce an inflammatory response in ECs and thus, might be a target for anti-angiogenesis treatments in cancer [119, 120]. However, in our study, a down-regulation of Tie-1 in placentas of obese dams was found, indicating that inflammatory effects observed herein are not mediated by Tie-1. Nonetheless, its down-regulation could be related to impaired vascularization observed by stereological analyses and this notion is further supported by simultaneous CD31 down-regulation on both mRNA and protein level, another well-known vascular marker.

This work presents evidence that EC homeostasis is significantly affected in the placental transfer zone by MO at E15.5, not only by down-regulation of EC markers on protein and mRNA-level, but more so due to both ultrastructural changes observed under EM and the increase in EC senescence specifically in the Lz. The increased electron density and condensed appearance of EC nuclei may indicate EC damage, and there was detachment of ECs from the BM. In certain instances, loss of contact of cells, like ECs, from the ECM and the BM lead to a form of programmed cell death, called anoikis [121-123]. However, this was not observed in placentas of obese dams in this study and increased cell death by apoptosis was also not detected by staining assays conducted *in vivo* for the Lz or *in vitro* in placental EC (HPVEC). On the other hand, γH2A.X staining suggests a significant increase in DNA-damage [124] in ECs in the Lz of obese dams which could explain the observed ultrastructural appearance. Classically, γH2A.X is not considered a senescence marker and is found in case of damaged DNA regions, like double strand breaks, and was even reported to be increased in proliferating cells [125, 126]. However, we investigated proliferation and apoptosis marker in ECs which allows a better estimation of senescence by γH2A.X staining [127] and found no changes in proliferation and apoptosis under MO, which makes EC senescence more likely. In whole placenta lysates, we evaluated γH2A.X protein level

together with markers for apoptosis (cleaved caspase-3 and PARP) and proliferation (cyclin D1 and PCNA) by western blot, but reported no differences in protein level between SD and HFD dams. This indicates that HFD does not simply cause more apoptosis, proliferation or senescence/DNA-damage than SD in the whole placenta and that instead specifically the EC in the transfer zone are affected by increased senescence. Hence, analysis of the transfer zone may be particularly relevant to study consequences of HFD for placental function rather than evaluating apoptosis, proliferation or senescence marker in whole placental lysates.

We showed that IL-6 serum level were increased under MO in our mouse model at E15.5 and previous reports showed that IL-6 can pass the placental barrier and reach the fetus [95, 128]. Therefore, we speculate that increased level of IL-6 from maternal serum in obese mice might affect placental EC homeostasis and cause the observed increase in senescence as well as alter EC appearance on the ultrastructural level. Cell culture studies indeed confirmed that IL-6 is capable to induce senescence, assessed in our work by senescence-associated beta-galactosidase activity in HPVEC [81], and others showed increased senescence in fibroblasts after IL-6 stimulation [129]. The IL-6R is the target of circulating IL-6 and is not expressed by ECs [130], yet IL-6 can still act on cells not harboring the IL-6R. In those situations, the cell surface receptor gp130 and IL-6 bound to the soluble IL-6R in the circulation, associate with each other and induce signaling. This way of signaling is called trans-signaling of IL-6 and is the most prominent inflammatory pathway for most cell types without a classical IL-6R [68, 131]. Regarding the origin of increased circulating IL-6 in maternal serum, we tested IL-6 mRNA expression and protein level in egWAT of obese dams at E15.5 which showed enlarged fat pads on section concomitant with weight gain. We found increased mRNA expression, albeit not statistically significant, and a strong tendency towards increased protein level of IL-6 in egWAT of obese dams. Mohamed-Ali et al. [132] and Coppack [133] reported that white adipose tissue can produce inflammatory cytokines and be the origin of circulating IL-6, and increased egWAT could therefore attribute to the systemically inflamed state under MO. As a result, we believe that the egWAT in our HFD dams could cause increased serum IL-6 level by egWAT hypertrophy and production. Serum IL-6 subsequently can reach the placenta and hence, lead to a “WAT - maternal serum - placenta” axis [81] which denotes a possible route of MO-induced EC damage in the placenta, propelling placental insufficiency. We aimed to further investigate this proposed route by applying an IL-6 signaling antibody therapy as well as an IL-$6^{-/-}$ mouse model, which are both discussed further below.

The formation of blood vessels is paramount for proper placental function and the above mentioned placental insufficiency due to EC damage could translate to an impaired placental vascular development. We investigated gross morphology and vascularization of the placenta by stereological means at E15.5. Placenta weight was similar between obese dams and controls, however total placenta volume was larger and the fraction of the Lz, which is the main vascularized part of the placenta, was significantly reduced in obese dams. Additionally, fetal vascular surface area and total capillary length were reduced under MO while capillary diameter seemed slightly increased. These results strongly suggest impaired vascular branching and development and a reduced area for materno-fetal exchange of nutrients, oxygen and disposal of waste [11, 24]. As a consequence, the placenta cannot fulfill its

function and the fetus might be undersupplied and develop the observed IUGR at E15.5, as there is a tight regulation of the three-dimensional development of the placenta and its strata. Indeed, deviations from this controlled growth processes were linked to placental insufficiencies and fetal development [11, 24, 25]. Additionally, a study showed that a reduced surface area in the placental transfer zone and decreased materno-fetal transfer could cause fetal growth restriction [83]. Our data further indicate that surface area and capillary length of SD placentas closely resemble what others reported for control dams at E15.5, while HFD placentas displayed surface area and capillary length at E15.5 which others observed at E14.5 in control dams [24]. This further indicates a disturbed development of the transfer zone under MO with direct consequences for placental function.

The catch-up in fetal weight development by E18.5 under MO could be attributed to enhanced glycogen-storage utilization in the placenta and increased protein level of GLUT1 and GLUT4-transporters [93]. These effects may compensate for the decreased relative size of the Lz observed at E15.5 under MO. However, further studies on the developmental dynamics of morphology and vascularization by stereological techniques before and after E15.5 could generate valuable insight into placental effects of MO. In another study utilizing an obesogenic diet, it was reported that fetal weight was also normalized around day 19 of gestation after IUGR was present at day 16, and placental transport proteins for specific nutrients might contribute to this normalization in fetal growth trajectory, even though placentas were smaller and morphologically altered [104]. Nonetheless, these and our results show that the placenta is severely affected regarding vascularization and function on a morphological and protein marker level by MO.

### 5.4 Impaired trophoblast differentiation, damaged placental basement membrane and AJ as well as lipid accumulation under MO

Not only did we observe changes in EC homeostasis and vascular morphology, trophoblasts that lie opposite of the BM in the placental transfer zone seem also affected by MO at E15.5. Proteomics profiling revealed a list of proteins that relate to processes relevant for trophoblasts in the transfer zone to be altered. We found significantly reduced E-cadherin level, not only in the proteomics screen of the Lz, but also in western blots of whole placenta samples, and could show by immune-staining that this protein is exclusively found in trophoblasts of the Lz. Originally, E-cadherin was described on epithelial cells before it was also shown to be expressed in human villous trophoblasts [28]. Cadherin proteins function as transmembrane molecules that are calcium-dependent for their adhesive properties. By homophilic interactions of the extracellular domain of cadherins, they produce dimers which bind to other cadherin dimers from adjacent cells. On the intracellular side, cadherins form connections to the cytoskeleton via binding to catenin family proteins, for example β-catenin [134, 135]. Furthermore, E-cadherin was reported to have an important regulatory function in epithelial barriers and as its expression is inhibited, this could lead to epithelial barrier and AJ disruption [135, 136]. In our cell culture studies, there was no effect observed on E-cadherin level after BeWo stimulation with isolated fatty acids. However, cadherins can be internalized to mitigate their adhesive function which also destabilizes AJ structures [137], and this mechanism was briefly touched in our investigation by IF staining of cells,

but yielded no conclusive results (data not shown). However, E-cadherin has an important role in epithelial-to-mesenchymal transition and trophoblast cell behavior which it thusly regulates [138]. From both, mRNA and protein quantitation of E-cadherin and β-catenin it can be deduced that AJ stability is negatively affected by MO, specifically in the placental transfer zone, since E-cadherin was exclusively detected in the Lz by IHC and IF. Furthermore, proteomics profiling of the Lz revealed significantly lower level of E-cadherin and a strong trend towards reduced β-catenin level. Next to E-cadherin, P-cadherin and VE-cadherin are part of AJ and regulate cell adhesion, signaling pathways and placental transfer. Unfortunately, IHC staining of VE-cadherin and IF staining of VE-cadherin and P-cadherin could not precisely show the localization of these cadherins to a specific cell layer within the Lz. However, P-cadherin seems to localize to the maternal blood sinus surface of SynT while E-cadherin occurred between SynT layers more strongly in the Lz of our samples. This is interesting since E- and P-cadherin were reported to occur jointly in embryonic and other tissues and P-cadherin was mentioned to be expressed more strongly [139]. Staining patterns were similar between SD and HFD placentas which further indicates no tremendous difference in expression pattern or localization.

The ultrastructure of the placenta in HFD dams at E15.5 showed that SynT homeostasis was affected and indicates a defect in SynT differentiation where the formation of two distinctly visible SynT layers is absent. This also implies that AJ could not form properly and cell-cell connections are disturbed, again, as mentioned above, indicating impaired placental development. Concomitantly, SynT exhibited altered cell-matrix interactions, as evidenced by the observed detachment from the BM in ultrastructure analysis and reduced level of focal adhesion marker Ptk2 detected by proteomics profiling, which is an important regulator of cell orientation and cell-matrix interaction [140, 141]. Furthermore, two subunits of laminin (Lamc1 and Lamb2) that were down-regulated under MO in the proteomics profile are relevant for BM integrity, further indicating disruption of the BM. These changes may have strong implications for permeability and transfer properties of the Lz [142]. Many of the detected proteins in proteomics profiling have not been characterized in expression, localization or function in the placenta, including Sdc4, Iqgap1/2 and Flot2, making it worthwhile to conduct further studies investigating the role of these proteins in the placenta. In the case of some focal adhesion-related proteins, they have already been mentioned to be involved in placental and embryonic development [143, 144]. Furthermore, the interaction between Ptk2 and VE-cadherin may be relevant for endothelial barrier function, and together with negative regulation of E-cadherin by Iqgap1 [141] might, in our eyes, have an effect on placental barrier integrity.

Another major ultrastructural difference in placentas of obese dams compared to controls was the accumulation of lipids in the transfer zone at E15.5. EM analysis displayed lipid and ECM depositions on the BM, as well as lipid droplets intracellular and extracellular of SynT which could have negative effects on the barrier integrity and cell homeostasis. The amount of lipid deposition, as quantified by Oil Red O staining, throughout the Lz was significantly higher in placentas of obese dams than controls, indicating that the placenta has the capacity to store lipids and these stores are hypertrophic under MO. Indeed, other studies reported that, like other non-adipose tissues, the placenta is able to store lipids in obese animal models [145, 146]. However, these lipid accumulations may have lipotoxic effects on the

placenta and its environment, leading to elevated oxidative stress, inflammation and metabolic effects in the fetus [147, 148]. In addition, a trophoblast-like cell line (BeWo) showed a tendency towards increased lipid accumulation upon stimulation with the isolated fatty acid OA at high concentration. This may suggest that there is a mechanism for certain fatty acids to pile up in placental cells, and consuming diets in which fatty acids are present in high amounts could promote accumulation of lipids in the placenta. This may have serious implications for offspring developing within a placental environment associated with augmented inflammation and fat deposits in the transfer zone, leading to fetal programming for obesity and lipid accumulation in tissues and organs later in life [77, 146, 148]. The HFD used in this study was, amongst others, enriched with PA, OA and LA from palm oil and animal lard (Appendix 6.4, Table 6.2). PA was reported to cause inflammation in placental cells [149] and cell death concomitant with impaired invasion of trophoblastic HTR-8/SVneo cells [150, 151]. In addition, in western style diets LA is frequently found and has been associated with oxidative and pro-inflammatory effects [152, 153]. Furthermore, cell viability was decreased and inflammatory responses as well as mitochondrial function in trophoblasts were affected by LA, which could translate to altered placental function [154]. Within the last years, we tried to establish a protocol for the isolation of murine trophoblasts and EC from placentas of obese dams in order to stimulate these primary cells with maternal serum from obese dams to elucidate if and how factors from maternal serum could affect cell homeostasis. However, such an isolation protocol is not established to date and in the future we will turn to commercially available murine placental trophoblast which recently became available and are isolated murine trophoblasts (SM-9) [155, 156].

Mid-gestation, days E10.5 to E12.5, in mice, where the definitive placenta is functional, has been suggested as equivalent to the end of first trimester in human pregnancy at which point organogenesis is completed [3]. Interestingly, we found that E-cadherin level in placentas of SD and HFD dams were lowest at E11.5, while VE-cadherin and CD31 level were highest at this point in mid-gestation. Lower level of E-cadherin early in placental development are associated with a more invasive and less epithelialized phenotype, and specific subsets of extravillous trophoblasts retain lower E-cadherin level to allow invasiveness [157]. At E11.5, the Lz already contains blood in its vessel system which is not observed 2 days prior [158]. From E11.5 to E15.5, E-cadherin level drastically increase and thus, it seems likely that trophoblast differentiation occurs, and trophoblasts of the syncytium intermit invasiveness. Vascular adhesion mediated by VE-cadherin is somewhat modified, causing a significant drop in VE-cadherin level from E11.5 to E15.5 in both SD and HFD placentas. This further supports that lower E-cadherin level at E15.5 in HFD placentas are a sign of impaired trophoblast and placental development, since E-cadherin expression is “behind schedule” in obese placentas. In line with the decrease in VE-cadherin from E11.5 to E15.5 is the decrease in phospho-Y654-β-catenin in both SD and HFD placentas. Phosphorylation of β-catenin at this tyrosine residue can lead to a reduction in cadherin-β-catenin interaction, increased WNT/β-catenin signaling and could thusly affect AJ stability [159, 160]. Similar to junction and focal adhesion markers Ptk2, Sdc4 and Iqgap1/2 mentioned above, phospho-Y654-β-catenin has not been functionally characterized in the placenta or trophoblast, making interpretations on its role in placental development difficult. However, one could carefully speculate that phospho-Y654-β-catenin mediates trophoblast invasiveness by inhibiting cadherin interaction between

cells on and before E11.5 to enable trophoblast migration and invasion. Once the placenta is fully functional and syncytial fusion has occurred, phosphorylation of β-catenin at Y654 is suppressed. At E15.5, phospho-Y654-β-catenin level appeared higher in placentas of obese dams, even with a considerable degree of variation between dams which could, nonetheless, support this speculation, since ultrastructure analysis showed the defect in syncytial fusion and trophoblast differentiation at E15.5. Total β-catenin expression was mildly affected by MO and displayed no change at E11.5 on protein level, but was down-regulated on mRNA and by tendency on protein level at E15.5 and on protein level at E18.5. These observations further indicate AJ destabilization, as β-catenin is a cadherin-anchoring protein to the cytoskeleton [30]. Interestingly, we found that the fatty acid LA was able to reduce β-catenin protein level in trophoblast-like BeWo cells, suggesting that the HFD might be a causing factor for reduced β-catenin level during gestation once blood supply to the placenta is fully established. Thus, with maternal blood reaching trophoblasts and fetal EC after E9.5, there is also contact of placental cells with nutrients and fatty acids from maternal blood, and these fatty acids might then exert their potentially negative effects on cells of the transfer zone leading to observable changes at E15.5. However, it might also be relevant to study further gestation days between E11.5 and E15.5 to elucidate these effects in more detail.

### 5.5 Impact of MO on placental transfer capacity

$^{14}$C-mannitol is an inert, non-metabolizable radioactive tracer that readily crosses the placental barrier via passive diffusion and accumulates in fetal tissues, and hence is used to study integrity of the feto-maternal transfer zone. This form of transfer of molecules across the placenta is responsible for a significant quantity of transfer, for example of up to 50% unidirectional flux of ions in humans. Consequently, any reduction in passive permeability of the placental barrier to hydrophilic substances and nutrients would have a direct consequence on total transfer capacity, and therefore also fetal supply and growth capability [83, 161, 162]. Next to hydrophilicity, steric properties of the molecules to be transferred are also important, which in the case of mannitol are quite similar to glucose. Additionally, morphological characteristics of the placenta are relevant for transfer [83, 104] which we assessed by stereological means, i.e. surface area and volume fractions. Results from our *in vivo* studies showed that materno-fetal transfer capacity of $^{14}$C-mannitol was significantly increased in obese dams at E15.5, even though the Lz:Jz ratio was reduced and Lz development seemed delayed at this stage. This might seem counterintuitive and one might expect a smaller Lz and impaired vascularization to lead to reduced transfer capacity, however there are possible explanations for the increased transfer capacity. First, it was described in our mouse model and elsewhere [83, 93] that in dams with IUGR offspring a catch-up growth between E15.5 and E18.5 can occur, which would demand increased transfer of nutrients and oxygen to the fetus to enhance its growth. However, not all nutrients are transported by passive diffusion, and altered morphology to enhance unidirectional transfer by maybe a margin of 50% can probably not solely compensate for fetal demands under IUGR. Therefore, investigation into active transport of e.g. GLUT-mediated glucose transport was conducted and revealed similar GLUT1/3 level in placentas of SD and HFD dams and slightly elevated GLUT4 level in placentas of HFD compared to SD dams at

E15.5 [93]. However, at E18.5 GLUT1 and GLUT4 level were both elevated in placentas of obese dams as described above, while GLUT3 level were similar to controls. These finding support the hypothesis of increased glucose flux to enable a catch-up growth between E15.5 and E18.5. On the other hand, the increase in $^{14}$C-mannitol could be a consequence of the disturbed ultrastructure in the transfer zone. We observed down-regulation of BM and ECM proteins, e.g. Lamc1 and Lamb2, as well as AJ markers concomitant with lipid accumulation, trophoblast differentiation defects and EC damage. These aspects could constitute a weakened placental barrier that might be unable to limit diffusion and, as a consequence, $^{14}$C-mannitol passes more readily from maternal to fetal circulation (Figure 5.4.1). A possible mechanism for this increase in permeability was presented by cell culture studies. We could show that BeWo cell layer permeability was significantly increased by stimulation with a high concentration of LA, a fatty acid found in high levels in HFD. Therefore, trophoblast cell layers in the placenta may be more permeable to substrate diffusion as a result of fatty acids from HFD in obese dams.

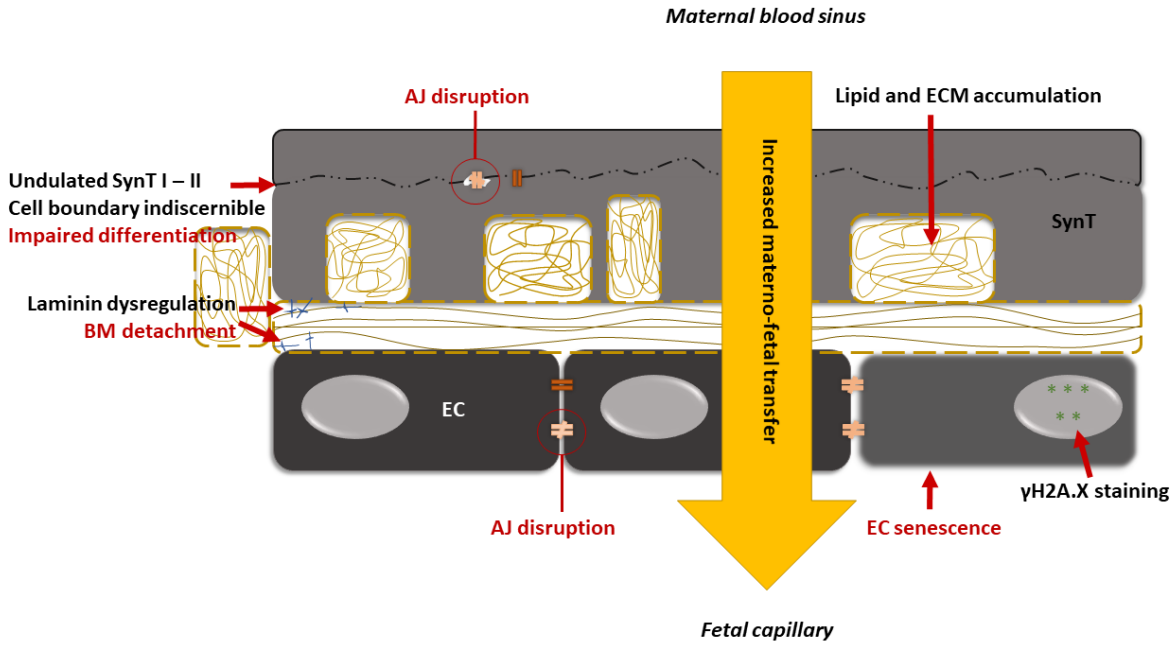


**Figure 5.4.1: Schematic illustration of the observed changes in the placental transfer zone under maternal obesity.** The figure illustrates damaged adherens junctions (AJ) and the differentiation defect in syncytiotrophoblast (SynT) concomitant with lipid and extracellular matrix (ECM) accumulation, also in the basement membrane (BM). Furthermore, endothelial cells (EC) were affected and might show disturbed AJ and increased γH2A.X staining which indicates a senescent phenotype. Additionally, stereology showed that the surface area of fetal capillaries was significantly reduced (not shown in this figure). These changes in cell homeostasis could lead to placental insufficiency and a defective placental barrier with increased materno-fetal transfer of inert hydrophilic substances. Trophoblast giant cells which are frequently observed superior to SynT were left out of this figure for simplification of the illustration and because they were not observed under EM in our HFD placentas.

Active substrate transport across the placenta was also touched in this work. $^{18}$F-FDG is a commonly used radioactive tracer in the clinic to assess tumor stages in a variety of cancers by PET scans which

are coupled to either computer tomography or MRT for precise tumor localization [163-165]. Moreover, PET scans coupled to MRT have also been performed on pregnant women in the past and yielded valuable information on $^{18}$F-FDG distribution and signal quantitation in placental and fetal tissues [166-168]. $^{18}$F-FDG PET scans have moreover been used in small animals, however studies in pregnant mice are very scarce [169]. Therefore, our $^{18}$F-FDG PET study is probably unique in that we investigated pregnant obese and control dams at E15.5. One challenge of determining accumulation of $^{18}$F-FDG in fetal tissues is the reference signal from maternal tissue [166]. We chose to apply the Padlak method and used maternal aorta as reference. We observed signal progression in the aorta of dams after injection into the tail vein and distribution in the circulation (Appendix 6.3, Figure 6.2.1) and normalized the signal in fetal tissues to the signal from the aorta. We could not find a significant difference in either $^{18}$F-FDG transfer or glucose metabolization rate in obese dams compared to controls, and regarding previous reports [93] might expect altered transfer rather at E18.5 than E15.5. Also, linear regression analysis was performed with various parameters and we found a significant, positive correlation of signal in fetal tissue and maternal blood glucose in control dams. This correlation was absent in obese dams, which showed high signals in fetal tissues even when maternal blood glucose was low. This suggests that obese dams have altered glucose distribution and that control dams favored maternal glucose supply with glucose over fetal supply when blood glucose level were low. Glucose is also the main energy source for the fetus and the placenta harbors glucose transporters, mostly GLUT1 and GLUT3, to mediate glucose accumulation [170]. Interestingly, it was reported that placentas under HFD showed increased GLUT1 expression at E18.5, but not E15.5 compared to SD placentas, as well as decreased glycogen cluster size from E15.5 to E18.5 in HFD placentas [93]. This may suggest that glucose accumulation in fetal tissues could be elevated later during gestation and hence, it would be reasonable to investigate $^{18}$F-FDG transfer capacity around E18.5, as mentioned above. Nonetheless, it has to be noted that a catch-up growth, as described, may not only require glucose, but also amino acids and fatty acids, and therefore increases in and increased activity of their transporters. Thus, amino acid and fatty acid transfer across the placenta need to be studied as well to fully understand fetal growth under MO [104].

### 5.6 Effect of anti-IL-6 signaling therapy on AJ marker and vascular development

We reported that IL-6 can induce EC senescence *in vitro* and proposed that this effect could lead to placental dysfunction, since IL-6 mRNA and protein level in egWAT and IL-6 serum level were increased and could potentially reach the placenta in obese dams. Hence, we aimed to determine whether IL-6 signaling blockade has positive effects on placental EC homeostasis and consequently on fetal outcome under MO. To this end, obese mice on HFD received either the IL-6 signaling blocking antibody mMR16-1 or the control antibody rat IgG and moreover, obese IL-6$^{-/-}$ mice on HFD were generated. Similar to HFD dams without antibody therapy, in mMR16-1 and IgG treated, as well as IL-6$^{-/-}$ dams, maternal and egWAT weight were significantly increased and fetal weight was strongly reduced at E15.5 compared to lean controls, showing an IUGR phenotype. Thus, the IL-6 signaling blockade by antibody therapy or IL-6$^{-/-}$ seem not to prevent an IUGR under MO. Also, litter size was not influenced by HFD

with or without mMR16-1 or IgG therapy or IL-6$^{-/-}$. However, resorption rates increased by more than 3-fold on average under HFD alone and mMR16-1 therapy when compared to SD, but this was without statistical significance. Nonetheless, absence of statistical significance does not prove absence of an effect [171] and hence, there might be an effect of HFD alone and mMR16-1 therapy on fetal resorption rate. Interestingly, up until now we could not show resorption of embryos in IL-6$^{-/-}$ dams which, of course, has to be interpreted with great care, since this cohort is very small, counting only 4 dams. Contrary to this observation is our personal experience and others (personal communication) that IL-6$^{-/-}$ dams became pregnant less frequently than HFD dams or antibody treated dams in this study, despite similar mating schemes with IL-6$^{-/-}$ males. However, there is some evidence in the literature that maternal immune activation modulates fetal development and further, knock-outs of cytokines in animal models have shown conflicting results in terms of fertility and pregnancy success, also regarding IL-6 knock-out [78, 172, 173]. Therefore, it is not surprising that pregnancy rate is somewhat lower in our IL-6$^{-/-}$ and a larger animal cohort might yield additional valuable insight.

ECs in the placenta can only react to IL-6 by soluble-IL6R (sIL-6R)/gp130-mediated trans-signaling, as described above, because they do not express the IL-6R [174]. Inflammatory signaling in ECs is thus mainly mediated by sIL6R/gp130 trans-signaling and leads to the activation of JAK/STAT3 and PI3K/AKT pathways, which therefore can also serve as read-out pathway when IL-6 trans-signaling is blocked [175-177]. To block IL-6 signaling in EC, it is required to e.g. block the IL-6 binding site in sIL-6R which is achievable by using an anti-IL-6R antibody, like tocilizumab in humans or mMR16-1 in mice [178-180]. The rat anti-murine IL-6R antibody mMR16-1 was used in pre-clinical studies to achieve FDA approval for tocilizumab and has been used in various other studies with non-pregnant C57BL/6 mice [84, 179, 181, 182].

Yoshida et al. [183] reported that MR16-1 induced an anti-rat IgG response after repeated administration in mice and hence, long-term application of MR16-1 could lead to antibody-mediated neutralization of MR16-1 and its effects. Therefore, MR16-1 was modified in the rat IgG1 FC part to generate a rat (Fab)-mouse FC chimeric antibody, mMR16-1, that should be less immunogenic and remain potent to block IL-6R for a longer period [84]. Serum level of SAA2, which is frequently used to evaluate IL-6 signaling blockade [84, 184], were not reduced in mMR16-1 treated dams compared to IgG treated dams in our study. This suggests that success of blocking IL-6 signaling may not be evaluated by SAA2 level after long-term application of mMR16-1 as we performed, or that IL-6 blockade was not successful in our setting. Wu et al. [84] showed that 7 days after mMR16-1 application, the SAA2 level returned to baseline which is the time-point at which dams in our study received the second injection with mMR16-1. Furthermore, it was reported that after 7 weeks of weekly application of MR16-1 (not mMR16-1), SAA level were significantly reduced compared to PBS injected mice, but not after 4 weeks of weekly application [185]. Thus, it remains unclear how multiple applications of mMR16-1 change expression of read-out marker like SAA2. On the other hand, in our model administration of mMR16-1 therapy over several weeks showed a significant increase in placental IL-6 level but no increase in SOCS3 level, a negative feedback regulator of IL-6 signaling. If elevated IL-6 level led to increased IL-6 signaling, SOCS3 level would likely be significantly increased to induce a negative feedback and block IL-6

signaling. However, this was not observed in mMR16-1 treated dams, indicating successful IL-6 signaling blockade and subsequent up-regulation of IL-6 level as compensation mechanism which was also reported elsewhere [84]. Moreover, we found suppression of Stat3 activation [182] and we also observed lower active p-Stat3 level in placentas of mMR16-1-treated dams. However, IgG therapy had a similar effect not only on p-Stat3 level, but also SOCS3 and total Erk1/2, which are also markers of JAK/STAT3 and PI3K/AKT pathways, respectively. Especially p-Stat3 remains difficult to evaluate as IL-6 signaling and blockade marker *in vivo* in our obesity model, since IL-6 serum level was elevated in HFD compared to SD dams, whereas p-Stat3 level were lower in placentas of HFD compared to SD dams (Figure 4.2.5.1). Nonetheless, mMR16-1 caused a strong increase in placental IL-6 protein level. We therefore believe that mMR16-1 does indeed block IL-6 signaling in parts, as the antibody is IL-6R specific, and suggest that p-Stat3 alone is not a sufficient *in vivo* marker for documenting blockade of IL-6 signaling after long-term mMR16-1 therapy. The use of a relevant control to the mMR16-1 antibody therapy is important for the study of mMR16-1-related effects and we chose a rat IgG antibody as control. Many other studies that utilized MR16-1 or mMR16-1 over variable time periods treated control animals with aqueous vehicles without an IgG antibody [182, 185, 186] or used an IgG similar to ours [84, 181, 187], making it difficult to compare existing literature and results of others with our work. This necessitates further investigation into mMR16-1 and its effects on IL-6 signaling blockade read-out markers, other than SAA2 and markers of JAK/STAT3 and PI3K/AKT pathways.

Administration of mMR16-1 or IgG led to a significant reduction of CD31 level in placentas compared to HFD dams without antibody therapy. In mMR16-1 treated dams, VE-cadherin and P-cadherin were also significantly decreased in placentas, compared to dams that received HFD without antibody therapy. This decrease of CD31 and VE-cadherin level may indicate a defect in placental vascularization that might be even further augmented under mMR16-1 therapy, when IL-6 signaling is blocked, than under HFD without antibody therapy compared to SD. The reduction in VE-cadherin and P-cadherin level in placentas of mMR16-1 treated dams indicates disturbed AJ compared to HFD dams without antibody therapy. Interestingly, level of VE-cadherin and P-cadherin in placentas of IgG treated dams seemed also reduced compared to HFD dams without antibody therapy, but failed to reach statistical significance. This suggests that IgG therapy causes less of an effect on AJ marker than mMR16-1 compared to the HFD without antibody therapy, possibly due to control IgG not blocking IL-6 signaling but inducing other unspecific side effects. As mentioned above, mMR16-1 and IgG therapy caused a reduction in placental p-Stat3 level and p-Stat3 has been associated with pre-eclampsia which is a pathology associated with vascular defects [188] and seems to regulate trophoblast invasion [189] as well as being involved in pregnancy loss in mice [190]. Hence, lower p-Stat3 level in the placenta may indicate defective vascular and placental development in mMR16-1 and IgG treated dams.

Taken together, the administration of either antibody, mMR16-1 or IgG control, in combination with HFD probably lead to an impaired placental development, placental dysfunction and fetal IUGR. Unfortunately, there is yet no data available on IL-6$^{-/-}$ placentas and level of these markers, together with stereological data that can be compared to data of mMR16, IgG and HFD without antibody therapy. Especially the stereological data would be particularly interesting, since these could show placental

vascularization and morphology under complete IL-6 knockout compared to temporary mMR16-1 antibody therapy and further elucidate the functional role of IL-6 signaling. Furthermore, IL-$6^{-/-}$ placentas could serve to decipher some of the mechanisms that are IL-6-related under MO in the context of placenta and fetal development on different gestation days (E11.5 to E18.5) since the IL-6 knockout persists constantly before and during pregnancy. However, based on the phenotypical data, it is safe to say that HFD was always associated with an IUGR phenotype, independent of IL-$6^{-/-}$ or IL-6 signaling blockade by mMR16-1, which probably limits the therapeutic potential of anti-IL-6 signaling strategies in obese pregnant patients. Literature on IL-6 antibody (tocilizumab) therapy in human pregnancies is scarce and only few case reports and expert opinions exist, and these suggest that tocilizumab should best be discontinued before and during pregnancy [191, 192].

As mentioned above, IL-6 signaling is required for normal pregnancy [172, 173] and IL-6 and other cytokines might play relevant roles in immune and fetal development [78, 172] and placental function [75]. Furthermore, Jones et al. showed that IL-6 is capable to up-regulate Stat3 and via this mechanism is linked to amino acid transporter increase in the placenta, and suggested that this occurs in combination with other pro-inflammatory cytokine signaling and can lead to fetal growth alterations [193]. Hence, influencing cytokine signaling, like IL-6, probably alters a spectrum of processes in the placenta. Since obesity alone alters inflammatory cytokine expression [79, 194], the combination of anti-IL-6 signaling therapy and obesity in our dams most certainly affected placental development and function. Hence, testing alternative concentrations of mMR16-1 antibody may be consequential, since the ideal concentration to allow healthy placenta development by simultaneously blocking negative effects in this organ due to increased IL-6 signaling under MO could not be determined herein, and the issue has not been addressed in this study.

### 5.7 Future perspectives

The impairment in placental development and function by HFD-induced MO was shown in this work, and it appears that EC as well as trophoblast homeostasis are affected during placental development under MO. Different markers of cell growth, differentiation and homeostasis were found to be altered, and ultrastructural changes fit the assumption of a disturbed cellular and extracellular environment. However, the ECM and especially the BM and cell-ECM interface were also affected by MO as indicated by proteomics profiling, and functional studies on markers of cell-ECM interaction like Ptk2 and Sdc4 are not discussed in the literature, yet. Therefore, we are currently busy with investigating changes in focal adhesion markers in placentas of obese and control dams. Furthermore, the period between E11.5 and E15.5 is probably very relevant for proper placental function and fetal development, since EC and AJ marker level that we investigated were unaltered at E11.5 between obese and control dams, however they were altered thereafter at E15.5. It might thus be possible that the placenta is fully functional in the first couple of days after first contact with maternal blood, between E9.5 and E11.5, but soon after develops insufficiencies and induces compensatory mechanisms. As a consequence, we observe the IUGR phenotype at E15.5 under MO, but lack valuable mechanistic insight on changes of placental

development that occur between E11.5 and E15.5, a period of 4 days out of about 20 days of total pregnancy duration.

Insights and findings from our murine maternal obesity model can serve as a basis for clinical investigations and a better understanding of the human placental health, pathologies and development. Over the past 2 years, we have gathered placenta and blood samples from pregnant human patients with lean, overweight and obese phenotypes with and without gestational diabetes in cooperation with the Gynecology and Obstetrics Department of the University Hospital in Cologne. These samples will be used to analyze EC homeostasis, vascularization as well as gene expression and protein level of various markers that were altered under MO in our mouse model. Despite morphological and cellular differences between murine and human placentas, the mechanisms of placental health and development show some astonishing similarities [7]. Hence, we believe that a lot of translational aspects of clinical relevance can be obtained from studying murine placentas under various maternal conditions. Additionally, serum from our patient cohort can be utilized in *in vitro* assays for placental cell stimulation to further decipher mechanisms of regulation and signaling in the placenta under MO, which might also pave the way for novel therapeutic approaches.

# 6. Appendix

## 6.1 Example of IL-6+/- genotyping

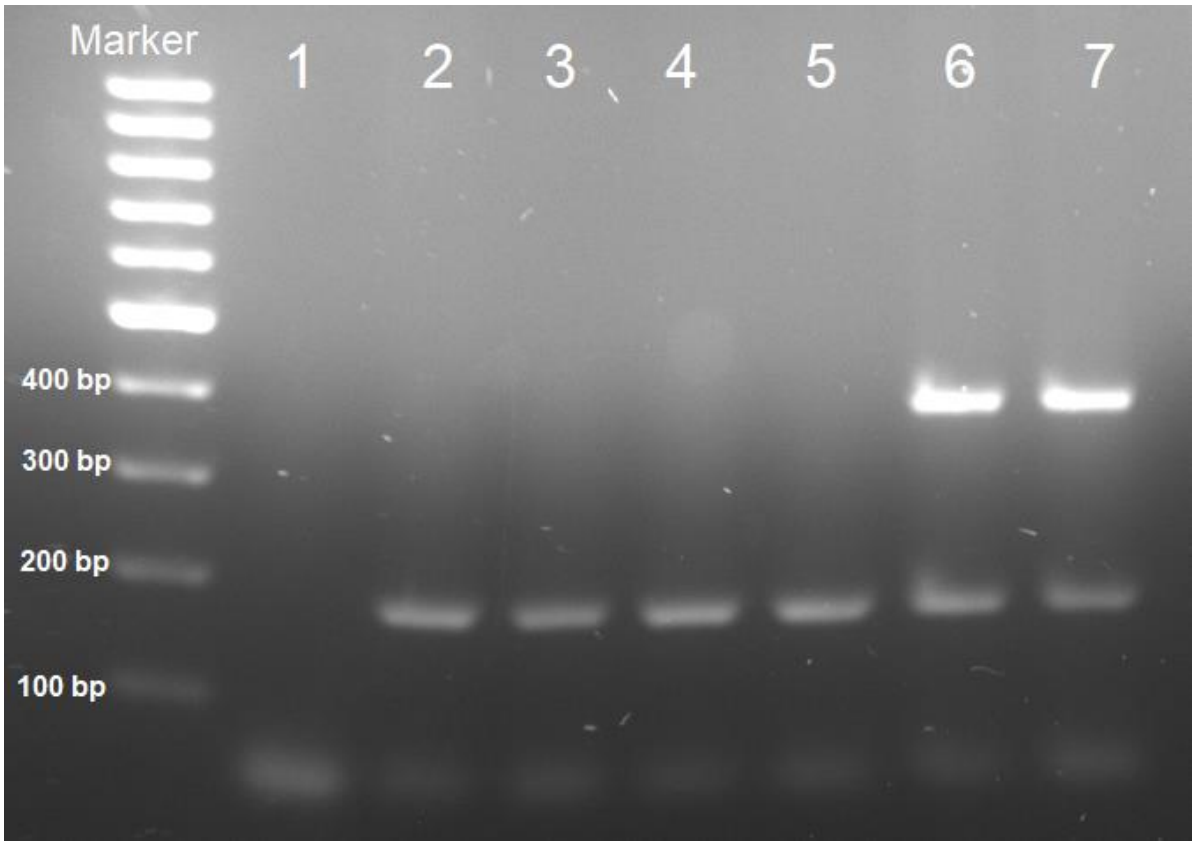


**Figure 6.1.1: Example of a genotyping agarose gel after electrophoresis.** The left side shows the gene marker with 100 bp intervals. Lane 1 is the negative control without genomic DNA. Lanes 2 to 5 show wild type samples with bands of approximately 174 base pairs only. Lanes 6 and 7 show two heterozygous IL-$6^{+/-}$ samples with bands at approximately 380 base-pairs (IL-6 mutant) and 174 base-pairs (wild type). Compare to example of the Jackson Lab at: https://www.jax.org/Protocol?stockNumber=002650&protocolID=22373).

## 6.2 Proteomics profile

Table 6.1: List of the 126 significantly altered proteins from proteomics profiling in HFD vs. SD transfer zone. The proteins are listed according to their Log2 difference (-1.0 represents fold-change of 0.5; 0 represents fold-change of 1; 1.0 represents fold-change of 2). The thick line shows transition from down-regulated to up-regulated protein level in HFD compared to SD samples. The *q* value of <0.05 denotes statistical significance.

| Protein ID | Gene names | Log2 difference HFD vs.SD | *q* value |
|---|---|---|---|
| P07356 | Anxa2 | -2,6168 | 0,0333684 |
| Q9DCN2 | Cyb5r3 | -2,59906 | 0,0084 |
| P50543 | S100a11 | -2,5607 | 0,0094 |
| Q91VB8 | haemaglobin alpha 2;Hba | -2,17721 | 0,013375 |
| P19096 | Fasn | -1,89499 | 0,0264419 |
| Q9ER00 | Stx12 | -1,78543 | 0 |

| | | | |
|---|---|---|---|
| Q8BHN3 | Ganab | -1,71235 | 0,0396699 |
| Q6EDY6 | Lrrc16a | -1,69647 | 0,0218485 |
| P57787 | Slc16a3 | -1,6913 | 0,007 |
| P14733 | Lmnb1 | -1,63922 | 0,0454553 |
| Q99PL5 | Rrbp1 | -1,61566 | 0,0346912 |
| P62192 | Psmc1 | -1,60362 | 0,0351379 |
| Q8JZU2 | Slc25a1 | -1,58432 | 0,0266429 |
| O55111 | Dsg2 | -1,52494 | 0,0302222 |
| O54724 | Ptrf | -1,47945 | 0,009 |
| Q8BH61 | F13a1 | -1,47331 | 0,0283725 |
| P09803 | Cdh1 | -1,45957 | 0,0351196 |
| O54988 | Slk | -1,44695 | 0,0355465 |
| Q91ZJ5 | Ugp2 | -1,40693 | 0,0342338 |
| P51150 | Rab7a | -1,40441 | 0,02828 |
| Q99LC5 | Etfa | -1,36717 | 0,0317458 |
| P16045 | Lgals1 | -1,33354 | 0,048063 |
| Q91YK2 | Rrp1b | -1,33122 | 0,0127059 |
| Q8K4I3 | Arhgef6 | -1,32215 | 0,0348854 |
| E9QAX7 | Cse1l | -1,30902 | 0,011625 |
| Q9Z1T1 | Ap3b1 | -1,29593 | 0,0347742 |
| Q9WTR1 | Trpv2 | -1,2713 | 0,0340128 |
| Q61753 | Phgdh | -1,21717 | 0,0145909 |
| P48678 | Lmna | -1,19905 | 0,0454758 |
| F8VPU2 | Farp1 | -1,19074 | 0,023725 |
| Q3TWV4 | Ap2m1 | -1,18023 | 0,0165172 |
| P97351 | Rps3a | -1,17537 | 0,0400625 |
| Q921G7 | Etfdh | -1,17352 | 0,0147895 |
| Q9D881 | Cox5b | -1,16998 | 0,036802 |
| D3YUP1 | Carm1 | -1,1574 | 0,0236579 |
| Q8VBZ3 | Clptm1 | -1,15313 | 0,0362323 |
| Q6W4W7 | Diap2;Diaph2 | -1,14764 | 0 |
| Q8CH18 | Ccar1 | -1,14342 | 0,00763636 |
| Q3UQ44 | Iqgap2 | -1,10754 | 0 |
| Q6P5E4 | Uggt1 | -1,08886 | 0,0337123 |
| O08553 | Dpysl2 | -1,08026 | 0,0218235 |
| Q3U4W8 | Usp5 | -1,07322 | 0,0397547 |
| O88844 | Idh1 | -1,07236 | 0,0341884 |
| Q61292 | Lamb2 | -1,07222 | 0,0217429 |
| Q5SQG5 | Phb | -1,0642 | 0,0338485 |
| Q9JLV5 | Cul3 | -1,04271 | 0,0322931 |
| Q8VDN2 | Atp1a1 | -1,03661 | 0,0461032 |
| Q6P5H2 | Nes | -1,03493 | 0,0452269 |
| Q8BML9 | Qars | -1,0222 | 0,0296923 |

| | | | |
|---|---|---|---|
| O08749 | Dld | -1,01181 | 0,0190323 |
| G3X971 | Ank3 | -0,986192 | 0,01416 |
| Q60634 | Flot2 | -0,982782 | 0,0305273 |
| E9Q6R4 | Arid1b | -0,981078 | 0 |
| P13707 | Gpd1 | -0,980603 | 0,034 |
| Q9D8N0 | Eef1g | -0,978909 | 0,0336716 |
| Q6P9R4 | Arhgef18 | -0,956909 | 0,0349091 |
| Q64521 | Gpd2 | -0,95459 | 0,0334634 |
| Q920Q4 | Vps16 | -0,954346 | 0,0393832 |
| Q810B6 | Ankfy1 | -0,941094 | 0,0386545 |
| P34152 | Ptk2 | -0,931865 | 0,0136154 |
| Q8VCQ8 | Cald1 | -0,911643 | 0,0428696 |
| Q9D0E1 | Hnrnpm | -0,909578 | 0,0328 |
| P70168 | Kpnb1 | -0,90501 | 0,0273673 |
| Q9JKF1 | Iqgap1 | -0,901555 | 0,0339125 |
| B2RX14 | Zcchc11 | -0,884978 | 0,0171667 |
| Q7TQ95 | Lnp | -0,856671 | 0,008375 |
| Q5H8C4 | Vps13a | -0,849888 | 0,0184375 |
| Q8CGB3 | Uaca | -0,833469 | 0,01405 |
| E9Q616 | Ahnak | -0,827819 | 0,0303585 |
| Q62318 | Trim28 | -0,817407 | 0,0341899 |
| Q9Z1G4 | Atp6v0a1 | -0,813168 | 0,0351222 |
| Q62383 | Supt6h | -0,802911 | 0,0340156 |
| Q3UMF0 | Cobll1 | -0,788507 | 0,0366275 |
| E9Q4K7 | Kif13b | -0,788062 | 0,0401333 |
| O35988 | Sdc4 | -0,762921 | 0,0390185 |
| J3QJX0 | Cul4b | -0,731063 | 0,0271875 |
| G5E898 | Ppl | -0,730015 | 0,0349278 |
| Q8R1K1 | Ubac2 | -0,721819 | 0,040018 |
| Q9Z0K8 | Vnn1 | -0,720036 | 0,0351905 |
| Q8BKG3 | Ptk7 | -0,718419 | 0,0342222 |
| P17156 | Hspa2 | -0,699641 | 0,0390092 |
| Q05793 | Hspg2 | -0,69063 | 0,0275111 |
| Q91V41 | Rab14 | -0,683975 | 0,0322807 |
| Q569Z5 | Ddx46 | -0,669953 | 0,03587 |
| Q8R0G9 | Nup133 | -0,66988 | 0,0349895 |
| Q99KI3 | Emc3 | -0,666976 | 0,0340714 |
| O35379 | Abcc1 | -0,654475 | 0,0347363 |
| Q9WVK4 | Ehd1 | -0,65194 | 0,0341231 |
| Q8C391 | Exoc4 | -0,651399 | 0,0336533 |
| Q9D2R0 | Aacs | -0,640354 | 0,0458279 |
| Q5SVG5 | Ap1b1 | -0,639239 | 0,0263404 |
| Q6PGF7 | Exoc8 | -0,620831 | 0,0253659 |

| | | | |
|---|---|---|---|
| F7BPW6 | Sec16a | -0,61018 | 0,0341311 |
| Q62261 | Sptbn1 | -0,602572 | 0,0397404 |
| Q91V89 | Ppp2r5d | -0,59464 | 0,0299821 |
| Q6TXD4 | Dnmbp | -0,548996 | 0,0210541 |
| F8VPK5 | Rock2 | -0,546932 | 0,0339054 |
| P46460 | Nsf | -0,546922 | 0,0450171 |
| D3YX34 | Dctn1 | -0,543849 | 0,026913 |
| A2AWA7 | Rabgap1 | -0,513952 | 0,040177 |
| F8VQJ3 | Lamc1 | -0,511355 | 0,0347419 |
| Q99MR8 | Mccc1 | -0,510445 | 0,0341806 |
| Q8C8U0 | Ppfibp1 | -0,508217 | 0,0446356 |
| Q91W86 | Vps11 | -0,497033 | 0,0359647 |
| Q9QXZ0 | Macf1 | -0,476136 | 0,0430776 |
| Q6P9Q4 | Fhod1 | -0,454446 | 0,0345783 |
| Q9CYH2 | Fam213a | 0,406607 | 0,0353617 |
| O08677 | Kng1 | 0,524401 | 0,045525 |
| P55065 | Pltp | 0,567094 | 0,0452562 |
| E9Q5B6 | Hnrnpd | 0,583015 | 0,0338765 |
| Q922U1 | Prpf3 | 0,614512 | 0,024 |
| Q99JY9 | Actr3 | 0,673098 | 0,0156111 |
| Q04447 | Ckb | 0,678408 | 0,0171071 |
| Q8BH95 | Echs1 | 0,710599 | 0,0421754 |
| Q9DBM2 | Ehhadh | 0,753224 | 0,0139565 |
| Q61233 | Lcp1 | 0,776454 | 0,045784 |
| Q3TQP6 | Me1 | 0,822377 | 0,00933333 |
| Q3TC93 | Hs1bp3 | 0,822602 | 0,0364184 |
| Q99KK9 | Hars2 | 0,847471 | 0,0100714 |
| O70310 | Nmt1 | 0,849706 | 0,0140952 |
| Q9CY58 | Serbp1 | 0,953535 | 0,0171111 |
| P58774 | Tpm2 | 1,10221 | 0,0277273 |
| Q61553 | Fscn1 | 1,10559 | 0,00771429 |
| P68040 | Gnb2l1 | 1,19011 | 0,0108462 |
| Q8K114 | Ints9 | 1,24664 | 0,0347528 |
| Q61781 | Krt14 | 1,50661 | 0,0211389 |

### 6.3 $^{18}$F-FDG time activity curve example

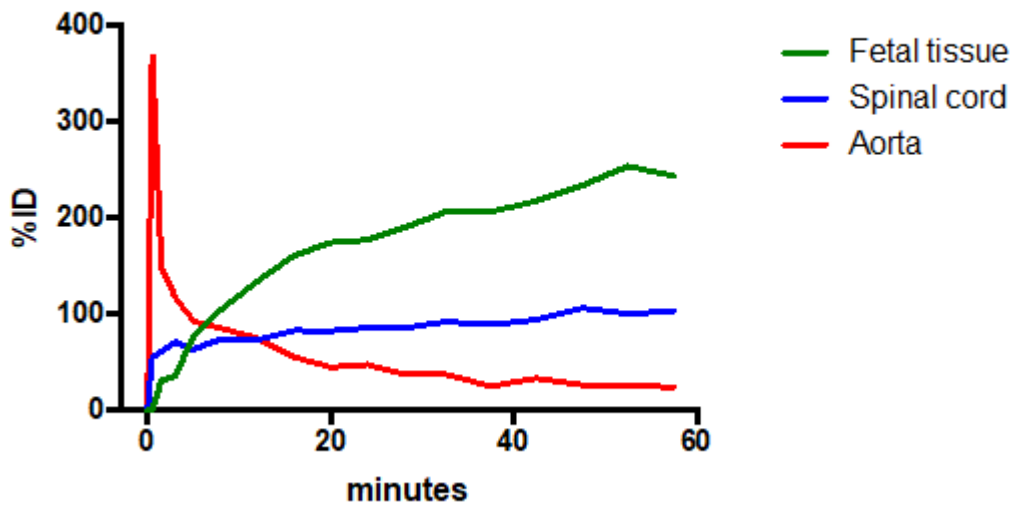


**Figure 6.2.1: Time activity curve example of $^{18}$F-FDG study.** The curve shows that first a signal from $^{18}$F-FDG is detected in the aorta (red curve) of dams directly after injection at minute 0 to 5 where the curve also has its peak. After some minutes, the signal increases in fetal tissue (green curve) and maternal spinal cord (blue curve) and reaches near maximum in spinal cord after about 10 minutes while the signal continuous to increase in fetal tissue until about minute 50.

### 6.4 Fatty acids found in the HFD

Table 6.2: Excerpt of the fatty acids found in the HFD used in this study. Table adapted from Kretschmer et al. [81], Table S1 and modified.

| Ingredient | Unit | Content |
|---|---|---|
| Crude fat | mg/kg | 350,921 |
| Crude protein | mg/kg | 204,600 |
| Saccharides | mg/kg | 256,291.3 |
| Metabolizable Energy | kcal/kg | 5,297.347 |
| Palmitic acid C-16:0 | mg/kg | 84,800 |
| Palmitoleic acid C-16:1 | mg/kg | 10,401 |
| Stearic acid C-18:0 | mg/kg | 48,600 |
| Oleic acid C-18:1 | mg/kg | 139,135 |
| Linoleic acid C-18:2 | mg/kg | 31,550 |
| Linolenic acid C-18:3 | mg/kg | 3,565 |
| Arachidic acid C-20:0 | mg/kg | 5,200 |
| Eicosaenic acid C-20:1 | mg/kg | 2,595 |
| Arachidonic acid C-20:4 | mg/kg | 120 |

## 7. References


1. Blumstein, D.T., *Handbook of the Mammals of the World edited by Don E. Wilson, Thomas E. Lacher, Russell A. Mittermeier, Albert Martínez-Vilalta, David Leslie, Erika Barthelmess, Toni Llobet, and Josep del Hoyo.* The Quarterly Review of Biology, 2017. 92(3): p. 343-344.
2. Blackburn, S.T., *Maternal, Fetal, & Neonatal Physiology: A Clinical Perspective*. 2007: Saunders Elsevier.
3. Georgiades, P., A.C. Ferguson-Smith, and G.J. Burton, *Comparative developmental anatomy of the murine and human definitive placentae.* Placenta, 2002. 23(1): p. 3-19.
4. Fox, H., *Pathology of the placenta*. 1997, London; Philadelphia: W.B. Saunders.
5. Dockery, P., J. Bermingham, and D. Jenkins, *Structure-function relations in the human placenta.* Biochem Soc Trans, 2000. 28(2): p. 202-8.
6. Schneider, H., *Placental Dysfunction as a Key Element in the Pathogenesis of Preeclampsia.* Dev Period Med, 2017. 21(4): p. 309-316.
7. Maltepe, E., A.I. Bakardjiev, and S.J. Fisher, *The placenta: transcriptional, epigenetic, and physiological integration during development.* J Clin Invest, 2010. 120(4): p. 1016-25.
8. Watson, E.D. and J.C. Cross, *Development of structures and transport functions in the mouse placenta.* Physiology (Bethesda), 2005. 20: p. 180-93.
9. Ayadi, A., et al., *Mouse large-scale phenotyping initiatives: overview of the European Mouse Disease Clinic (EUMODIC) and of the Wellcome Trust Sanger Institute Mouse Genetics Project.* Mamm Genome, 2012. 23(9-10): p. 600-10.
10. Perez-Garcia, V., et al., *Placentation defects are highly prevalent in embryonic lethal mouse mutants.* Nature, 2018. 555(7697): p. 463-468.
11. De Clercq, K., et al., *High-resolution contrast-enhanced microCT reveals the true three-dimensional morphology of the murine placenta.* Proc Natl Acad Sci U S A, 2019. 116(28): p. 13927-13936.
12. Mu, J. and S.L. Adamson, *Developmental changes in hemodynamics of uterine artery, utero- and umbilicoplacental, and vitelline circulations in mouse throughout gestation.* Am J Physiol Heart Circ Physiol, 2006. 291(3): p. H1421-8.
13. Rossant, J. and J.C. Cross, *Placental development: lessons from mouse mutants.* Nat Rev Genet, 2001. 2(7): p. 538-48.
14. Furukawa, S., Y. Kuroda, and A. Sugiyama, *A comparison of the histological structure of the placenta in experimental animals.* Journal of toxicologic pathology, 2014. 27(1): p. 11-18.
15. Adamson, S.L., et al., *Interactions between trophoblast cells and the maternal and fetal circulation in the mouse placenta.* Dev Biol, 2002. 250(2): p. 358-73.
16. Pardi, G., A.M. Marconi, and I. Cetin, *Placental-fetal interrelationship in IUGR fetuses--a review.* Placenta, 2002. 23 Suppl A: p. S136-41.
17. Constância, M., et al., *Placental-specific IGF-II is a major modulator of placental and fetal growth.* Nature, 2002. 417(6892): p. 945-8.
18. Jones, H.N., T.L. Powell, and T. Jansson, *Regulation of placental nutrient transport--a review.* Placenta, 2007. 28(8-9): p. 763-74.
19. Coan, P.M., et al., *Origin and characteristics of glycogen cells in the developing murine placenta.* Dev Dyn, 2006. 235(12): p. 3280-94.
20. Tetro, N., et al., *The Placental Barrier: the Gate and the Fate in Drug Distribution.* Pharm Res, 2018. 35(4): p. 71.
21. Chen, Y., et al., *Instigation of endothelial Nlrp3 inflammasome by adipokine visfatin promotes inter-endothelial junction disruption: role of HMGB1.* J Cell Mol Med, 2015. 19(12): p. 2715-27.
22. Gruber, L., et al., *High fat diet accelerates pathogenesis of murine Crohn's disease-like ileitis independently of obesity.* PLoS One, 2013. 8(8): p. e71661.
23. Burton, G.J. and A.L. Fowden, *Review: The placenta and developmental programming: balancing fetal nutrient demands with maternal resource allocation.* Placenta, 2012. 33 Suppl: p. S23-7.
24. Coan, P.M., A.C. Ferguson-Smith, and G.J. Burton, *Developmental dynamics of the definitive mouse placenta assessed by stereology.* Biol Reprod, 2004. 70(6): p. 1806-13.
25. Coan, P.M., A.C. Ferguson-Smith, and G.J. Burton, *Ultrastructural changes in the interhaemal membrane and junctional zone of the murine chorioallantoic placenta across gestation.* J Anat, 2005. 207(6): p. 783-96.
26. Riquelme, G., *Review: Placental syncytiotrophoblast membranes--domains, subdomains and microdomains.* Placenta, 2011. 32 Suppl 2: p. S196-202.

27. Cross, J.C., D.G. Simmons, and E.D. Watson, *Chorioallantoic morphogenesis and formation of the placental villous tree.* Ann N Y Acad Sci, 2003. 995: p. 84-93.
28. Batistatou, A., et al., *Expression of dysadherin and E-cadherin in trophoblastic tissue in normal and abnormal pregnancies.* Placenta, 2007. 28(5-6): p. 590-2.
29. Gumbiner, B.M., *Regulation of cadherin-mediated adhesion in morphogenesis.* Nat Rev Mol Cell Biol, 2005. 6(8): p. 622-34.
30. Dejana, E., *Endothelial cell-cell junctions: happy together.* Nat Rev Mol Cell Biol, 2004. 5(4): p. 261-70.
31. Dejana, E. and C. Giampietro, *Vascular endothelial-cadherin and vascular stability.* Curr Opin Hematol, 2012. 19(3): p. 218-23.
32. Leach, L., et al., *Molecular organization of tight and adherens junctions in the human placental vascular tree.* Placenta, 2000. 21(5-6): p. 547-57.
33. Cattelino, A., et al., *The conditional inactivation of the beta-catenin gene in endothelial cells causes a defective vascular pattern and increased vascular fragility.* J Cell Biol, 2003. 162(6): p. 1111-22.
34. Sonderegger, S., J. Pollheimer, and M. Knöfler, *Wnt signalling in implantation, decidualisation and placental differentiation--review.* Placenta, 2010. 31(10): p. 839-47.
35. Marciniak, A., et al., *Fetal programming of the metabolic syndrome.* Taiwan J Obstet Gynecol, 2017. 56(2): p. 133-138.
36. Myatt, L. and A. Maloyan, *Obesity and Placental Function.* Semin Reprod Med, 2016. 34(1): p. 42-9.
37. Alexander, B.T., J.H. Dasinger, and S. Intapad, *Fetal programming and cardiovascular pathology.* Compr Physiol, 2015. 5(2): p. 997-1025.
38. Stubert, J., et al., *The Risks Associated With Obesity in Pregnancy.* Dtsch Arztebl Int, 2018. 115(16): p. 276-283.
39. Reijnders, I.F., et al., *The impact of periconceptional maternal lifestyle on clinical features and biomarkers of placental development and function: a systematic review.* Hum Reprod Update, 2019. 25(1): p. 72-94.
40. Burton, G.J., et al., *Pre-eclampsia: pathophysiology and clinical implications.* Bmj, 2019. 366: p. l2381.
41. Cresswell, J.A., et al., *Effect of maternal obesity on neonatal death in sub-Saharan Africa: multivariable analysis of 27 national datasets.* The Lancet, 2012. 380(9850): p. 1325-1330.
42. Mensink, G.B., et al., *[Overweight and obesity in Germany: results of the German Health Interview and Examination Survey for Adults (DEGS1)].* Bundesgesundheitsblatt Gesundheitsforschung Gesundheitsschutz, 2013. 56(5-6): p. 786-94.
43. Cedergren, M.I., *Maternal morbid obesity and the risk of adverse pregnancy outcome.* Obstet Gynecol, 2004. 103(2): p. 219-24.
44. Liang, C., K. DeCourcy, and M.R. Prater, *High-saturated-fat diet induces gestational diabetes and placental vasculopathy in C57BL/6 mice.* Metabolism, 2010. 59(7): p. 943-50.
45. Desai, M., J.K. Jellyman, and M.G. Ross, *Epigenomics, gestational programming and risk of metabolic syndrome.* Int J Obes (Lond), 2015. 39(4): p. 633-41.
46. Janesick, A.S. and B. Blumberg, *Obesogens: an emerging threat to public health.* American journal of obstetrics and gynecology, 2016. 214(5): p. 559-565.
47. Trasande, L., et al., *Incremental charges, costs, and length of stay associated with obesity as a secondary diagnosis among pregnant women.* Med Care, 2009. 47(10): p. 1046-52.
48. Suzuki, K., *The developing world of DOHaD.* J Dev Orig Health Dis, 2018. 9(3): p. 266-269.
49. Nelson, S.M., P. Matthews, and L. Poston, *Maternal metabolism and obesity: modifiable determinants of pregnancy outcome.* Hum Reprod Update, 2010. 16(3): p. 255-75.
50. Zhang, C., S. Rawal, and Y.S. Chong, *Risk factors for gestational diabetes: is prevention possible?* Diabetologia, 2016. 59(7): p. 1385-1390.
51. Kintiraki, E., et al., *Pregnancy-Induced hypertension.* Hormones (Athens), 2015. 14(2): p. 211-23.
52. Brett, K.E., et al., *Maternal-fetal nutrient transport in pregnancy pathologies: the role of the placenta.* Int J Mol Sci, 2014. 15(9): p. 16153-85.
53. Sharma, D., S. Shastri, and P. Sharma, *Intrauterine Growth Restriction: Antenatal and Postnatal Aspects.* Clin Med Insights Pediatr, 2016. 10: p. 67-83.
54. Vijayaselvi, R. and A. Cherian, *Risk assessment of intrauterine growth restriction.* Current Medical Issues, 2017. 15(4): p. 262-266.

55. Woods, L., V. Perez-Garcia, and M. Hemberger, *Regulation of Placental Development and Its Impact on Fetal Growth-New Insights From Mouse Models.* Front Endocrinol (Lausanne), 2018. 9: p. 570.
56. Kingdom, J.C., et al., *A placenta clinic approach to the diagnosis and management of fetal growth restriction.* Am J Obstet Gynecol, 2018. 218(2s): p. S803-s817.
57. Huang, L., et al., *Maternal prepregnancy obesity is associated with higher risk of placental pathological lesions.* Placenta, 2014. 35(8): p. 563-9.
58. Kovo, M., et al., *The Effect of Maternal Obesity on Pregnancy Outcome in Correlation With Placental Pathology.* Reprod Sci, 2015. 22(12): p. 1643-8.
59. Hayes, E.K., et al., *Adverse fetal and neonatal outcomes associated with a life-long high fat diet: role of altered development of the placental vasculature.* PLoS One, 2012. 7(3): p. e33370.
60. Hayes, E.K., et al., *Trophoblast invasion and blood vessel remodeling are altered in a rat model of lifelong maternal obesity.* Reprod Sci, 2014. 21(5): p. 648-57.
61. Challier, J.C., et al., *Obesity in pregnancy stimulates macrophage accumulation and inflammation in the placenta.* Placenta, 2008. 29(3): p. 274-81.
62. Frias, A.E., et al., *Maternal high-fat diet disturbs uteroplacental hemodynamics and increases the frequency of stillbirth in a nonhuman primate model of excess nutrition.* Endocrinology, 2011. 152(6): p. 2456-64.
63. Kim, D.W., et al., *Obesity during pregnancy disrupts placental morphology, cell proliferation, and inflammation in a sex-specific manner across gestation in the mouse.* Biol Reprod, 2014. 90(6): p. 130.
64. Denison, F.C., et al., *Obesity, pregnancy, inflammation, and vascular function.* Reproduction, 2010. 140(3): p. 373-85.
65. Christian, L.M. and K. Porter, *Longitudinal changes in serum proinflammatory markers across pregnancy and postpartum: effects of maternal body mass index.* Cytokine, 2014. 70(2): p. 134-40.
66. Stewart, F.M., et al., *Longitudinal assessment of maternal endothelial function and markers of inflammation and placental function throughout pregnancy in lean and obese mothers.* J Clin Endocrinol Metab, 2007. 92(3): p. 969-75.
67. Pantham, P., I.L. Aye, and T.L. Powell, *Inflammation in maternal obesity and gestational diabetes mellitus.* Placenta, 2015. 36(7): p. 709-15.
68. Scheller, J., et al., *The pro- and anti-inflammatory properties of the cytokine interleukin-6.* Biochim Biophys Acta, 2011. 1813(5): p. 878-88.
69. Barnes, T.C., et al., *Endothelial activation and apoptosis mediated by neutrophil-dependent interleukin 6 trans-signalling: a novel target for systemic sclerosis?* Ann Rheum Dis, 2011. 70(2): p. 366-72.
70. Blecharz-Lang, K.G., et al., *Interleukin 6-Mediated Endothelial Barrier Disturbances Can Be Attenuated by Blockade of the IL6 Receptor Expressed in Brain Microvascular Endothelial Cells.* Transl Stroke Res, 2018. 9(6): p. 631-642.
71. Krueger, J., et al., *Expression and function of interleukin-6 in epithelial cells.* J Cell Biochem, 1991. 45(4): p. 327-34.
72. Tossetta, G., et al., *IL-1β and TGF-β weaken the placental barrier through destruction of tight junctions: an in vivo and in vitro study.* Placenta, 2014. 35(7): p. 509-16.
73. Kobayashi, K., H. Miwa, and M. Yasui, *Inflammatory mediators weaken the amniotic membrane barrier through disruption of tight junctions.* J Physiol, 2010. 588(Pt 24): p. 4859-69.
74. Resi, V., et al., *Molecular inflammation and adipose tissue matrix remodeling precede physiological adaptations to pregnancy.* Am J Physiol Endocrinol Metab, 2012. 303(7): p. E832-40.
75. Howell, K.R. and T.L. Powell, *Effects of maternal obesity on placental function and fetal development.* Reproduction, 2017. 153(3): p. R97-r108.
76. Appel, S., et al., *Leptin does not induce an inflammatory response in the murine placenta.* Horm Metab Res, 2014. 46(6): p. 384-9.
77. Janoschek, R., et al., *Dietary intervention in obese dams protects male offspring from WAT induction of TRPV4, adiposity, and hyperinsulinemia.* Obesity (Silver Spring), 2016. 24(6): p. 1266-73.
78. Kopf, M., et al., *Impaired immune and acute-phase responses in interleukin-6-deficient mice.* Nature, 1994. 368(6469): p. 339-42.
79. **Appel, S., et al.**, *Maternal obesity attenuates predelivery inflammatory reaction in C57BL/6N mice.* J Reprod Immunol, 2017. 122: p. 10-13.

80. **Nüsken, E.**, et al., *Maternal High Fat Diet and in-Utero Metformin Exposure Significantly Impact upon the Fetal Renal Proteome of Male Mice.* J Clin Med, 2019. 8(5).
81. **Kretschmer, T.**, et al., *Effect of Maternal Obesity in Mice on IL-6 Levels and Placental Endothelial Cell Homeostasis.* Nutrients, 2020. 12(2).
82. Fowler, J.S. and A.P. Wolf, *Synthesis of carbon-11, fluorine-18, and nitrogen-13 labeled radiotracers for biomedical applications*. 1981, ; Brookhaven National Lab., Upton, NY (USA). p. Medium: ED; Size: Pages: 124.
83. Sibley, C.P., et al., *Placental-specific insulin-like growth factor 2 (Igf2) regulates the diffusional exchange characteristics of the mouse placenta.* Proc Natl Acad Sci U S A, 2004. 101(21): p. 8204-8.
84. Wu, G., et al., *Monoclonal anti-interleukin-6 receptor antibody attenuates donor-specific antibody responses in a mouse model of allosensitization.* Transpl Immunol, 2013. 28(2-3): p. 138-43.
85. Suvarna, K.S., C. Layton, and J.D. Bancroft, *Bancroft's Theory and Practice of Histological Techniques E-Book*. 2012: Elsevier Health Sciences.
86. Altunkaynak, B.Z., et al., *A brief introduction to stereology and sampling strategies: basic concepts of stereology.* NeuroQuantology: An Interdisciplinary Journal of Neuroscience and Quantum Physics, 2012. 10: p. 31+.
87. Hughes, C.S., et al., *Single-pot, solid-phase-enhanced sample preparation for proteomics experiments.* Nat Protoc, 2019. 14(1): p. 68-85.
88. Hegen, M., et al., *MAPKAP kinase 2-deficient mice are resistant to collagen-induced arthritis.* J Immunol, 2006. 177(3): p. 1913-7.
89. Livak, K.J. and T.D. Schmittgen, *Analysis of relative gene expression data using real-time quantitative PCR and the 2(-Delta Delta C(T)) Method.* Methods, 2001. 25(4): p. 402-8.
90. Fischer, M., et al., *I. A bioactive designer cytokine for human hematopoietic progenitor cell expansion.* Nat Biotechnol, 1997. 15(2): p. 142-5.
91. Kipkeew, F., et al., *CCN1 (CYR61) and CCN3 (NOV) signaling drives human trophoblast cells into senescence and stimulates migration properties.* Cell Adh Migr, 2016. 10(1-2): p. 163-78.
92. Benjamini, Y. and Y. Hochberg, *Controlling the false discovery rate: a practical and powerful approach to multiple testing.* Journal of the Royal statistical society: series B (Methodological), 1995. 57(1): p. 289-300.
93. Appel, S., et al., *A Potential Role for GSK3β in Glucose-Driven Intrauterine Catch-Up Growth in Maternal Obesity.* Endocrinology, 2019. 160(2): p. 377-386.
94. Dahlgren, J., et al., *Interleukin-6 in the maternal circulation reaches the rat fetus in mid-gestation.* Pediatr Res, 2006. 60(2): p. 147-51.
95. Zaretsky, M.V., et al., *Transfer of inflammatory cytokines across the placenta.* Obstet Gynecol, 2004. 103(3): p. 546-50.
96. von Mering, C., et al., *STRING: known and predicted protein-protein associations, integrated and transferred across organisms.* Nucleic Acids Res, 2005. 33(Database issue): p. D433-7.
97. Bae-Gartz, I., et al., *Running Exercise in Obese Pregnancies Prevents IL-6 Trans-signaling in Male Offspring.* Med Sci Sports Exerc, 2016. 48(5): p. 829-38.
98. Nilsson, C., et al., *Laboratory animals as surrogate models of human obesity.* Acta Pharmacol Sin, 2012. 33(2): p. 173-81.
99. Kleinert, M., et al., *Animal models of obesity and diabetes mellitus.* Nat Rev Endocrinol, 2018. 14(3): p. 140-162.
100. Hariri, N. and L. Thibault, *High-fat diet-induced obesity in animal models.* Nutr Res Rev, 2010. 23(2): p. 270-99.
101. Speakman, J.R., *Use of high-fat diets to study rodent obesity as a model of human obesity.* International Journal of Obesity, 2019. 43(8): p. 1491-1492.
102. Odermatt, A., *The Western-style diet: a major risk factor for impaired kidney function and chronic kidney disease.* Am J Physiol Renal Physiol, 2011. 301(5): p. F919-31.
103. Varlamov, O., *Western-style diet, sex steroids and metabolism.* Biochim Biophys Acta Mol Basis Dis, 2017. 1863(5): p. 1147-1155.
104. Sferruzzi-Perri, A.N., et al., *An obesogenic diet during mouse pregnancy modifies maternal nutrient partitioning and the fetal growth trajectory.* Faseb j, 2013. 27(10): p. 3928-37.
105. Camacho-Buenrostro, D., et al., *THE ASSOCIATION BETWEEN PRE-PREGNANCY OBESITY AND WEIGHT GAIN IN PREGNANCY, WITH GROWTH DEVIATIONS IN NEWBORNS.* Nutr Hosp, 2015. 32(1): p. 124-9.
106. Goldstein, R.F., et al., *Association of Gestational Weight Gain With Maternal and Infant Outcomes: A Systematic Review and Meta-analysis.* Jama, 2017. 317(21): p. 2207-2225.

107. Nardozza, L.M., et al., *Fetal growth restriction: current knowledge.* Arch Gynecol Obstet, 2017. 295(5): p. 1061-1077.
108. Burton, G.J. and E. Jauniaux, *Pathophysiology of placental-derived fetal growth restriction.* Am J Obstet Gynecol, 2018. 218(2s): p. S745-s761.
109. Sultana, Z., et al., *Oxidative stress, placental ageing-related pathologies and adverse pregnancy outcomes.* Am J Reprod Immunol, 2017. 77(5).
110. Greenberg, A.S. and M.S. Obin, *Obesity and the role of adipose tissue in inflammation and metabolism.* Am J Clin Nutr, 2006. 83(2): p. 461s-465s.
111. Zhang, L., et al., *The inflammatory changes of adipose tissue in late pregnant mice.* J Mol Endocrinol, 2011. 47(2): p. 157-65.
112. Coelho, M., T. Oliveira, and R. Fernandes, *Biochemistry of adipose tissue: an endocrine organ.* Arch Med Sci, 2013. 9(2): p. 191-200.
113. Arrowsmith, S., S. Wray, and S. Quenby, *Maternal obesity and labour complications following induction of labour in prolonged pregnancy.* Bjog, 2011. 118(5): p. 578-88.
114. Azaïs, H., et al., *Effects of adipokines and obesity on uterine contractility.* Cytokine Growth Factor Rev, 2017. 34: p. 59-66.
115. Kyank, H., *[Endothelial cell damage in pre-eclampsia].* Zentralbl Gynakol, 1991. 113(9): p. 487-92.
116. Iantorno, M., et al., *Obesity, inflammation and endothelial dysfunction.* J Biol Regul Homeost Agents, 2014. 28(2): p. 169-76.
117. Song, L., et al., *Prenatal high-fat diet alters placental morphology, nutrient transporter expression, and mtorc1 signaling in rat.* Obesity (Silver Spring), 2017. 25(5): p. 909-919.
118. Savant, S., et al., *The Orphan Receptor Tie1 Controls Angiogenesis and Vascular Remodeling by Differentially Regulating Tie2 in Tip and Stalk Cells.* Cell Rep, 2015. 12(11): p. 1761-73.
119. Chan, B. and V.P. Sukhatme, *Suppression of Tie-1 in endothelial cells in vitro induces a change in the genome-wide expression profile reflecting an inflammatory function.* FEBS Lett, 2009. 583(6): p. 1023-8.
120. Yang, P., et al., *Tie-1: A potential target for anti-angiogenesis therapy.* J Huazhong Univ Sci Technolog Med Sci, 2015. 35(5): p. 615-622.
121. Onyeisi, J.O.S., et al., *Heparan sulfate proteoglycans as trastuzumab targets in anoikis-resistant endothelial cells.* J Cell Biochem, 2019. 120(8): p. 13826-13840.
122. Guadamillas, M.C., A. Cerezo, and M.A. Del Pozo, *Overcoming anoikis--pathways to anchorage-independent growth in cancer.* J Cell Sci, 2011. 124(Pt 19): p. 3189-97.
123. Hayden, M.R., J.R. Sowers, and S.C. Tyagi, *The central role of vascular extracellular matrix and basement membrane remodeling in metabolic syndrome and type 2 diabetes: the matrix preloaded.* Cardiovasc Diabetol, 2005. 4: p. 9.
124. Bonner, W.M., et al., *GammaH2AX and cancer.* Nat Rev Cancer, 2008. 8(12): p. 957-67.
125. Rogakou, E.P., et al., *Megabase chromatin domains involved in DNA double-strand breaks in vivo.* J Cell Biol, 1999. 146(5): p. 905-16.
126. Ichijima, Y., et al., *Phosphorylation of histone H2AX at M phase in human cells without DNA damage response.* Biochem Biophys Res Commun, 2005. 336(3): p. 807-12.
127. Lawless, C., et al., *Quantitative assessment of markers for cell senescence.* Experimental Gerontology, 2010. 45(10): p. 772-778.
128. Dahlgren, J., et al., *Interleukin-6 in the maternal circulation reaches the rat fetus in mid-gestation.* Pediatr Res, 2006. 60(2): p. 147-51.
129. Kojima, H., et al., *The STAT3-IGFBP5 axis is critical for IL-6/gp130-induced premature senescence in human fibroblasts.* Cell Cycle, 2012. 11(4): p. 730-9.
130. Romano, M., et al., *Role of IL-6 and its soluble receptor in induction of chemokines and leukocyte recruitment.* Immunity, 1997. 6(3): p. 315-25.
131. Rose-John, S., *IL-6 trans-signaling via the soluble IL-6 receptor: importance for the pro-inflammatory activities of IL-6.* Int J Biol Sci, 2012. 8(9): p. 1237-47.
132. Mohamed-Ali, V., J.H. Pinkney, and S.W. Coppack, *Adipose tissue as an endocrine and paracrine organ.* Int J Obes Relat Metab Disord, 1998. 22(12): p. 1145-58.
133. Coppack, S.W., *Pro-inflammatory cytokines and adipose tissue.* Proc Nutr Soc, 2001. 60(3): p. 349-56.
134. Navarro, P., et al., *Catenin-dependent and -independent functions of vascular endothelial cadherin.* J Biol Chem, 1995. 270(52): p. 30965-72.
135. Hartsock, A. and W.J. Nelson, *Adherens and tight junctions: structure, function and connections to the actin cytoskeleton.* Biochim Biophys Acta, 2008. 1778(3): p. 660-9.

136. Abe-Yutori, M., et al., *Decreased expression of E-cadherin by Porphyromonas gingivalis-lipopolysaccharide attenuates epithelial barrier function.* J Periodontal Res, 2017. 52(1): p. 42-50.
137. Delva, E. and A.P. Kowalczyk, *Regulation of cadherin trafficking.* Traffic, 2009. 10(3): p. 259-67.
138. Kokkinos, M.I., et al., *Cadherins in the human placenta--epithelial-mesenchymal transition (EMT) and placental development.* Placenta, 2010. 31(9): p. 747-55.
139. Radice, G.L., et al., *Precocious mammary gland development in P-cadherin-deficient mice.* J Cell Biol, 1997. 139(4): p. 1025-32.
140. Kleinschmidt, E.G. and D.D. Schlaepfer, *Focal adhesion kinase signaling in unexpected places.* Curr Opin Cell Biol, 2017. 45: p. 24-30.
141. Quadri, S.K., *Cross talk between focal adhesion kinase and cadherins: role in regulating endothelial barrier function.* Microvasc Res, 2012. 83(1): p. 3-11.
142. Risteli, J., et al., *The basement membrane proteins laminin and type IV collagen in isolated villi in pre-eclampsia.* Placenta, 1984. 5(6): p. 541-50.
143. Chatzizacharias, N.A., G.P. Kouraklis, and S.E. Theocharis, *The role of focal adhesion kinase in early development.* Histol Histopathol, 2010. 25(8): p. 1039-55.
144. Xin, L., et al., *Proteomics study reveals that the dysregulation of focal adhesion and ribosome contribute to early pregnancy loss.* Proteomics Clin Appl, 2016. 10(5): p. 554-63.
145. Strakovsky, R.S. and Y.X. Pan, *A decrease in DKK1, a WNT inhibitor, contributes to placental lipid accumulation in an obesity-prone rat model.* Biol Reprod, 2012. 86(3): p. 81.
146. Heerwagen, M.J., et al., *Transgenic increase in N-3/n-6 Fatty Acid ratio reduces maternal obesity-associated inflammation and limits adverse developmental programming in mice.* PLoS One, 2013. 8(6): p. e67791.
147. Delhaes, F., et al., *Altered maternal and placental lipid metabolism and fetal fat development in obesity: Current knowledge and advances in non-invasive assessment.* Placenta, 2018. 69: p. 118-124.
148. Saben, J., et al., *Maternal obesity is associated with a lipotoxic placental environment.* Placenta, 2014. 35(3): p. 171-7.
149. Shirasuna, K., et al., *Palmitic acid induces interleukin-1β secretion via NLRP3 inflammasomes and inflammatory responses through ROS production in human placental cells.* J Reprod Immunol, 2016. 116: p. 104-12.
150. Yang, C., et al., *Down-regulation of stearoyl-CoA desaturase-1 increases susceptibility to palmitic-acid-induced lipotoxicity in human trophoblast cells.* J Nutr Biochem, 2018. 54: p. 35-47.
151. Manuel, C.R., et al., *Saturated and unsaturated fatty acids differentially regulate in vitro and ex vivo placental antioxidant capacity.* Am J Reprod Immunol, 2018. 80(3): p. e12868.
152. Naughton, S.S., et al., *Australia's nutrition transition 1961-2009: a focus on fats.* Br J Nutr, 2015. 114(3): p. 337-46.
153. Ramsden, C.E., et al., *Lowering dietary linoleic acid reduces bioactive oxidized linoleic acid metabolites in humans.* Prostaglandins Leukot Essent Fatty Acids, 2012. 87(4-5): p. 135-41.
154. Shrestha, N., et al., *Linoleic Acid Increases Prostaglandin E2 Release and Reduces Mitochondrial Respiration and Cell Viability in Human Trophoblast-Like Cells.* Cell Physiol Biochem, 2019. 52(1): p. 94-108.
155. Holtz, R., et al., *Class II Transactivator (CIITA) Promoter Methylation Does Not Correlate with Silencing of CIITA Transcription in Trophoblasts1.* Biology of Reproduction, 2003. 69(3): p. 915-924.
156. Murphy, S.P., et al., *Repression of MHC class II gene transcription in trophoblast cells by novel single-stranded DNA binding proteins.* Molecular reproduction and development, 1997. 47(4): p. 390-403.
157. Vićovac, L. and J.D. Aplin, *Epithelial-mesenchymal transition during trophoblast differentiation.* Acta Anat (Basel), 1996. 156(3): p. 202-16.
158. Müntener, M. and Y.C. Hsu, *Development of trophoblast and placenta of the mouse. A reinvestigation with regard to the in vitro culture of mouse trophoblast and placenta.* Acta Anat (Basel), 1977. 98(3): p. 241-52.
159. van Veelen, W., et al., *β-catenin tyrosine 654 phosphorylation increases Wnt signalling and intestinal tumorigenesis.* Gut, 2011. 60(9): p. 1204-12.
160. Roura, S., et al., *Regulation of E-cadherin/Catenin association by tyrosine phosphorylation.* J Biol Chem, 1999. 274(51): p. 36734-40.

161. Sibley, C.P. and R.D. Boyd, *Control of transfer across the mature placenta.* Oxf Rev Reprod Biol, 1988. 10: p. 382-435.
162. Sibley, C.P., *Review article: mechanisms of ion transfer by the rat placenta: a model for the human placenta?* Placenta, 1994. 15(7): p. 675-91.
163. Caresia Aroztegui, A.P., et al., *18F-FDG PET/CT in breast cancer: Evidence-based recommendations in initial staging.* Tumour Biol, 2017. 39(10): p. 1010428317728285.
164. Yeh, R., et al., *The Role of 18F-FDG PET/CT and PET/MRI in Pancreatic Ductal Adenocarcinoma.* Abdom Radiol (NY), 2018. 43(2): p. 415-434.
165. Singnurkar, A., R. Poon, and U. Metser, *Comparison of 18F-FDG-PET/CT and 18F-FDG-PET/MR imaging in oncology: a systematic review.* Ann Nucl Med, 2017. 31(5): p. 366-378.
166. Zanotti-Fregonara, P., et al., *In vivo quantification of 18f-fdg uptake in human placenta during early pregnancy.* Health Phys, 2009. 97(1): p. 82-5.
167. Zanotti-Fregonara, P., et al., *Radiation dose to the fetus from [(18)F]-FDG administration during the second trimester of pregnancy.* Health Phys, 2012. 102(2): p. 217-9.
168. Zanotti-Fregonara, P., R. Laforest, and J.W. Wallis, *Fetal Radiation Dose from 18F-FDG in Pregnant Patients Imaged with PET, PET/CT, and PET/MR.* J Nucl Med, 2015. 56(8): p. 1218-22.
169. Zheleznyak, A., et al., *Preclinical Positron Emission Tomographic Imaging of Acute Hyperoxia Therapy of Chronic Hypoxia during Pregnancy.* Mol Imaging, 2015. 14: p. 366-72.
170. Baumann, M.U., S. Deborde, and N.P. Illsley, *Placental glucose transfer and fetal growth.* Endocrine, 2002. 19(1): p. 13-22.
171. Amrhein, V., S. Greenland, and B. McShane, *Scientists rise up against statistical significance.* Nature, 2019. 567(7748): p. 305-307.
172. Smith, S.E., et al., *Maternal immune activation alters fetal brain development through interleukin-6.* J Neurosci, 2007. 27(40): p. 10695-702.
173. Chaouat, G., S. Dubanchet, and N. Ledée, *Cytokines: Important for implantation?* J Assist Reprod Genet, 2007. 24(11): p. 491-505.
174. Kaplanski, G., et al., *IL-6: a regulator of the transition from neutrophil to monocyte recruitment during inflammation.* Trends Immunol, 2003. 24(1): p. 25-9.
175. Zegeye, M.M., et al., *Activation of the JAK/STAT3 and PI3K/AKT pathways are crucial for IL-6 trans-signaling-mediated pro-inflammatory response in human vascular endothelial cells.* Cell Commun Signal, 2018. 16(1): p. 55.
176. Valle, M.L., et al., *Inhibition of interleukin-6 trans-signaling prevents inflammation and endothelial barrier disruption in retinal endothelial cells.* Exp Eye Res, 2019. 178: p. 27-36.
177. Garbers, C., S. Aparicio-Siegmund, and S. Rose-John, *The IL-6/gp130/STAT3 signaling axis: recent advances towards specific inhibition.* Curr Opin Immunol, 2015. 34: p. 75-82.
178. Tanaka, T., M. Narazaki, and T. Kishimoto, *Anti-interleukin-6 receptor antibody, tocilizumab, for the treatment of autoimmune diseases.* FEBS Lett, 2011. 585(23): p. 3699-709.
179. Hohki, S., et al., *Blockade of interleukin-6 signaling suppresses experimental autoimmune uveoretinitis by the inhibition of inflammatory Th17 responses.* Exp Eye Res, 2010. 91(2): p. 162-70.
180. Jones, S.A., J. Scheller, and S. Rose-John, *Therapeutic strategies for the clinical blockade of IL-6/gp130 signaling.* J Clin Invest, 2011. 121(9): p. 3375-83.
181. Wang, X., et al., *Rapid monocyte infiltration following retinal detachment is dependent on non-canonical IL6 signaling through gp130.* J Neuroinflammation, 2017. 14(1): p. 121.
182. Akita, K., et al., *An Interleukin-6 Receptor Antibody Suppresses Atherosclerosis in Atherogenic Mice.* Front Cardiovasc Med, 2017. 4: p. 84.
183. Yoshida, H., et al., *Induction of high-dose tolerance to the rat anti-mouse IL-6 receptor antibody in NZB/NZW F1 mice.* Rheumatol Int, 2011. 31(11): p. 1445-9.
184. Liang, B., et al., *Evaluation of anti-IL-6 monoclonal antibody therapy using murine type II collagen-induced arthritis.* J Inflamm (Lond), 2009. 6: p. 10.
185. Izumiyama, T., et al., *The effect of anti-IL-6 receptor antibody for the treatment of McH-lpr/lpr-RA1 mice that spontaneously developed destructive arthritis and enthesitis.* BMC Musculoskelet Disord, 2019. 20(1): p. 286.
186. Suzuki, M., et al., *Blockade of interleukin-6 receptor enhances the anti-arthritic effect of glucocorticoids without decreasing bone mineral density in mice with collagen-induced arthritis.* Clin Exp Immunol, 2015. 182(2): p. 154-61.
187. Kim, I., et al., *Anti-interleukin 6 receptor antibodies attenuate antibody recall responses in a mouse model of allosensitization.* Transplantation, 2014. 98(12): p. 1262-70.

188. Qu, H.M., et al., *Overexpressed HO-1 is associated with reduced STAT3 activation in preeclampsia placenta and inhibits STAT3 phosphorylation in placental JEG-3 cells under hypoxia.* Arch Med Sci, 2018. 14(3): p. 597-607.
189. Fitzgerald, J.S., et al., *Trophoblast invasion: the role of intracellular cytokine signalling via signal transducer and activator of transcription 3 (STAT3).* Hum Reprod Update, 2008. 14(4): p. 335-44.
190. Garcia, M.G., et al., *High expression of survivin and down-regulation of Stat-3 characterize the feto-maternal interface in failing murine pregnancies during the implantation period.* Placenta, 2007. 28(7): p. 650-7.
191. Götestam Skorpen, C., et al., *The EULAR points to consider for use of antirheumatic drugs before pregnancy, and during pregnancy and lactation.* Ann Rheum Dis, 2016. 75(5): p. 795-810.
192. Gerosa, M., et al., *The use of biologics and small molecules in pregnant patients with rheumatic diseases.* Expert Rev Clin Pharmacol, 2018. 11(10): p. 987-998.
193. Jones, H.N., T. Jansson, and T.L. Powell, *IL-6 stimulates system A amino acid transporter activity in trophoblast cells through STAT3 and increased expression of SNAT2.* Am J Physiol Cell Physiol, 2009. 297(5): p. C1228-35.
194. Segovia, S.A., et al., *Maternal obesity, inflammation, and developmental programming.* Biomed Res Int, 2014. 2014: p. 418975.

## List of Abbreviations

| | |
|---|---|
| $^{18}$F-FDG | Fluorodeoxyglucose ($^{18}$F) |
| 2N $H_2SO_4$ | Sulfuric acid |
| ACTB | Beta-actin, β-actin |
| AJ | Adherens junction |
| APS | Ammonium persulfate |
| AU | Arbitrary units |
| BCA | Bicinchoninic acid |
| BM | Basement membrane |
| BrdU | Bromodeoxyuridine |
| BSA | Bovine serum albumin |
| CAA | Chloroacetamide |
| CAT | Catalase |
| CD31 | Platelet endothelial cell adhesion molecule, cluster of differentiation 31 |
| CD45 | Cluster of differentiation 45 |
| CDH1 | Cadherin 1, epithelial cadherin, E-cadherin |
| CDH3 | Cadherin 3, P-cadherin |
| CDH5 | Cadherin 5, vascular endothelial cadherin, VE-cadherin |
| cDNA | Copy DNA |
| CECAD | Cologne Excellence Cluster on Cellular Stress Responses in Aging-Associated Diseases |
| CI | Confidence interval |
| CMMC | Center for Molecular Medicine Cologne |
| $CO_2$ | Carbon dioxide |
| CTNNB1 | Catenin beta-1, β-catenin |
| CXCL1 | C-X-C Motif Chemokine Ligand 1 |
| CXCL10 | C-X-C Motif Chemokine Ligand 10 |
| CYBA | Cytochrome B-245 Alpha Chain |
| CYBB | Cytochrome B-245 Beta Chain |
| DAB | 3,3'-Diaminobenzidine |
| DAPI | 4',6-Diamidino-2-phenylindole |
| Db | Decidua basalis |
| DEPC | Diethyl pyrocarbonate |
| DMEM | Dulbecco's Modified Eagle's Medium |
| DNA | Deoxyribonucleic acid |
| dNTP | Deoxyribose nucleoside triphosphate |
| D-PBS | Dulbecco's phosphate-buffered saline |
| DTT | Dithiothreitol |
| EC | Endothelial cell (plural: ECs) |
| ECM | Extracellular matrix |
| EDTA | Ethylenediaminetetraacetic acid disodium salt dehydrate |
| EGTA | ethylene glycol-bis(β-aminoethyl ether)-N,N,N′,N′-tetraacetic acid |
| egWAT | epigonadal white adipose tissue |
| ELISA | Enzyme-linked immunosorbent assay |
| EM | Electron microscopy |
| ERK1/2 | Extracellular signal-regulated kinases or classical Mitogen-Activated Protein kinases |
| Fab | Fragment antigen-binding |
| FBS | Fetal bovine serum |
| Fc | Fragment crystallizable region |
| FC | Fetal capillary |

| | |
|---|---|
| FDR | False discovery rate |
| FE | Fetal endothelium |
| GLUT | Glucose transporter 1/3 (GLUT1/3) |
| GPX | Glutathione Peroxidase |
| $H_2O$ | Water |
| HEPES | 4-(2-hydroxyethyl)-1-piperazineethanesulfonic acid |
| HFD | High fat diet |
| HIER | Heat-induced epitope retrieval |
| HPLC | High-performance liquid chromatography |
| HPRT | Hypoxanthine-guanine phosphoribosyltransferase |
| HPVEC | Human placental vein endothelial cells |
| HRP | Horseradish peroxidase |
| IF | Immunofluorescence |
| IgG | Immunoglobulin G |
| IHC | Immunohistochemistry |
| IL-1α | Interleukin 1 alpha |
| IL-1β | Interleukin 1 beta |
| IL-6 | Interleukin 6 |
| $IL\text{-}6^{-/-}$ | IL-6 knock-out |
| IL-6R | Interleukin 6 receptor |
| IUGR | Intrauterine growth restriction |
| Jz | Junctional zone |
| kDA | Kilo Dalton |
| LA | Linoleic acid |
| LC/MS | Liquid chromatography mass spectrometry |
| LCM | Laser-capture microdissection |
| LFQ | Label-free quantification |
| Log2 | Binary logarithm |
| Lys-C | Lysyl Endopeptidase |
| Lz | Labyrinth zone |
| m/z | Mass-to-charge ratio |
| MBS | Maternal blood sinus |
| MCP1 | Monocyte Chemoattractant Protein 1 |
| MDA | Malondialdehyde |
| $MgCl_2$ | Magnesium chloride |
| M-MLV | Moloney Murine Leukemia Virus |
| mMR16-1 | Mousenized rat-anti-mouse IL-6R |
| MO | Maternal obesity |
| MRT | Magnet resonance tomography |
| MTB | Mononuclear trophoblast |
| $Na_3VO4$ | Sodium orthovanadate |
| NaCl | Sodium chloride |
| NaF | Sodium fluoride |
| NCF1 | Neutrophil Cytosolic Factor 1 |
| NCF2 | Neutrophil Cytosolic Factor 2 |
| NOX4 | NADPH (Nicotinamide adenine dinucleotide) Oxidase 4 |
| O/N | Overnight |
| $O_2$ | Molecular oxygen |
| OA | Oleic acid |
| OD | Optical density |
| PA | Palmitic acid |
| PARP | Poly (ADP-ribose) polymerase |
| PBS | Phosphate-buffered saline |

| | |
|---|---|
| PBS-T | Phosphate-buffered saline with Tween20 |
| PCNA | Proliferating cell nuclear antigen |
| PCR | Polymerase chain reaction |
| PenStrep | Penicillin-Streptomycin |
| pERK1/2 | Thr202/Tyr204-phosphorylated ERK1/2 |
| PET | Positron Emission Tomography |
| PMSF | Phenylmethylsulfonyl fluoride |
| p-Stat3 | Tyr705-phosphorylated Stat3 |
| pY654-β-catenin | Tyr654-phosphorylated β-catenin |
| qPCR | Quantitative PCR |
| R/T | Room temperature |
| R/T | Room temperature |
| RIPA | Radio-immunoprecipitation assay |
| RNA | Ribonucleic acid |
| SAA2 | Serum amyloid A2 |
| SD | Standard diet |
| SDS | Sodium dodecyl sulfate |
| SDS-PAGE | Sodium dodecyl sulfate-polyacrylamide gel electrophoresis |
| SEM | Standard error of the mean |
| SOCS3 | Suppressor of cytokine signaling 3 |
| SOD | Superoxide dismutase |
| Stat3 | Signal transducer and activator of transcription 3 |
| SynT | Syncytiotrophoblast |
| TAE | TRIS acetic acid EDTA |
| TBA | Thiobarbituric acid |
| TBST | Tris-buffered saline with Tween 20 |
| TEAB | Triethylammonium bicarbonate |
| TEMED | N,N,N',N'-Tetramethylethylendiamin |
| TMB | 3,3′,5,5′-Tetramethylbenzidine |
| TNFα | Tumor necrosis factor alpha |
| TRIS | 2-Amino-2-(hydroxymethyl)propane-1,3-diol |
| TUNEL | Terminal deoxynucleotidyl transferase-mediated deoxy uracil triphosphate-biotin nick end labeling |
| UDG | uracil-DNA-glycosylase |
| USA | United States of America |
| UV | Ultra violet |
| v/v | volume concentration, volume/volume |
| vWF | Von-Willebrand-factor |
| w/v | weight concentration, weight/volume |
| γH2A.X | Phosphorylated form of H2A histone family member X |

## List of Figures

## List of Tables

## Acknowledgements

First and foremost, I would like to thank my supervisors Dr. Sarah Appel and Prof. Dr. Jörg Dötsch who not only made this entire work possible, but are also great advisors, motivators and scientists of huge enthusiasm. Thriving as a scientists over the last 4 years with a lot of freedom to test and explore was possible through their guidance and I have always found advice and help when I needed it. I am especially thankful and proud for their trust in my work which helped me fulfill my duties.

I would like to extent my appreciation to all the talented members of the Research Group Appel and Dötsch, in particular to Marion Handwerk, Maria Wohlfarth and Eva-Maria Turnwald with whom I work vigorously throughout this whole study and who taught me a great deal of practical and organizational skills. It is a privilege to work with such friendly, open-hearted and enthusiastic people.

Furthermore, I am thankful to the Research Groups of Dr. Nüsken, Dr. Dr. Hucklenbruch-Rother and of Prof. Dr. Dr. Alcazar who contributed valuable scientific input and technical support to this work. Working alongside these colleagues was a great pleasure and surly had an impact on the success of this work.

I would also like to acknowledge our collaboration partners, PD Dr. Heike Endepols from the Department of Nuclear Medicine, University Hospital Cologne, and Prof. Dr. Wilhelm Bloch from the German Sports University Cologne with whom I enjoyed working together and who made many successful experiments possible.

I would further like to acknowledge the technical support and service of the CECAD Imaging facility regarding microscopy and image analysis especially by Peter Zentis, and the Proteomics facility regarding sample preparation, measurements and data analysis. Also, I am thankful to the TEHU of the CMMC for providing service and technical advice on histologic sample preparation. Furthermore, I appreciate the service and support in animal handling and housing by the animal care takers of the decentralized animal facilities at the Institute of Pharmacology.

I am very thankful for the support of my tutors, Prof. Dr. Mario Fabri and Prof. Dr. Matthias Hammerschmidt who guided me through this work and towards graduation with valuable feedback. Furthermore, I appreciate the lecturers and organizers of the IPMM who assisted in developing skills and gaining knowledge required for a successful promotion and scientific career.

Lastly, a great deal of appreciation goes to my friends and family who supported me in many ways and made sure professional and social progress went well alongside over the last 4 years. An open ear of a true friend or family member can truly safe the day.

## Erklärung an Eides statt

Ich versichere, dass ich die von mir vorgelegte Dissertation selbstständig angefertigt, die benutzten Quellen und Hilfsmittel vollständig angegeben und die Stellen der Arbeit - einschließlich Tabellen, Karten und Abbildungen -, die anderen Werken im Wortlaut oder dem Sinn nach entnommen sind, in jedem Einzelfall als Entlehnung kenntlich gemacht habe; dass diese Dissertation noch keiner anderen Fakultät oder Universität zur Prüfung vorgelegen hat; dass sie - abgesehen von unten angegebenen Teilpublikationen - noch nicht veröffentlicht worden ist sowie, dass ich eine solche Veröffentlichung vor Abschluss des Promotionsverfahrens nicht vornehmen werde.

Die Bestimmungen dieser Promotionsordnung sind mir bekannt. Die von mir vorgelegte Dissertation ist von Frau Dr. Sarah Appel und Herrn Prof. Dr. Jörg Dötsch betreut worden.

Nachfolgende Teilpublikationen liegen vor:

1. Sarah Appel*, Merle Schulze-Edinghausen*, **Tobias Kretschmer***, Sarah Storck, Ruth Janoschek, Inga Bae-Gartz, Marion Handwerk, Maria Wohlfarth, Kai-Dietrich Nüsken, Eva Hucklenbruch-Rother, Malte Heykants , Esther Mahabir, Jörg Dötsch. *Maternal obesity attenuates predelivery inflammatory reaction in C57BL/6N mice*. J Reprod Immunol, 2017. 122: p. 10-13. *These authors contributed equally to this work.

2. Eva Nüsken, Eva-Maria Turnwald, Gregor Fink, Jenny Voggel, Christopher Yosy, **Tobias Kretschmer**, Marion Handwerk, Maria Wohlfarth, Lutz T Weber, Eva Hucklenbruch-Rother, Jörg Dötsch, Kai-Dietrich Nüsken, Sarah Appel. *Maternal High Fat Diet and in-Utero Metformin Exposure Significantly Impact upon the Fetal Renal Proteome of Male Mice*. J Clin Med, 2019. 8(5).

3. **Tobias Kretschmer**, Merle Schulze-Edinghausen, Eva-Maria Turnwald, Ruth Janoschek, Inga Bae-Gartz, Peter Zentis, Marion Handwerk, Maria Wohlfarth, Astrid Schauss, Eva Hucklenbruch-Rother, Jörg Dötsch, Sarah Appel. *Effect of Maternal Obesity in Mice on IL-6 Levels and Placental Endothelial Cell Homeostasis. Nutrients*, 2020. 12(2)

4. **Tobias Kretschmer**, Eva-Maria Turnwald, Ruth Janoschek, Peter Zentis, Inga Bae-Gartz, Tim van Beers, Marion Handwerk, Maria Wohlfarth, Mojgan Ghilav, Wilhelm Bloch, Eva Hucklenbruch-Rother, Jörg Dötsch, and Sarah Appel. *Maternal, high fat diet-induced obesity affects trophoblast differentiation and placental function in mice*. Submitted on June 9th, 2020 to Biology of Reproduction.

Ich versichere, dass ich alle Angaben wahrheitsgemäß nach bestem Wissen und Gewissen gemacht habe und verpflichte mich, jedmögliche, die obigen Angaben betreffenden Veränderungen, dem Promotionsausschuss unverzüglich mitzuteilen.

Ort, Datum Unterschrift (Tobias Kretschmer)